

POLITECNICO DI TORINO

Facoltà di Ingegneria Meccanica, Aerospaziale,
dell'Autoveicolo e della Produzione
Master Degree course in Automotive Engineering

Master Degree Thesis

Cockpit-opening optimization of a CFRP monocoque

Applied study on an FSAE race-car



Supervisor
Prof. Andrea Tonoli

Candidate
Alessio Canuto

ACADEMIC YEAR 2019-2020

*"Adding power makes you faster on
the straights; subtracting weight
makes you faster everywhere."*

Colin Chapman

Summary

Formula Student competitions are exciting events in which teams from all over the world compete against each other in a battle for performances, design quality and project sustainability. To succeed in this event, teams exploit cutting-edge technologies in every field. Considering the chassis, because of its structural, performance and safety relevance, the choice of the solution is extremely important since it influences the entire project. The most performing choice is represented by a Carbon Fibre Reinforced Polymers (CFRP) monocoque, which design must be carefully executed. An aspect of particular relevance is the cockpit opening, namely, the aperture which allows the pilot to enter/exit from the chassis itself. It represents the area of the monocoque which suffers major stiffness losses and stress concentration. Thus, its design and optimization are of paramount importance.

The objectives of this paper are both to report in detail the investigations and the structural analyses performed to achieve the best performances in terms of stiffness over mass ratio for the 2017 Squadra Corse FSAE prototype (SC17) and to provide a useful reference for future chassis designers inside the team.

Starting from the analysis of the results of an asymmetric torsion test performed on the 2016 prototype, the paper will then describe the steps followed during the design process of the SC17. Not only the theoretical results are presented, but also the practical implementations of the analyzed solutions.

In addition to this, further investigations are reported to show the influence of some geometrical and constructional parameters on the specific torsional stiffness, together with some possible future developments.

As demonstrated by the excellent results obtained by the team during the 2017 championship, SC17 has been an extremely competitive prototype, thanks, also to a stiff and light composite monocoque that owes these characteristics to the combination of an integrated firewall frame and a foam reinforcement ring around the cockpit opening.

Acknowledgements

QUESTO lavoro di tesi conclude un percorso iniziato qualche anno fa, fatto di tanti momenti speciali: alcuni non facili, soprattutto all'inizio, ma che sono serviti da lezione. Questi, sono stati anni di crescita, non solo tecnica, ma soprattutto personale. Dietro a questa maturità ci sono tante persone e tante esperienze.

I primi che devo ringraziare sono mamma e papà. Grazie per non aver mai ostacolato le mie scelte, nonostante fosse evidente che avrebbero complicato non poco le cose, sia quando sono entrato in Squadra Corse, sia quando ho deciso di seguire il mio sogno di lavorare in F1 senza aver finito l'università, in Toro Rosso prima ed ora in Ferrari.

Anche Ricky merita un ringraziamento a parte. Non solo mi ha dato un tetto sotto cui stare ma mi ha anche sempre sopportato, anche nei momenti in cui l'armanach marcava patele!

Non da meno sono stati tutti gli amici che mi hanno fatto compagnia durante questo percorso. Tra tutti, devo un ringraziamento speciale a Gino e Pino. Voglio anche ringraziare i nuovi amici conosciuti durante la Ferrari F1 Academy, grazie a loro quest'avventura è stata indimenticabile.

Chi bin as ancamin-a,.. a l'ha 'ncora tut ël travaj da fé.

Maranello,
Marzo 2020

Contents

List of Tables	7
List of Figures	8
1 Introduction	11
2 FSAE and Squadra Corse PoliTO	15
2.1 Formula Student	15
2.1.1 Static events	16
2.1.2 Dynamic Events	16
2.2 Squadra Corse PoliTO	18
3 Introduction to chassis	21
3.1 Introduction to vehicles chassis	21
3.2 Chassis design procedure	26
3.3 Introduction to types of structures	27
3.4 Introduction to the problem of the cockpit opening	30
3.4.1 SCXV torsional stiffness test	30
3.4.2 Further structural and non-structural considerations	37
3.5 Cockpit opening FSAE rules	41
4 Propaedeutic concepts	43
4.1 Introduction to composites materials	44
4.1.1 Reinforcements	46
4.1.2 Matrix	50
4.2 Introduction to the Finite Element Method: most important steps	51
4.2.1 Procedure	51
4.3 Introduction to the Classical Laminated Plate theory	55
5 The SC17 project	65
5.1 Load-cases	69
5.2 SC17 FEM model	71

5.2.1	Monocoque CAD model: the surfaces resulting from the first design phase	71
5.2.2	Monocoque convergence analysis	74
5.3	Cockpit-opening detailed analysis	78
5.4	Practical implementation of the designed solutions	86
5.5	The SC17: a brief overview of the project results	89
5.6	Possible future developments	92
6	Further studies on the cockpit opening	95
6.1	Influence of fillet radii	97
6.2	Influence of aperture dimensions	102
7	Conclusion	105

List of Tables

3.1	Comparison between space-frame and monocoque	29
5.1	Running load-cases: forces and moments at the tyre-ground contact patch	70
5.2	FSAE alternative frame rules load-cases	70
5.3	Convergence analysis summary	75
6.1	Local convergence analysis summary	96
6.2	Influence of fillet radii on torsional stiffness over mass ratio	98

List of Figures

2.1	Score distribution of a Formula Student event	17
2.2	SC05	18
2.3	SC06	18
2.4	SC07	18
2.5	SC08	18
2.6	SC08H	19
2.7	SCX	19
2.8	SCXX	19
2.9	SC12e	19
2.10	SCR	19
2.11	SCXV	19
2.12	SC17	20
3.1	Relationship between vehicle relative stiffness and chassis torsional stiffness	25
3.2	Space-frame chassis example	27
3.3	Hybrid chassis example	28
3.4	Monocoque chassis example	28
3.5	Representation of a symmetric torsion test	31
3.6	Representation of an asymmetric torsion test	31
3.7	Squadra Corse asymmetric torsion test layout	32
3.8	Displacements measurement on front dampers	33
3.9	Displacements measurement on front roll hoop	33
3.10	Displacements measurement in the middle of the cockpit opening	34
3.11	Displacements measurement at the end of the cockpit opening	34
3.12	Displacements measurement after the cockpit opening	35
3.13	Displacements measurement at the rear-end	35
3.14	Example of a hysteresis cycle	36
3.15	Rotational displacements over length	36
3.16	Real torsional stiffness values for SCXV and load-displacements curve	37
3.17	Variation of torsional stiffness over length	37
3.18	Stresses due to torsion load-case	38

3.19	Loads on a simplified chassis in three parts: I, a closed profile, II, an open profile and III, a tubular space frame	39
3.20	Fibres direction for panel subjected to: shear (left) and bending (right)	39
3.21	Examples of cockpit opening solution: low inertia and no ply edges (left), increased edge bending stiffness (centre) and a combination of these measure (right)	40
3.22	Cockpit opening FSAE template	42
4.1	Laminate example	45
4.2	Intralaminar shear stresses	47
4.3	Load transfer process in continuous (a) and discontinuous fiber (b) .	47
4.4	Example of weaving patterns	48
4.5	3D detail of a woven fabric	49
4.6	Photomicrograph of a fabric-reinforced composite lamina	49
4.7	Stress resultant	59
5.1	SC17 chassis design process	66
5.2	Packaging of the prototype SCXV	67
5.3	Cockpit opening FSAE template	72
5.4	First cockpit opening geometry	72
5.5	Actual position of driver shoulder during driving conditions	73
5.6	SC17 actual cockpit opening geometry	73
5.7	FEM model: mesh-size 20 mm	75
5.8	FEM model: mesh-size 15 mm	75
5.9	FEM model: mesh-size 10 mm	76
5.10	FEM model: mesh-size 5 mm	76
5.11	FEM model detail: mesh-size 5 mm	76
5.12	Torsional stiffness calculation	76
5.13	Convergence analysis: number of nodes per iteration	76
5.14	Convergence analysis: run-time per iteration	76
5.15	Convergence analysis: z-displacement per iteration	77
5.16	Convergence analysis: error percentage per iteration	77
5.17	Convergence analysis: displacements comparison	77
5.18	FEM model with ring	78
5.19	Detail of the Rohacell ring	78
5.20	Study of the influence of Rohacell density on torsional stiffness . . .	79
5.21	Strain energy density of the different Rohacell solutions	80
5.22	Percentage increase of stiffness/mass ratio as a function of different Rohacell solutions	80
5.23	Study of the influence of Rohacell density and UD on torsional stiffness	81
5.24	Z-coordinate displacement comparison between baseline model (left), Rohacell reinforcement (centre) and Rohacell and UD (right)	81
5.25	Z-coordinate displacement comparison between firewall fixed frame with: T200 at 0° (left) and T200 at 45° (right)	82

5.26	Z-coordinate displacement comparison between firewall fixed frame with: M46J at 0° (left) and M46J at 45° (right)	83
5.27	Firewall fixed frame z-coordinate displacement comparison between: T200 (left), M46J (centre), UD (right)	83
5.28	Z-coordinate displacement comparison between two firewall laminate solutions: fixed frame M46J laminate (left), same laminate but with additional two UD balanced plies (right)	84
5.29	Strain energy density of the resulting model when subjected to torsion	84
5.30	Strain energy density of the resulting model when considering maximum envelope of: running load-cases (left), FSAE alternative frame rules (right)	85
5.31	Comparison between the baseline model (left) and the resulting model (right)	85
5.32	Lamination of the top half of the monocoque	86
5.33	Lamination of the top half: detail of the cockpit opening Rohacell reinforcement	87
5.34	Integrated firewall frame	88
5.35	Packaging of the prototype SC17	90
5.36	CFD simulation of the SC17	91
5.37	SC17 in the wind tunnel of Centro Ricerche FIAT during the validation of the aero-pack	91
5.38	Stiffened composite panel	93
5.39	Monocoque sandwich foam core	93
6.1	Local convergence analysis. Stress in the cockpit opening	96
6.2	Baseline geometry (left) and absence of rear-end fillets (right) . . .	98
6.3	Absence of rear-end fillets (left) and a fillet R=100 mm (right) . . .	99
6.4	Fillet R=100 mm (left) and fillet R=134 mm (right)	99
6.5	Baseline geometry (left) and absence of front-end fillets (right) . . .	100
6.6	Baseline geometry (left) and rear-end with additional structure (right)	100
6.7	TuFast 2019 electric prototype	101
6.8	AMZ electric prototype	101
6.9	Baseline geometry (left) and aperture at the limit with the FSAE dimensions (right)	102
6.10	Aperture at the limit with the FSAE dimensions (left) and the same geometry but 5 mm wider	103
7.1	Squadra Corse team together with the teams's faculty advisor during design event in Varano 2017	106
7.2	SC17 team during the prizegiving in Varano 2017 - Third place overall	106

Chapter 1

Introduction

This Master thesis will cover in detail the design and analysis of a specific area of a composite monocoque, namely the cockpit opening. The cockpit opening of a chassis corresponds to the opening which allows the drivers to enter/exit into the survival cell. What will be presented in the following chapters is given by two contributions: the first one is a portion of the entire design and analysis process followed by the author during the 2016-2017 Formula Student season (which brought, thanks to the efforts of the entire team, to a prototype capable of significant achievements after several years of difficulties and poor results), while the second contribution is constituted by a set of investigations performed specifically for this paper.

The design and analysis process followed by the chassis department for the SC17 monocoque could be divided into two macro-steps:

- Design, analysis, and development of the chassis geometries as well as its composite laminate (thickness, orientation, lay-up);
- Design, analysis, and optimization of the cockpit opening area, considering not only the opening itself but also the surrounding components (i.e. the firewall and the firewall frame).

The first topic will not be covered in this paper since it has been already illustrated in [3].

The second point represents the first of the two contributions mentioned above. In fact, because of the high torsional stiffness target required by the vehicle dynamic department and the need to further reduce the mass of the chassis, this detailed analysis became essential in the project of the SC17.

This aperture causes weakening effects on the structure and due to the loading conditions at which the chassis is subjected to when on the track, it represents a critical area of the monocoque, both concerning stiffness, stresses, and strains.

The final aim of this work is not only to provide a series of useful information but also to be a repository of tested solutions, concepts and encountered problems,

that can be used by the future engineers of Squadra Corse during the design and production phases of the new chassis to speed up the design process and to obtain a reliable solution with improved performances.

The design phase of a new FSAE (Formula Society of Automotive Engineers, FSAE from now on) prototypes is usually characterized by a remarkable amount of excitements. Unfortunately, the time at disposal is very limited because both the design phase and the production process will have to be performed by the students themselves. It is then advantageous, as in this case, to exploit the thesis and other technical papers to gather knowledge inside the team. This to improve the technical quality of the car, aiming at more performances, reliability and safety, true milestones of every Formula Student project.

The technical solutions when dealing with FSAE chassis, and so cockpit openings, are multiple and the decisions depend on many factors: from money to time, from experience to priorities. This leads to the fact that every team develops its specific solution and they can be quite different from team to team. Another interesting factor is the type of prototype considered: electric vehicles have different needs compared to internal combustion engine ones. A typical example is, in case of electric vehicles, the need to avoid electromagnetic interference between high and low-voltage wiring systems, which could lead to having wires passing in different areas of the cockpit (an example could be having the high voltage wires arranged at the bottom of the chassis because they weight more, and the low voltage ones passing through the top of the cockpit). On the other hand, internal combustion engine vehicles could be more interested in fuel tank arrangements.

In particular, concerning Squadra Corse, the chassis underwent a dramatic development over years: from the first steel tubes space-frame to the first complete carbon fiber monocoque (2014) up to the last and more recent one, the performances, especially in terms of stiffness over mass ratio, increased dramatically (more details are summarized in table 3.1. Nevertheless, inside the team, there was no documentation about detailed studies on the cockpit opening.

Again, the contribution of this thesis will be to represent a valuable tool through which future chassis designers of Squadra Corse will be able to address the design of this delicate region of the chassis. The field of interest itself which, as mentioned above, has never been studied in detail, represents an innovative aspect.

In order to allow a comprehensive understanding of this work and the logic path behind, the next paragraphs will briefly describe the contents of the following chapters..

In particular:

- Chapter 2 - FSAE and Squadra Corse PoliTO

This chapter will introduce Formula Student and Squadra Corse PoliTO. This section will give an insight into what is the context within which FSAE teams develop their prototypes.

- Chapter 3 - Introduction to chassis

Being the chassis the article under investigation, Chapter 3 will provide an introduction about chassis (most common solutions, their advantages, and disadvantages, which are the most important parameters affecting the performances, their main objectives, and constraints).

- Chapter 4 - Composites and Finite Element Analysis

The chassis analyzed in this paper is made by fiber-reinforced composites. Chapter 4 will start with the basics of composites materials: from a general introduction, the attention will then move specifically on carbon-fiber composites.

This thesis is mainly simulation-oriented and most of the results will be the output of various Finite Elements Method (FEM) analyses. Because of this, the following section of Chapter 4 will introduce the fundamental of the FEM method. Many relevant books have been written since the introduction and the development of this numerical method and this section is not intended to be exhaustive, but to give just a first insight on FEA (Finite Element Analysis).

The following section will deal with the integration of the topics mentioned above, namely, it will report how the FEM method deals with composites.

- Chapter 5 - SC17 project

Chapter 5 will introduce the project of the 2017 prototype focusing in particular, on the chassis. This to understand what there was behind the design and development of the SC17 monocoque. This chapter contains also the results of the analyses performed to define the cockpit opening and its surroundings. These studies have been carried out during the design phase of the SC17, and thus represents the first contribution given to the study of the cockpit opening.

- Chapter 6 - Further studies on monocoque cockpit opening This chapter contains some further investigations about the parameters affecting the cockpit opening performances performed a posteriori with respect to what analyzed in Chapter 5. This because of the limited time available during the actual design phase of the SC17, which did not allow more in-depth research on the topic.

- Chapter 7 - Conclusion This chapter reports the outcomes of the considerations outlined in the above-mentioned chapters.

Chapter 2

FSAE and Squadra Corse PoliTO

2.1 Formula Student

Formula SAE [15] is a student design competition organized by SAE (Society of Automotive Engineers), SAE from now on, International with the aim of inspiring students to design, build and develop a single seater prototype and make it race against other universities' teams. The competition started in 1978 and was originally called SAE Mini Indy.

The main goal of the competition is to spread out the “learn by doing” attitude and to prepare students to face the working environment immediately after the graduation. The competition takes place all over the world in the most important motorsport circuits and an overall ranking is made on the base of the single events results.

As clearly pointed out in [2], the concept behind Formula SAE is that a fictional manufacturing company has contracted a student design team to develop a small Formula-style race car. The prototype race car is to be evaluated for its potential as a production item. The target marketing group for the race car is the non-professional weekend autocross racer. Each student team designs, builds and tests a prototype based on a series of rules, whose purpose is both ensuring on-track safety (the cars are driven by the students themselves) and promoting clever problem solving.

During a Formula SAE event, the cars are evaluated by judges in a series of static and dynamic events, which include technical inspections, evaluations on the design of the car and its performance in the race, aimed to evaluate how well the vehicle behaves and goodness of its design and production. The maximum score assigned during a SAE event is 1000 points, 675 are made available by the dynamic events and 325 from the static ones.

2.1.1 Static events

This section will describe briefly each static event, its objectives and the maximum amount of points assigned. The total amount of points for these events is 325 points.

- Technical Inspection (no points)

The objective of these controls is to assess the safety of the prototype, evaluating its compliance with the FSAE rules.

- Cost Report (100 points)

This event requires the development of document which reports the costs of all the parts of the vehicle, its total costs and manufacturability. In addition to this, team members are asked to face a "Real Case Scenario", which is used to test students ability to face costs and manufacturing challenges.

- Business Presentation (75 points)

The objective of the presentation event is to evaluate the team's ability to develop and deliver a comprehensive business case that will convince the executives of a corporation that the teams design best meets the demands of the amateur, weekend competition market, and that it can be profitably manufactured and marketed.

- Design (150 points)

Engineering Design is one of the more prestigious events during the competition. During this event the students defend their knowledge of the car and engineering concepts to a panel of judges. The students should explain to the judges the entire design process of their car, from the concept to the manufacturing and discuss with the judges all the pros and cons of their choices.

2.1.2 Dynamic Events

This section shortly describes the dynamic events and specifies the amount of points assigned to each of them. The total amount of points for these events is 675 points.

- Acceleration (75 points)

This events evaluate the acceleration performances of a prototype over 75m.

- Skid Pad (50 points)

The objective of the skid-pad event is to measure the cars cornering ability on a closed circuit with two constant radius corners of 8m to the right and left. The faster car gets the highest score.

- Autocross (150 points)

Autocross is a one lap sprint usually 1-2km long. The objective of the autocross event is to evaluate the car’s maneuverability and handling qualities on a tight course without the hindrance of competing cars. The autocross course will combine the performance features of acceleration, braking, and cornering into one event.

- Endurance (300 points) The Endurance Event is a closed circuit race of 22km long. There are two drivers, each driving half of the distance

- Efficiency (100 points)

The cars fuel economy will be measured in conjunction with the Endurance Event. The fuel economy shows how well the car has been tuned for the competition. This is a compromise event because the fuel economy score and endurance score will be calculated from the same heat. No refueling is allowed during an endurance heat.

Figure 2.1 illustrates the score distribution during a FSAE event.

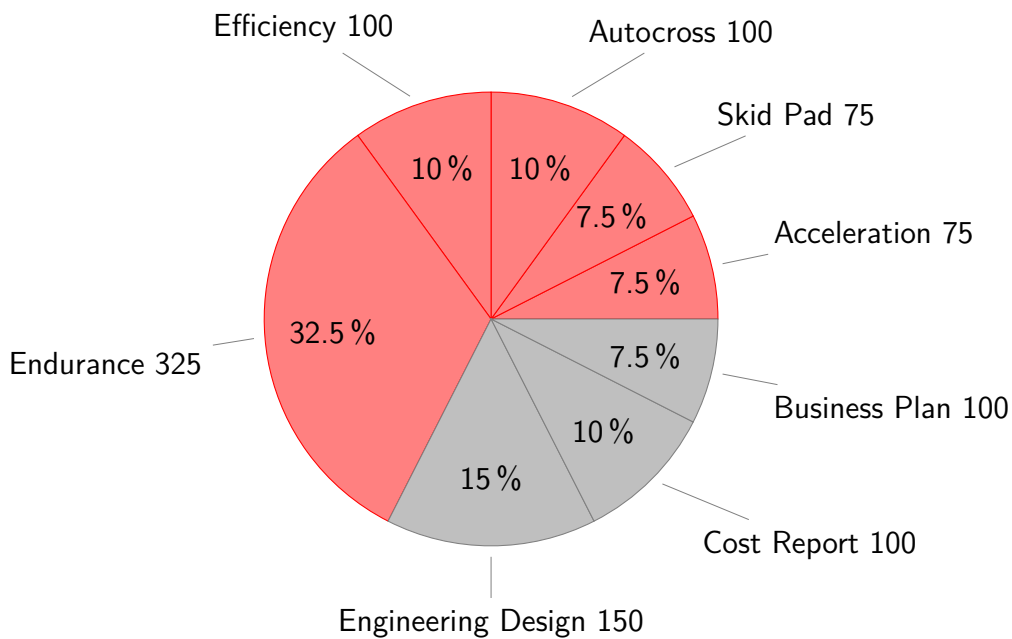


Figure 2.1: Score distribution of a Formula Student event

2.2 Squadra Corse PoliTO

Squadra Corse PoliTO [17] is the Formula Student team of Politecnico di Torino. It has been established in 2005 by a modest group of students united by their passion for motorsport. Squadra Corse’s prototype, SC05, took part in the competition the same year. The following years were characterized by continuous improvements of the internal combustion engine prototypes, such as the introduction of an electronically-actuated sequential gearbox, variable geometry intake manifold, traction control, launch control, and telemetry system

In 2011 the team designed the first full-electric prototype, the SC12e, to participate in the student competition of 2012, reaching outstanding results.

The prototypes developed in the following maintained the full electric power-train but featured further developments, such as composite monocoque, firstly implemented in 2014, and Full Wheel Drive (FWD) transmission, designed for the first time in 2015.

Since 2015 the main layout remained the same. The design process is now focusing on lightness and reliability, refining the details time by time.

Pictures 2.2, 2.3, 2.4, 2.5, 2.6, 2.7, 2.8, 2.9, 2.10, 2.11, 2.12, represent the prototypes designed by Squadra Corse over the years, from its establishment to the 2017 prototype.



Figure 2.2: SC05



Figure 2.3: SC06



Figure 2.4: SC07



Figure 2.5: SC08



Figure 2.6: SC08H



Figure 2.7: SCX



Figure 2.8: SCXX



Figure 2.9: SC12e



Figure 2.10: SCR



Figure 2.11: SCXV

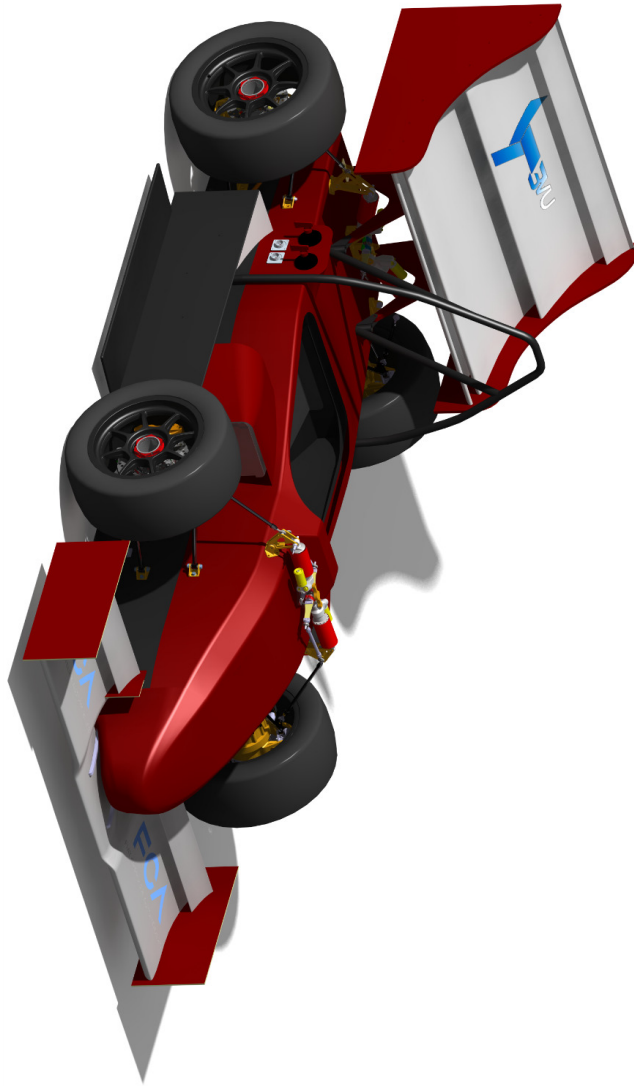


Figure 2.12: SC17

Chapter 3

Introduction to chassis

3.1 Introduction to vehicles chassis

The chassis is one of the most important components of a vehicle, and even more so concerning a race-car. It has the aims of both containing all the required sub-assemblies necessary for the proper functioning of the vehicle and to connect the front and rear suspension systems. The structure must be capable of withstanding the external loads coming from the interactions between tires and ground, which, in turn, are transmitted to the chassis by means of the suspension arms.

Generally, safety should have the highest priority, especially in FSAE competitions, where the purpose is learning by doing, and students perform both the design and manufacturing phases. The chassis embodies the way through which the pilot is protected from side, front and rear impacts. The chassis, combined with roll-overs, protect the driver also from rollover.

The fact that the chassis connects the suspension systems lead to the definition of one of the most important parameter about race-cars, namely, torsional stiffness. It is universally recognized that torsional stiffness is one of the most important properties of a vehicle chassis.

The two fundamental parameters characterizing race-cars chassis are:

- Mass: it must be as low as possible. Chassis' mass represent one of the three most important contributions to the overall vehicle's mass, together with the driver and the engine. The order depends on which category of racing cars is considered. About FSAE prototypes, the mass of the pilot represents the main contribution, followed by the engine (internal combustion) or the battery pack (full electric), and finally by the chassis.

The overall vehicle's mass should be kept to the minimum, in order to enhance the performances during the dynamic manoeuvres the car will be subject to during a race. In FSAE competitions, the two most important dynamic events, autocross and endurance, have a format in which speed and direction suddenly

change. [6] states that Overall vehicle weight reduction enhances the ability to rapidly change vehicle speed and direction;

- Stiffness: it can be divided into flexural and torsional stiffness. Actually, only this last influences the loads transferred to the tyres, and so the performances. According to Sampò et al [16], lack of chassis torsional stiffness affects the lateral load transfer distribution, it allows displacements of the suspension hard-points, modifying suspension kinematics and it triggers unwanted dynamic effects, such as resonance phenomena and vibrations.

When a load is applied to a wheel, it may cause a deformation of the chassis due to the load path passing thru the suspension system. Thus, the chassis can be seen as a torsion bar. Its deformation has a remarkable influence on the dynamic behaviour of the car. As an example, let's consider the entry phase of a turning manoeuvre. The steering wheel turns and the front tyres start providing lateral grip. This action induces a lateral acceleration of the front-end, which in turn, traduces into lateral load transfer at the front, with the load shifting toward the outer wheel. At this instant, the rear wheels are not delivering yet lateral forces. If the torsional stiffness of the chassis is too low, rear wheels will take longer to experience lateral load transfer. The car must be more inside the corner to activate the load transfer at the rear and thus generating lateral grip in rear tyres too. This happens because of the filtering action of the chassis.

This means that torsional stiffness, together with the front and rear weight distribution, defines the dynamic distribution of lateral load transfer between front and rear ends. This finally influences the over-/under-steering properties of the vehicle. It has been proven by [5] that cars with low torsional stiffness are mostly under-steering. Deformations may nullify the suspensions effect, shifting the roll centres.

In other words, the torsional deformation of the chassis causes rotation around the roll axis, which sums up with the suspension ones, interfering with them in the control of the attitude. As a consequence, the higher the torsional stiffness, the lower will be the influence of the chassis on the suspension behaviour, with an improvement in term of handling and safety.

In addition, if the torsional stiffness is not high enough, it will behave as a filter during suspension systems set-up, reducing the impact of these changes and may cause a strange feeling for the pilot.

A sufficiently stiff chassis improve the response to set-up changes. This is fundamental, especially in testing sessions where a too small torsional stiffness would lead to big set-up changes without significant improvements in performances. As stated in [9], to find an optimum in suspension setup, the smallest variation in front and rear anti-roll stiffness should be felt immediately by

drivers. To ensure this, high torsional rigidity of the chassis with respect to the anti-roll stiffness is required.

Defining a priori a value of the torsional stiffness is almost impossible. It depends on the kind of car (passenger car, segment, mass, architecture, if coupè or spider and so forth) and on its tasks. In a formula-like race-car, this value must be high enough to allow the proper functioning of the suspension systems: the unique elastic deformation caused by external load must be due to spring and dampers. In general, as a rule of thumb, the torsional stiffness of the chassis must be about 10 times the suspensions roll stiffness.

Another approach to defining the torsional stiffness target is reported in [9].

The value of the torsional stiffness of a chassis can range ideally from zero to infinite. Which is the best value to choose from? As mentioned above in this section, the vehicle dynamics, concerning suspension kinematics only, would suggest an infinitely stiff chassis. Unfortunately, this is not feasible. The approach illustrated in the aforementioned paper consists of relating the behavior of a vehicle with a finite stiff chassis with respect to a vehicle with an infinitely stiff chassis. To do so, the equivalent torsional stiffness of a vehicle is divided by the total torsional stiffness of the suspension systems. For the sake of simplicity, a vehicle can be thought of as a series of three torsion springs: a first one representing the torsional stiffness of the front suspension, a central one representing the chassis and finally a third one for the rear suspension system. Assuming that both suspension systems have the same torsional stiffness, the total vehicle resistance to torsional deflection when dealing with a finite stiff chassis can be computed as shown in Eq.3.1 and Eq.3.2.

Let's now consider the case in which the chassis has an infinitely high torsional stiffness. The equivalent torsional stiffness of the vehicle provided with that chassis is given by Eq. 3.3. Finally, Eq.3.4 defines a relative stiffness which, as stated before, compares the performances of the vehicle with respect to a vehicle provided with a stiff chassis. K_{Rel} assumes values from zero to one. If the chassis stiffness is null, then the relative stiffness is nulls, while when the stiffness tends to infinite, K_{Rel} tends to one.

The plot of the relative stiffness as a function of the chassis stiffness helps to determine how the chassis stiffness influences the relative vehicle behavior (Figure 3.1). This chart is then useful to define a chassis torsional stiffness target: assuming a relative stiffness desired target of 0.9, the stiffness of the chassis is about 200 kNm/rad. The shape of the chart allows also to do another consideration: increasing the chassis stiffness is not quite effective above a certain value. To get the missing 0.1 relative stiffness, the chassis stiffness should increase to values at which the mass would become an important penalizing factor. To summarize, to determine the target torsional stiffness, the

reader should, once knowing the value of the suspension stiffness, choose the relative stiffness percentage on the y axis. From here the reader should look for the intersection with the curve and finally, moving downward, determine the chassis stiffness.

$$\frac{1}{K_{car}} = \frac{1}{K_{susp}} + \frac{1}{K_{chassis}} + \frac{1}{K_{susp}} \quad (3.1)$$

Where:

- K_{susp} represents the torsional stiffness of the suspension (front as well as rear);
- $K_{chassis}$ is the torsional stiffness of the chassis.

Eq.3.1 can be rewritten as,

$$K_{car} = \frac{K_{susp}K_{chassis}}{2K_{chassis} + K_{susp}} \quad (3.2)$$

$$\frac{1}{K_{car(Rigidchassis)}} = \frac{1}{K_{susp}} + \frac{1}{K_{susp}} = \frac{2}{K_{susp}} \quad (3.3)$$

$$K_{Rel} = \frac{K_{car}}{K_{car(Rigidchassis)}} = \frac{\cancel{K_{susp}}K_{chassis}}{(2K_{chassis} + K_{susp})\cancel{K_{susp}}} \frac{2}{\cancel{K_{susp}}} = \frac{1}{1 + \frac{K_{susp}}{2K_{chassis}}} \quad (3.4)$$

Furthermore, if the chassis undergoes big elastic deformations, then the elastic deformation energy will be initially stored, but then released in an uncontrolled way, like through vibrations and oscillations. This phenomenon may cause a reduction of the dimension of the tyres contact-patch, and lead to imprecision of the steering system, reducing the dynamic performances of the whole car.

The problem of assessing the influence of the chassis torsional stiffness on the vehicle dynamics can be analyzed by means of advanced multi-body codes, where the mode shapes determined through a FEM analysis are used within the multi-body code. This approach allows to obtain accurate results but requires a number of input usually not available during the preliminary phase of the design process.

To summarise, as specified in [16], there are several factors that make torsional rigidity an important figure in vehicle dynamics. There are several problems connected to a too small torsional stiffness:

1. The control of the lateral load transfer distribution is difficult and the vehicle does not respond as expected to set-up changes;

Relative stiffness as a function of the chassis torsional stiffness

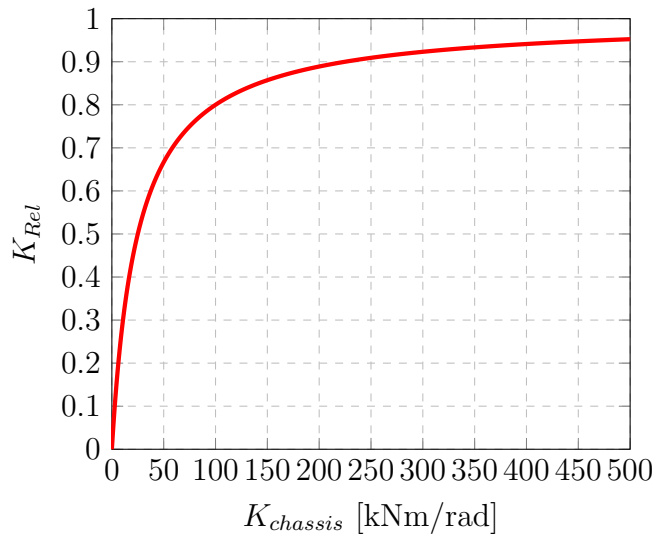


Figure 3.1: Relationship between vehicle relative stiffness and chassis torsional stiffness

2. Displacements of the suspension attachment points occur, so that the desired control of the movement of the tires cannot be guaranteed;
3. Dynamic effects like vibrations can occur;
4. Fatigue phenomena are more marked;
5. Ride quality is poor.

For sport and race-cars, these problems are particularly important.

Concerning more about the vehicle dynamic aspects, the document of Ing. Moroni [13] states clearly how the torsional stiffness influences the vehicle dynamic behaviour. The results presented in the paper are:

- The chassis torsional stiffness has an influence on the car steady-state handling balance similar to other traditional set-up parameters;
- The chassis torsional stiffness has an influence on the lap-time performances only through changes in driveability due to the handling balance variations;
- The tuning of set-up parameters related to the car's transient behaviour (damper characteristics, has to take into account the chassis torsional stiffness);
- The chassis torsional stiffness has more influence than some common set-up parameters (springs stiffness, Anti-Roll Bar (ARB) stiffness), on the high frequency range of steering control capacity.

3.2 Chassis design procedure

The starting point when designing a chassis is to understand what are its main characteristics and how each aspect influences the properties of the final product.

The main aspects to take into account are:

- **Safety:** FSAE rules underline the importance of the driver cell's safety which is asked to protect the driver. It is designed to face front and lateral impacts, rollover, contact with high temperature substances and must be electrically insulated;
- **Mass and stiffness:** these quantities are strictly linked. It is fundamental to find the right compromise. The chassis must be stiff enough so to not compromise the kinematic of the suspensions but this stiffness must not lead to a too heavy chassis which would be, in turn, detrimental to the overall dynamic properties. Usually what defines the shape of a chassis are packaging (inside) and suspension hard-points (outside).

Aerodynamics can be considered too. This means that to increase the torsional stiffness the solutions are using materials with better performances or using more material, which lead to mass increase;

- **Accessibility and maintainability:** a chassis is designed around the packaging. It must be able to contain all the necessary sub-assemblies, which must be accessible for an easy maintenance. When dealing with composites chassis, the fixing points must be defined during the design phase because it is really difficult to integrate new components a posteriori;
- **Ergonomics:** SAE defines strict rules concerning the dimensions of the cockpit opening and the driver must be able to exit from the car in 5 second, starting from a racing position (steering wheel mounted and safety belts fastened). This, together with the need to have the best possible feeling when driving, lead to carry on studies on ergonomics and visibility. Especially about the driving position, it is a compromise between visibility, comfort and centre of gravity height;
- **Cost:** monocoques are much more expensive than space-frame chassis but usually this is worth it when comparing the performances, especially the stiffness over weight ratio;
- **Manufacturability:** the best design is useless if it is not producible. The definition of the geometry and of the manufacturing process must take into account the timing of a FSAE championship.

3.3 Introduction to types of structures

The section above highlighted the importance of the chassis and its main characteristics. This section will briefly present the most common solutions that can be adopted as FSAE chassis.

Usually, a FSAE prototype uses a space-frame (made either with steel tubes or with composite ones), aluminum monocoque or composite monocoque. Hybrid solutions with monocoque in the front and space-frame at the rear are usually employed in internal combustion engine vehicles.

Space frames are the most common solution, in particular the one based on steel tubes. The solution with composite tubes is rarely applied. The main pros are that it is much simpler to design, to produce and to manage. Furthermore, it is easier to manage a posteriori modifications, since it is enough to cut and/or weld other components. The major cons rely in the need to add, because of the rules, anti-intrusion panels, which increase dramatically the weight. There are some non-negligible aspects that must be taken into account when dealing with a monocoque: it requires technical and theoretical expertise and the extensive use of Computer Aided Engineering (CAE) and Finite Element Analysis (FEA) tools. Materials require proper management, both in terms of storage and manufacturing (curing) and the production process itself is more complex.

The pictures below are examples of the different kind of solution mentioned above.

The first picture represents a steel tubes space-frame. The second picture shows a hybrid solution. Finally, an example of composite monocoque.

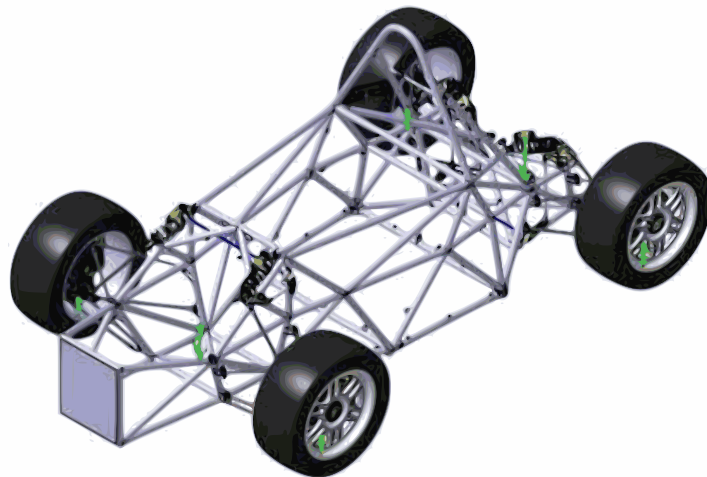


Figure 3.2: Space-frame chassis example

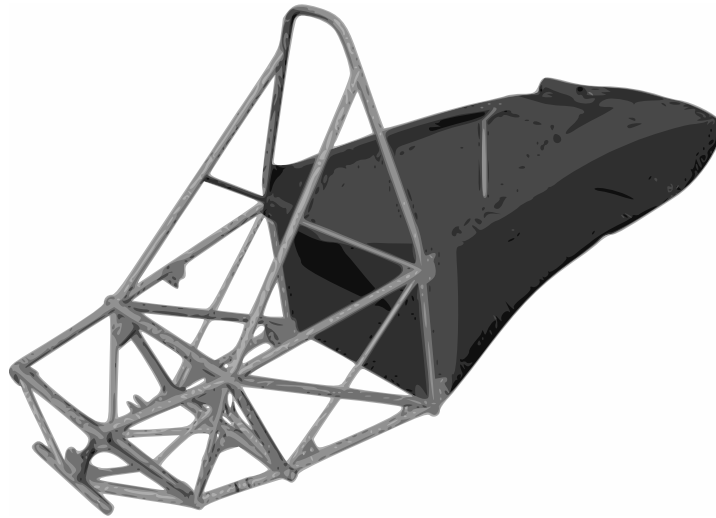


Figure 3.3: Hybrid chassis example



Figure 3.4: Monocoque chassis example

Monocoques represent the best solution about pure performances: highest stiffness with the same weight. The table below reports the mass and the torsional stiffness values of the most refined space-frame chassis of Squadra Corse, compared to the first monocoque.

In the table 3.1, K_t stands for torsional stiffness. The most important data in the table are the ones contained in the last column, namely, the stiffness (torsional)

Table 3.1: Comparison between space-frame and monocoque

Car	Chassis	Mass [kg]	Kt [Nm/rad]	Kt/mass [Nm/rad*kg]
SC12e	Steel tubes space-frame	44.5	72404	1509
SCR	CFRP monocoque	28.5	84008	2947

over weight ratio. As it possible to see, the value related to the monocoque is about 95% higher than the corresponding value of the space-frame. It must also be underlined that, being this data referred to the first ever built monocoque there was a lot margin from improvements.

3.4 Introduction to the problem of the cockpit opening

The information reported in the sections above, together with the results of the torsional stiffness test campaign developed for SCXV, reported in the following section, and the outcomes from FEM analysis, will demonstrate how the cockpit-opening region is characterized by the major loss of torsional stiffness and stress concentration.

3.4.1 SCXV torsional stiffness test

This section describes in details the torsional stiffness tests performed on the SCXV prototype. These results are reported in this paper because they have been relevant during the design phase of the SC17. In fact, as it will be mentioned in the following sections, one of the milestone of the design of the SC17 was a more detailed analysis of the cockpit opening. This because of the very high torsional stiffness target required by the vehicle dynamic department, which required to perform this kind of analysis for the first time in the history of Squadra Corse

First of all, this test was conducted in order to:

1. Determine the actual value of the torsional stiffness and to compare this value with the numerical one, resulting from FEM analysis. This was useful for assessing the correlation between the two and to determine the eventual discrepancies between the virtual simulation environment and the real product after the manufacturing process;
2. Study the torsional stiffness trend along the vehicle axis to determine if and where there were non negligible losses;
3. Study the hysteresis of the system (mainly due to friction and gap in the uni-ball joints of the suspensions).

In order to pursue these objectives a considerable number of loading-unloading cycles have been performed in several positions along the longitudinal axis of the prototype.

Torsion tests can be either symmetric or asymmetric.

Symmetric tests are characterized by two equal and opposite loads applied, for example, to the front uprights. The rear uprights are usually constrained. The vehicle is forced to rotate around its longitudinal axes. The problem of this kind of test is the need of a specific equipment capable of allowing the rotation around the central axes and the application of equal and opposite loads.

Image 3.5 represent a scheme of an equipment for symmetric torsion tests.

Asymmetric torsion tests are, on the contrary, characterized by the application of the load on just one of the front uprights. The other one is constrained, as well as the rear ones. In this case, the rotation axes does not correspond perfectly with the longitudinal axes of the car but there will a deviation deriving by this asymmetry.

Image 3.6 represent a scheme of an equipment for asymmetric torsion tests.

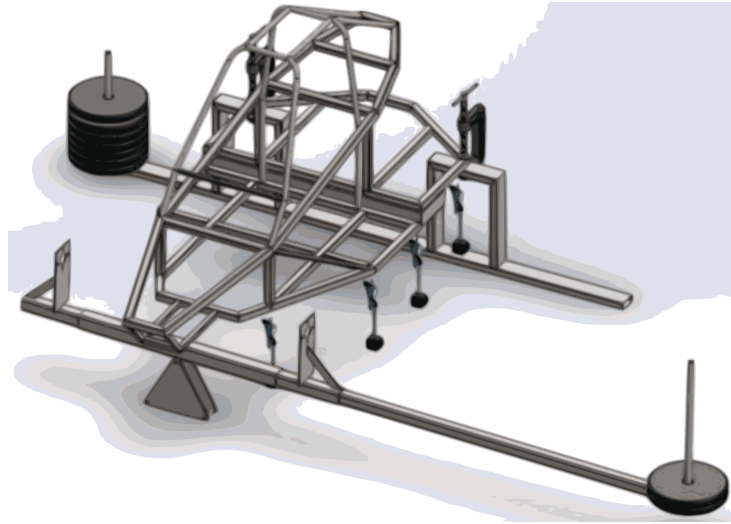


Figure 3.5: Representation of a symmetric torsion test

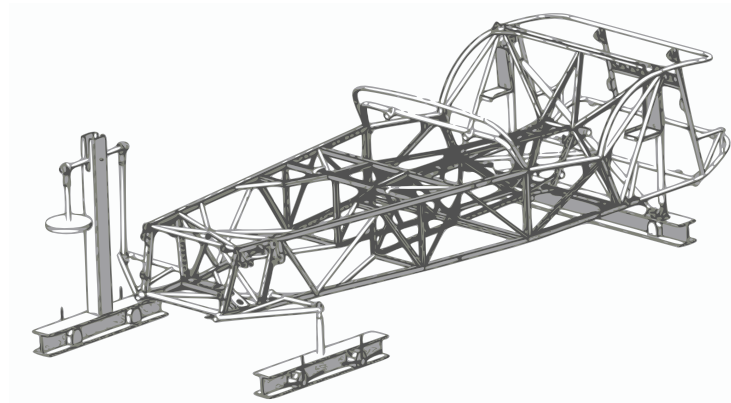


Figure 3.6: Representation of an asymmetric torsion test

Ideally, is preferable to perform a symmetric torsion test. Unfortunately, at the time this test was performed in Squadra Corse, only an equipment for asymmetric torsion test was available.

Picture 3.7 shows the overall set-up utilized. It consisted of a crane used to both raise the car, which weight was about 250 kg, and as a safety device, in case one or more of the constraints failed. As mentioned above the test was asymmetric. This

means that three over four uprights were constrained. There were two different kind of constraints:

1. Rear upright constraints: they were triangular structures provided by a bearing allowing the motion both in yz plane and in the xy one, allowing the hubs to be free to move. This to avoid an over-constrained structure, which stiffness would have been overestimated because of the constraints;
2. Front (right) upright constraint: this constraint was a rod at the top of which the same bearing system describe before was used. This rod was attached to a basis by means of hinge, again allowing a certain degree of motion to avoid to be over-constrained.



Figure 3.7: Squadra Corse asymmetric torsion test layout

The test, as mentioned before, was performed repeating several loading-unloading cycles. Each phase was divided in further sub-steps in which the load was gradually increased/decreased. The available steps were 10, 5, 2 and 1 kg. The z -coordinate displacements were measured by means of a mechanical device, attached to a magnetic base. It is possible to see this device in the pictures showing in detail the measurement locations. The section were these measures have been taken were selected in order to determine the trend of the torsional stiffness over the longitudinal axes. Pictures 3.8, 3.9, 3.10, 3.11, 3.12, 3.13 show more in details these

measurements.



Figure 3.8: Displacements measurement on front dampers



Figure 3.9: Displacements measurement on front roll hoop

The first outcomes of this test were the hysteresis curves. Pictures 3.14 shows how, after a loading-unloading cycle, the final displacement is not null. This phenomenon can be explained taking into consideration internal friction phenomena. The area bounded by the loading and unloading curves represents the work done by the friction forces and thus the energy dissipated as heat.

Another interesting result is represented by the curves describing the variation of the rotation angle over the longitudinal axis of the vehicle. Pictures 3.15 show these trends for each of the load steps. It should be noticed that the shape of the trend is similar for all the curves. They are shifted because of the increasing load (and so the torque). What is underlined by these curves is a step increase of the angular displacements for values of x around 415 mm, which correspond to the central section of the cockpit opening. Here the effects of the opening on the structure are the maximum and the structural contributions of both the rear part, with the main roll hoop, and the front one, with the front roll hoop, is no longer

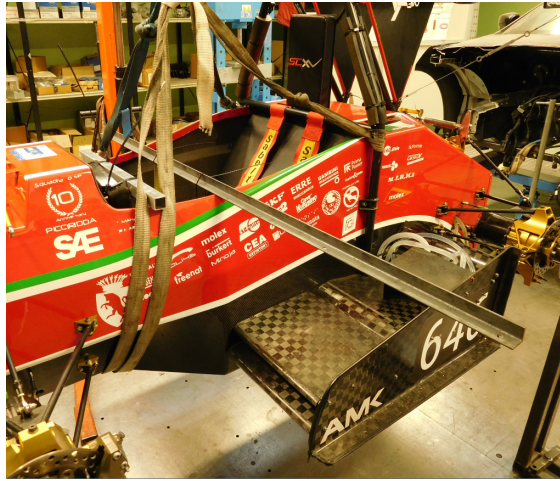


Figure 3.10: Displacements measurement in the middle of the cockpit opening



Figure 3.11: Displacements measurement at the end of the cockpit opening

available. This traduces into a local reduction of the torsional stiffness.

Another important upshot is represented by the real values of torsional stiffness (3.16). This gives an important insight of how the target in design phase traduces in the car after both design and manufacturing. These results are also important because they suggest what is the coefficient of ignorance that must be used to increase the FEM torsional stiffness target. For the SCXV the design target was 180 kNm/rad and this became about 140 kNm/rad (a difference of 25 %). It should be underlined, though, that this test was performed on a two years old chassis which was subjected to both aging and several races and tests. The discrepancy between

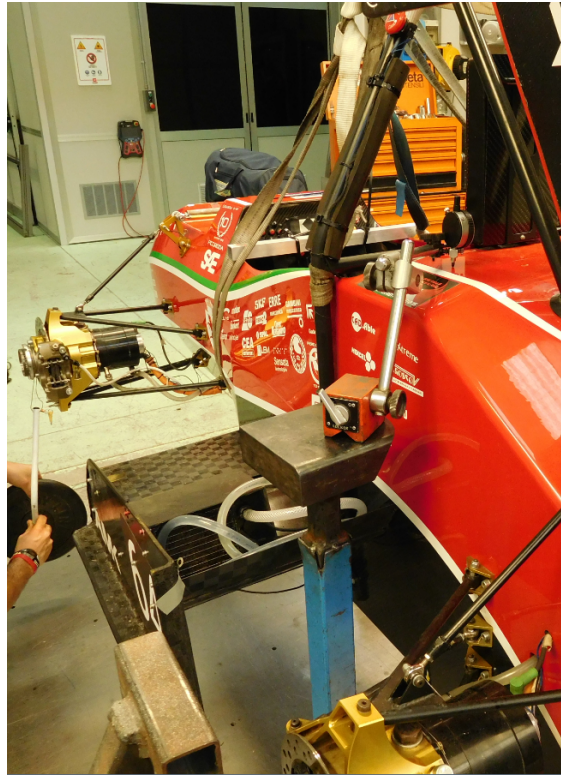


Figure 3.12: Displacements measurement after the cockpit opening



Figure 3.13: Displacements measurement at the rear-end

the theoretical value and the actual one, together with the necessity to guarantee great dynamic performances brought to set the torsional stiffness design target to values higher than the previous prototype. It must be underlined that higher torsional stiffness could bring to a heavier prototype, so the best torsional stiffness

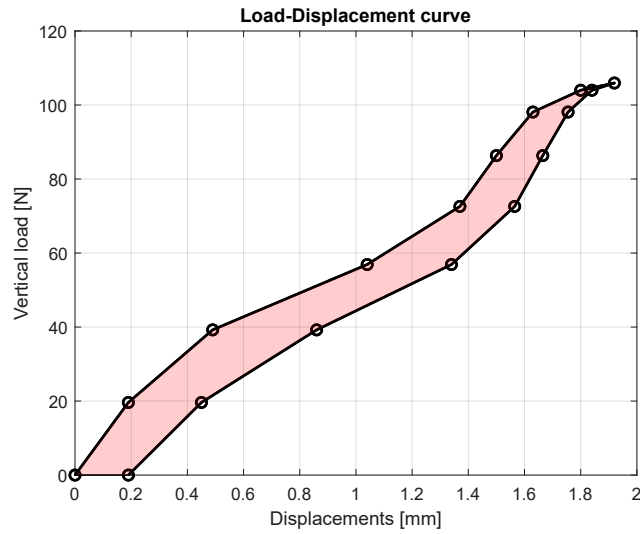


Figure 3.14: Example of a hysteresis cycle

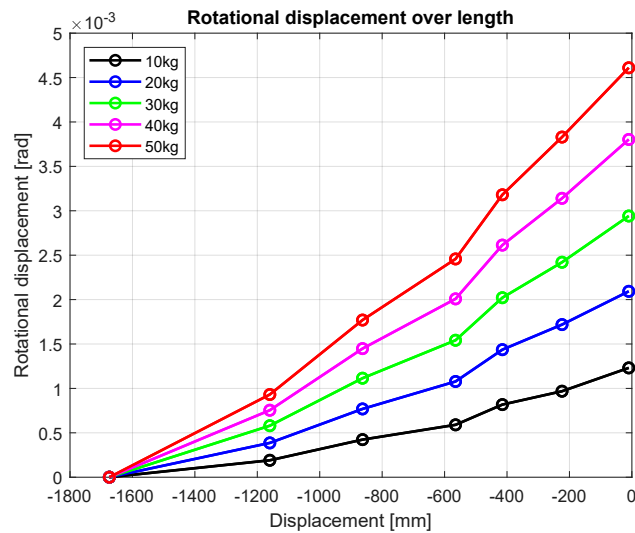


Figure 3.15: Rotational displacements over length

over weight ratio represents the parameter a designer has to bear in mind when designing a chassis.

Further post-processing and analysis bring to picture 3.17.

The angle θ represent the angle around the chassis' roll axis. As it is possible to see, θ increases dramatically, together with its derivative, in the cockpit opening region. The higher the value of theta, the lower the torsional stiffness. The cockpit opening represents the region of the curves where the values are maximum. Thus,

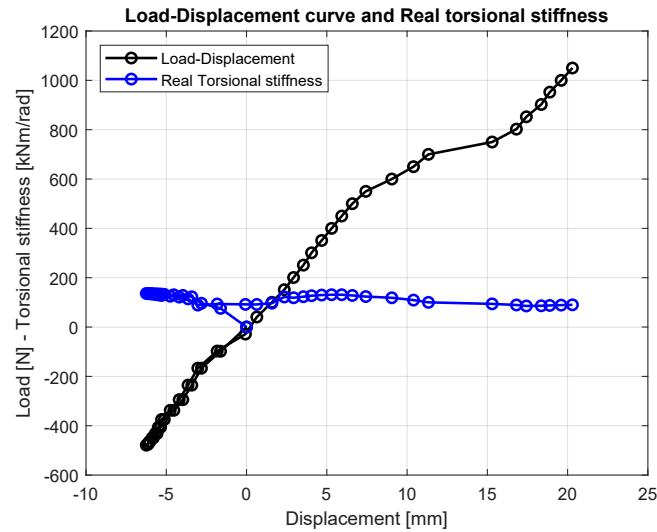


Figure 3.16: Real torsional stiffness values for SCXV and load-displacements curve

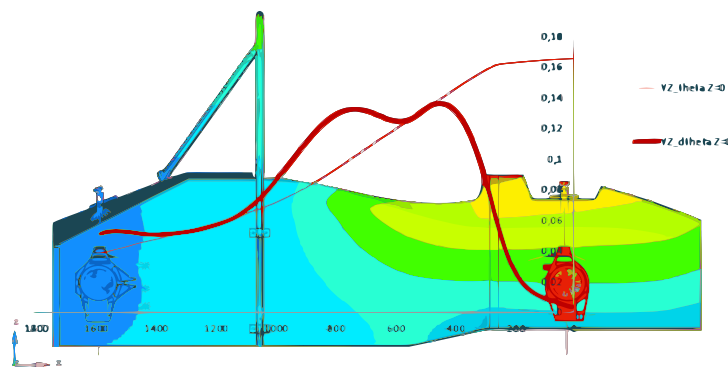


Figure 3.17: Variation of torsional stiffness over length

it is the area where the torsional stiffness suffers the greatest loss.

In addition to this, because of the geometrical variations and to the stress concentration factors induced by the opening and its surrounding, the cockpit opening is where stresses concentrates the most (when dealing with a torsional load-case).

The picture 3.18 shows the stress concentration in the cockpit-opening when dealing with a torsional load-case.

3.4.2 Further structural and non-structural considerations

The study performed by [9], allows to introduce some further considerations concerning the influence of the type of structure on its behaviour.

For closed box structures, very high torsional stiffness can be achieved even with

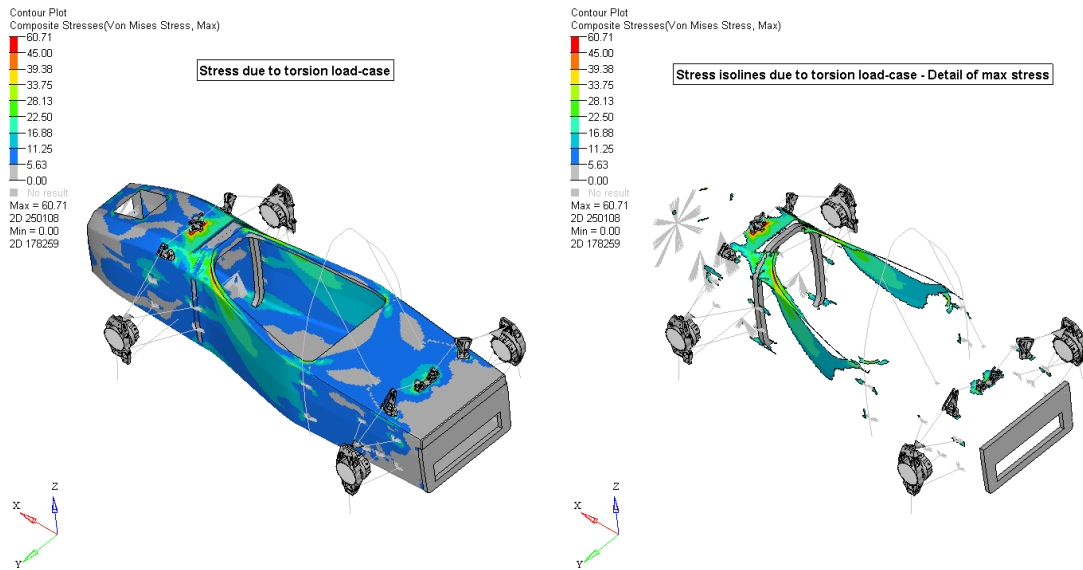


Figure 3.18: Stresses due to torsion load-case

reduced wall thickness, provided that the cross sections remain more or less with same shape along the length. In FSAE prototypes, the cockpit opening minimum dimensions are stated by the rules, which because of safety oblige the usage of an opening template. In FSAE vehicles, the dimension of this template is remarkable with respect to the dimension of the chassis. Thus, FSAE monocoques must be considered as open box structures. If closed boxed structures are subjected to shear loads only, open ones are subjected to bending and tend to deform into a "S-shaped" structure (i.e. the sides of the opening). Figure 3.19 illustrates how the closed edges are subjected to shear stresses only, while the open ones experience bending ones.

In these regards, dealing with fibres-based composite, to improve the strength of the panels fibres must be placed under $\pm 45^\circ$ and $0^\circ - 90^\circ$ for shear and bending respectively. This is shown in picture 3.20.

To further enhance the structural behaviour, bulkheads could be introduced to constraint the shape of the cross-sections, increasing the resistance to torsional deflection. It should be underlined, though, that load is not just pure torsion but there are in-plane components that must also be taken into account.

The open cross-section of the cockpit opening represents the weakest point of the structure and in order to obtain satisfactory results both concerning stiffness and strength, this region must be carefully designed. Being the bending stiffness of these panels a function of EI , the two most immediate solutions are improving the material or increasing I . Dealing with materials with higher performances is not always feasible, especially because of costs. Furthermore, the need to avoid open ply-ends led, in our case, to spend more time investigating a better geometry.

Picture 3.21 illustrates some possible solutions. The solution on the left has a

smaller inertia and open ply ends. The central one has a higher inertial contribution but still open ply-end. Finally, the third solution, which has been chosen for SC17, provide both better inertia and lamination.

Another relevant aspect is the impact on aerodynamic. This part of the mono-coque is characterized by the biggest cross-sectional area, and the more the structure is large the greater is its impact on aerodynamic drag.

What stated so far motivates the need of a detailed study of this region of the chassis, so that it will be able to comply with all its structural, ergonomics and safety targets, without compromising dynamic and aerodynamic performances.

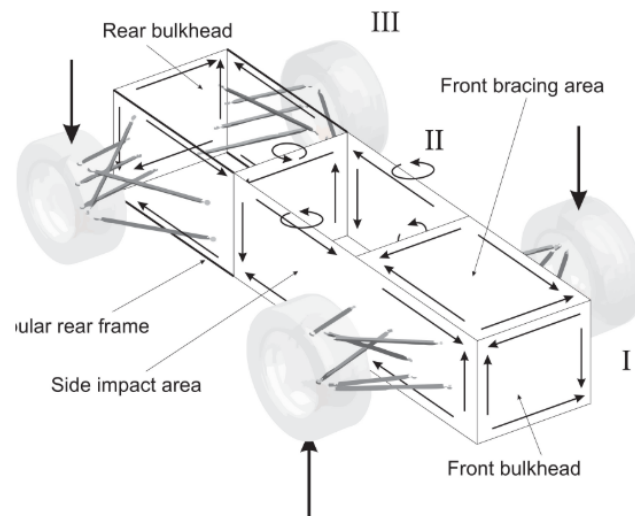


Figure 3.19: Loads on a simplified chassis in three parts: I, a closed profile, II, an open profile and III, a tubular space frame

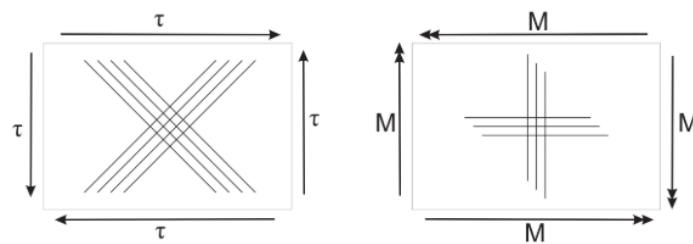


Figure 3.20: Fibres direction for panel subjected to: shear (left) and bending (right)

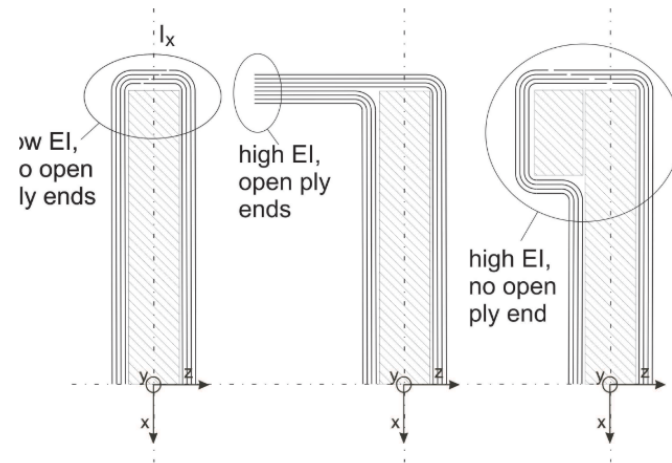


Figure 3.21: Examples of cockpit opening solution: low inertia and no ply edges (left), increased edge bending stiffness (centre) and a combination of these measure (right)

3.5 Cockpit opening FSAE rules

This section briefly contains the articles of the FSAE rules book [15] which deal with the chassis cockpit opening and the other components which can be relevant (i.e. firewall). The next list shows the set of rules describing the cockpit opening template.

- T4.1.1 In order to ensure that the opening giving access to the cockpit is of adequate size, the template shown in Figure 8 will be inserted into the cockpit opening;
- T4.1.2 The template will be held horizontally, parallel to the ground, and inserted vertically from a height above any Primary Structure or bodywork that is between the Front Hoop and the Main Hoop until it has passed below the top bar of the Side Impact Structure (or until it is 350 mm (13.8 inches) above the ground for monocoque cars). Fore and aft translation of the template is permitted during insertion;
- T4.1.3 During this test, the steering wheel, steering column, seat and all padding may be removed. The shifter or shift mechanism may not be removed unless it is integral with the steering wheel and is removed with the steering wheel. The firewall may not be moved or removed;
- As a practical matter, for the checks, the steering column will not be removed. The technical inspectors will maneuver the template around the steering column shaft, but not the steering column supports;

The following list contains the list of articles describing the firewall.

- T4.5.1 A firewall must separate the driver compartment from all components of the fuel supply, the engine oil, the liquid cooling systems and any high voltage system (PART EV - EV1.1). It must protect the neck of the tallest driver. It must extend sufficiently far upwards and/or rearwards such that any point less than 100 mm (4 ins.) above the bottom of the helmet of the tallest driver must not be in direct line of sight with any part of the fuel system, the cooling system or the engine oil system;
- T4.5.2 The firewall must be a non-permeable surface made from a rigid, fire resistant material;
- T4.5.3 Any firewall must seal completely against the passage of fluids, especially at the sides and the floor of the cockpit, i.e. there must be no holes in a firewall through which seat belts pass;

- T4.5.4 Pass-through for wiring, cables, etc. are allowable if grommets are used to seal the pass-through. Also, multiple panels may be used to form the firewall but must be sealed at the joints;

In addition, a firewall must separate the driver compartment from all tractive system components, including any High Voltage (HV) wiring.

The tractive system firewall must be composed of two layers:

1. One layer, facing the tractive system side, must be made of aluminum with a thickness between 0.5 and 0.7 mm. This part of the tractive system firewall must be grounded according to FSAE Rule PART EV - EV4.3;
2. The second layer, facing the driver, must be made of an electrically insulating material. The material used for the second layer must meet UL94-V0, FAR25 or equivalent. The second layer must not be made of CFRP;
3. The thickness of second layer must be sufficient to prevent penetrating this layer with a 4 mm wide screwdriver and 250N of force. The firewall must be rigidly mounted.

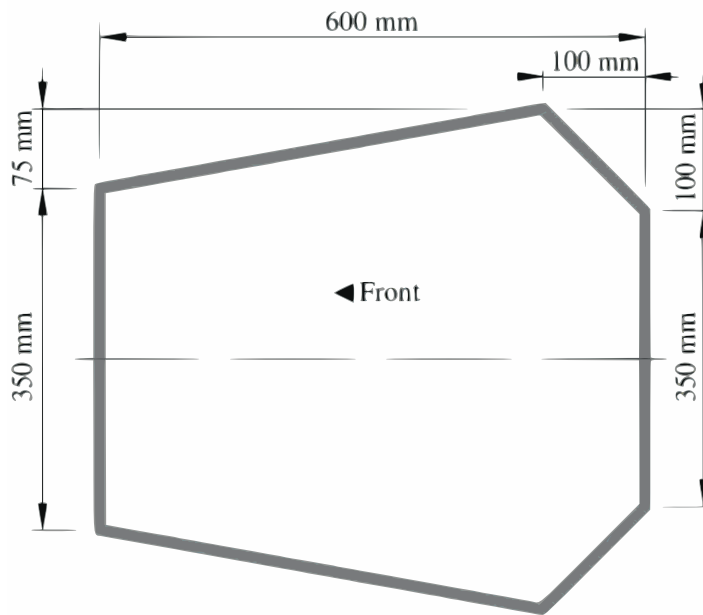


Figure 3.22: Cockpit opening FSAE template

Chapter 4

Propaedeutic concepts

"I was crossing the English
Channel with a carbon-fiber wing
on my back"

Felix Baumgartner

This thesis is based on two main topics, namely, composite materials and Finite Element Analysis (FEA). These subjects are usually not tackled, or not in deep, during automotive engineering courses.

These are the reasons behind this chapter. The author intends to provide all the necessary tools the reader will have to use to understand the process, the decisions and the results of the next chapters.

First composite materials will be introduced ¹, followed by an in-details study of carbon-based composites.

The next section will introduce the Finite Element Method (FEM from now on). Since there are already many books which describes this numerical method in detail ², this section will cover only the most important steps.

¹The information contained in this section are mostly taken from [1]

²Relevant references about this topic are [7], [10], [12], [14], [19], [20]

4.1 Introduction to composites materials

The most common and generic definition of composite materials specifies that they are materials formed by the combination of two or more distinct materials, to form a new material which is characterized by enhanced property with respect to its constitutive ones. These materials, called constituents, are separated by a well defines interface. Composites could seems to be new and exotic, and this is true, to a certain extent. It must be pointed out, though, that nature invented composites billions of years ago. Wood is probably one of the most common, together with bones.

The first man-made composites date back to straw-reinforced clay, used for bricks. Modern composites use metal, ceramics or polymer binders, reinforced with a variety of fibers and particles. When more than one reinforcement is used, composites are called hybrid. An example of hybrid composite is reinforced concrete, where steel rods further reinforced the composite made by stones and concrete.

Being such complicated materials, composites can be classified accordingly to different parameters. They are:

- Reinforcements
 - Continuous long fibres (Unidirectional, bidirectional and random orientation)
 - Discontinuous fibres (Random or preferential orientation);
- Laminate configuration
 - Unidirectional laminate (Single ply or multiple plies, all with the same orientation);
 - Laminate (Not all the plies have the same direction);
 - Bulk (Laminae cannot be identified);
- Hybrid structure
 - Different material in various laminae (Es. sandwich structures);
 - Different reinforcements in a lamina.

Composites can be designed depending on the needs and this guides to different choices of both matrix and reinforcements. Reinforcements in the form of fibers are usually preferred because most materials are stronger in fiber form than in bulk one. The reasons behind are mainly related to the number of defects, which is much lower in fibers compared to those in bulk form.

Fibers are characterized by remarkable values of strength over weight ratio as well as stiffness over weight one. These values are higher than most other materials,

such as metals. Unfortunately, fibers cannot be used alone because they are not able to withstand neither compression loads, nor shear loads. This justifies the presence of a matrix that performs different tasks: it holds the reinforcements together, provides load transfer between fibers and between composites and external loads or supports, protects them from the external environment, ensuring typical composites corrosion resistance.

Fibers, instead, provide most of the stiffness and strength. The mechanical properties of the matrix are negligible compared to the reinforcements' ones. This means that the mechanical properties of the composite material are much lower than that of the fibers, but, still, composites are stiffer and stronger than most conventional material, when viewed on a per unit weight basis. The reduction from fiber to composite properties is proportional to the amount of matrix used (mixture rule).

The main advantage of composites materials is their strength/weight ratio. This motivates their diffusion in all the fields of technology and engineering in which mass represents a critical factor, like aerospace and motor-sport. Furthermore, they show high fatigue resistance compared to metals. In addition to this, since the matrix can be shaped into complex forms, a single composites object can replace many others, assembled with different techniques. This parts-reduction translates into a reduction of costs associated with assembly, inventory, and maintenance, which compensate for higher material costs.

It must be underlined that the great mechanical properties of the fibers mentioned above are limited to tensile loads only. Fibers, in fact, are not able to withstand both compression and forces perpendicular to their direction. For this reason, plies need to be lay-up, to constitute laminates, with plies oriented in several directions, as shown in picture 4.1.

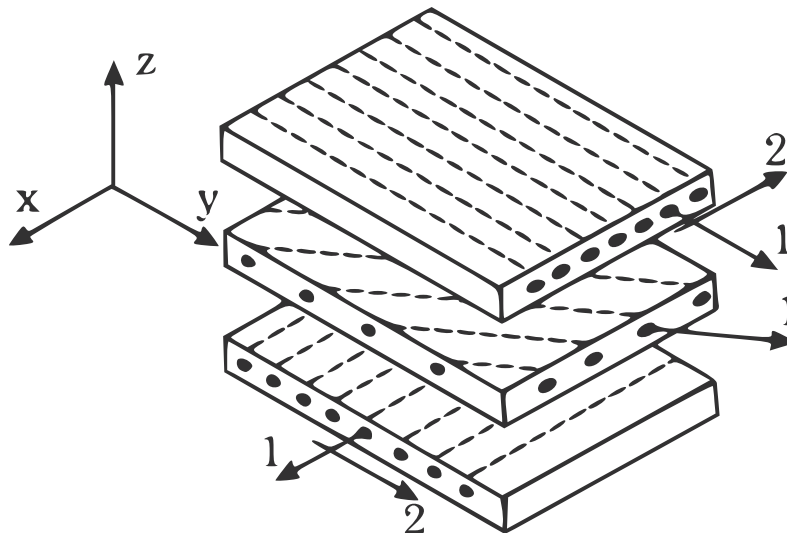


Figure 4.1: Laminate example

Although a laminate like this can withstand loads from various orientations, its properties in one specific direction are lower when compared to a unidirectional laminate.

Unidirectional plies are not the only ones available. Woven composites are characterized by fibers woven in two directions, warp and weft. Again, they can withstand loads from multiple directions but their properties are lower than unidirectional in one specific direction. It is also possible to stack plies to obtain the so-called "quasi-iso" configuration, in which the properties are similar in all directions. When high bending loads are acting on composites, it is common to use a hybrid panel, called a sandwich plate, in which laminates are separated by a core (foam or metal honeycomb). The core separates the two faces so that the second moment of area, I , provided by the faces is large, resulting in high bending stiffness.

Since composites are a mix of reinforcements and matrix, the next sections will deal with reinforcement and binder in detail.

The design of composite components requires simultaneous structural and material design. This last allows tuning the properties of the material zone by zone, depending on the need. This can be performed by the proper management of constituents and lay-up. The following sections will analyze in detail both the main reinforcements and the binder.

4.1.1 Reinforcements

Fibers are a particular form of a certain material, treated properly so to obtain this shape and properties. They present better mechanical properties compared to the original material in bulk form. This because both the alignment of the molecules along the fibers and the reduced amount and size of defects. Fibers do not have a single value of strength but rather individual fiber strength that follows a Weibull distribution. They can be used either as continuous or discontinuous reinforcements. In the first case, the length of the fibers is the same as the ply (at least in one direction). On the contrary, in the second one, the fibers are short, chopped or as particles. The mechanical properties of plies are influenced by the reinforcements together with the matrix. Unidirectional composites exhibit maximum properties along with the fiber and minimum properties perpendicular to them. Matrix dictates creep properties. Composites reinforced with short reinforcements may experience noticeable creep even at room temperature. This is one of the main reasons why continuous fibers reinforcements are employed in structural applications.

As reported by [1], a wide variety of fibers can be used as reinforcements in structural applications. Fibers can be classified by their length: short, long; according to their strength and/or stiffness: low (LM), medium (MM), high (HM), and ultrahigh modulus (UHM); or according to their chemical composition: organic and inorganic.

An aspect of paramount importance is the fiber-matrix compatibility. This is promoted by an agent, called "sizing", which covers the fibers and serves three purposes:

1. Lubricate and prevent static friction between fibers and tooling;
2. Group fibers in bundles;
3. Promote fiber-matrix bonding. This interaction is responsible for the intralaminar shear strength.

The intralaminar shear phenomenon can be either matrix-dominated or affected by the fiber-matrix bond strength. The first case takes place when shear stresses are acting on planes parallel to the direction of the fibers and thus these last are not resisting shear. The second case appears when shear stresses appear along the fibers' direction. Figure 4.2 shows the aforementioned shear stresses. As mentioned before, fibers can be classified as continuous, discontinuous and particles. Continuous fibers allow achieving maximum stiffness and strength while reducing matrix creep. The fibers oriented in the load direction carry most of the load. They are the most costly. Discontinuous reinforcements are a cheaper solution in which matrix transfer the load between fibers. The load transfer mechanism is different between these two solutions. In discontinuous fibers, the fiber does not carry the load along its entire length but the fiber-matrix interface plays a crucial role. The fiber is subjected to tensile stress only at its center, while at its ends shear stresses between fiber and matrix are dominant. What described above is not only what happens with discontinuous fibers, but it is also what takes place when a continuous fiber fails. This phenomenon is illustrated in figure 4.3.

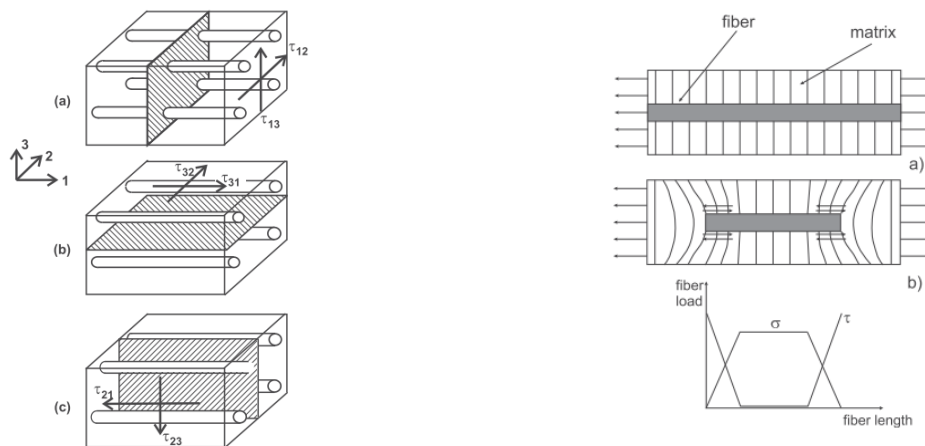


Figure 4.2: Intralaminar shear stresses

Figure 4.3: Load transfer process in continuous (a) and discontinuous fiber (b)

Reinforcements are usually in the form of unidirectional plies or fabrics. These last can be either non-woven or woven. As pointed out in [1], a non-woven fabric is usually called a mat, which is made by randomly oriented chopped fibers such as chopped strand mat, randomly oriented short fibers, or swirled tows or rovings. On the other hand, woven fabrics are obtained by interlacing yarns in a weaving machine. Yarns are usually arranged along with two perpendicular directions, called warp and weft. If the same yarn is used in both directions, it is possible to obtain balanced properties. The most common outcomes of this bi-axial weaving process are a wide variety of weaving patterns, such as plain, twill and satin fabrics. Example of these patterns are illustrated in picture 4.4.

Unidirectional continuous fibers offer better mechanical performances compared to fabric reinforcements. This is due to the deformation of the woven fibers. Figure 4.5 illustrates a 3D detail of woven fibers. In addition, image 4.6 illustrates the photomicrograph of a fabric-reinforced composite lamina.

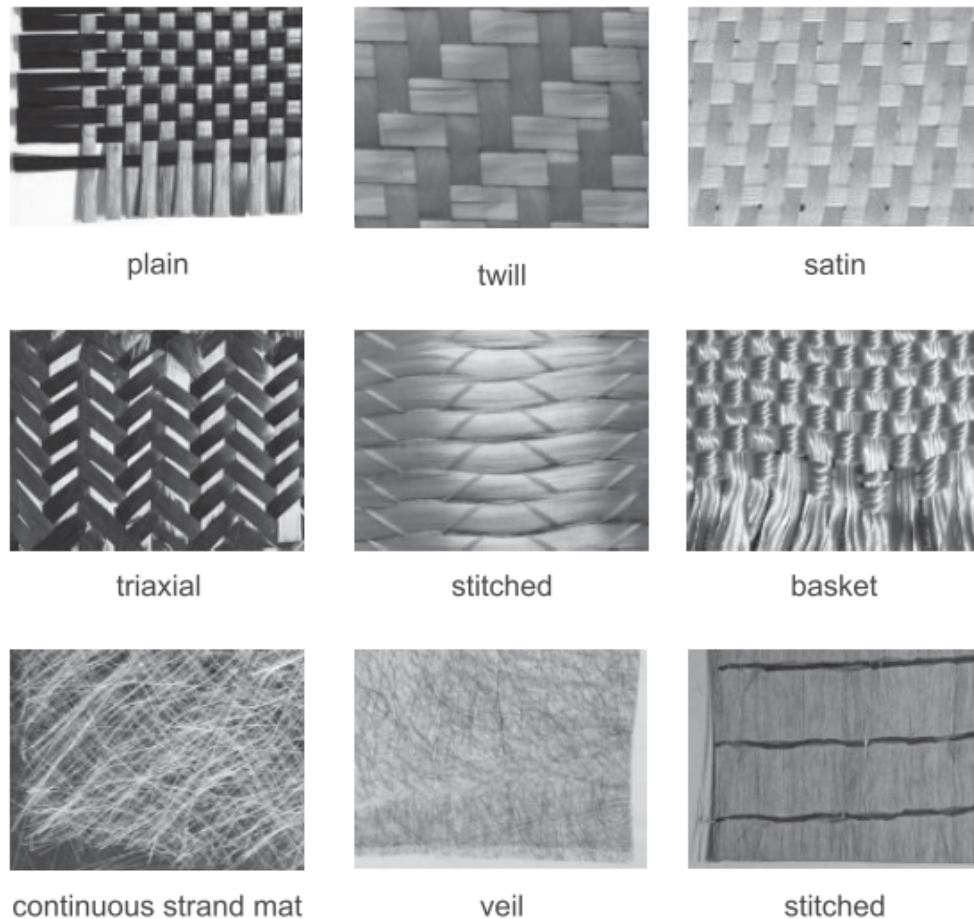


Figure 4.4: Example of weaving patterns

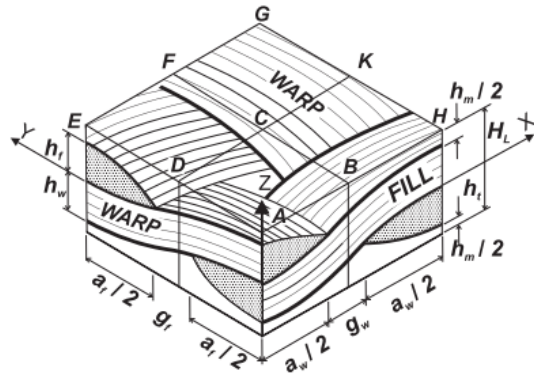


Figure 4.5: 3D detail of a woven fabric

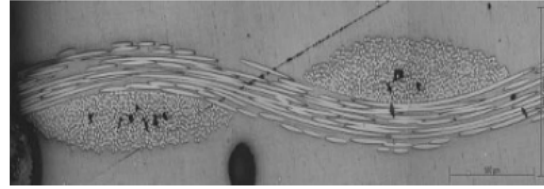


Figure 4.6: Photomicrograph of a fabric-reinforced composite lamina

Carbon fibers

Carbon fibers are obtained from precursors, typically polymeric, which are subjected to oxidation and pyrolysis. The most common precursors are polyacrylonitrile (PAN), cellulose (rayon) or pitch, obtained from petroleum distillation. Depending on the precursor, fibers are distinguished in PAN-based, rayon-based and pitch-based.

As underlined by [1], stiffness and strength are controlled by the thermal treatment because this determines the carbon content and the orientation of the strongest carbon links along the direction of the fibers' axis, and so in turn, stiffness and strength. The manufacturing process for PAN-based and rayon-based is structured in more steps, depending on the final aim. Fibers are maintained under tension and subjected to a first heat-treatment, followed by stabilization and partial oxidation. In the next step, they are pyrolyzed at high temperatures (1000°C). This phase is immediately followed by heating up to over $1300\text{-}1500^{\circ}\text{C}$ in an inert environment, for material canonization. For high and ultra-high-modulus fibers, the temperature can reach almost 3000°C , where graphitization is almost complete.

Their stiffness enhances fatigue behavior. The higher the stiffness of the fiber, the lower the loads and the strains on the matrix for a given load. Furthermore, carbon fibers are good electrical conductors.

Cost is the main limiting factor when dealing with carbon fibers. They are employed only in the fields where the mass is a serious penalty in terms of investments. They are also brittle, which limits the toughness.

The latest outcomes concerning carbon-based fibers are carbon nanotubes. As suggested by the name, they are tubes with a diameter in the range of 1 nm , or a few μm . Their properties overcome those of traditional carbon fibers because of the more precise orientation of the strongest links and the near-zero presence of defects. They are employed as nano-composites since they are filled with matrix

and then used as reinforcements in a binder.

4.1.2 Matrix

The most important tasks of the matrix are: providing stress transfer among fibers, protect them from chemical attack and abrasion and carrying loads such as transverse stress, intralaminar shear stress and bearing stress. The matrix determines the allowable service condition (temperature range, chemical resistance, and abrasion), the conductivity (thermal and electrical), the flammability resistance and, finally, aesthetics..

The most common matrix materials are:

- Polymers;
- Metals;
- Ceramics.

Polymeric matrix systems are the most common thanks to their capability to form complex geometries with relatively low tooling costs and low manufacturing costs. Employed polymers can be either thermoplastic or thermoset. Being thermoset used in Advanced Composite Materials (ACM), they will be briefly described in the following. Thermoset matrix systems provide their mechanical properties thanks to a chemical reaction that transforms the resin into a cross-linked polymer matrix. The process is irreversible. The change is so dramatic that usually the polymer is called resin before being cured and matrix right after. Depending on the choice of initiator, curing systems, catalyst and the reactivity of the resin, curing cycles can last from minutes to several hours and they can take place at room temperature or high ones, inside an autoclave. The most common thermoset resins are:

- Polyester resins;
- Vinyl ester resins;
- Epoxy resins;
- Phenolic resins;

Epoxy resins are quite common. Their main advantages are a wide range of mechanical properties, low shrinkage, which, in turns means low residual stresses, and, chemical resistance.

4.2 Introduction to the Finite Element Method: most important steps

As mentioned at the beginning of this chapter, there is already a great extent of books that explain in detail the Finite Element Method. For this reason, this section will report the most important steps only. This section takes inspiration from an analogous section of [11].

The scientific world describes phenomena through mathematical terms whose relationships are defined by equations that describe the phenomenon object of study. In most practical applications these equations are complex and it is not possible to find analytical solutions in closed form. The Finite Element Method (FEM from now on) has been developed to provide a numerical method capable of computing an approximate solution to these problems. FEM is widely employed in structural mechanics since the problems involved in this field can be solved analytically. Apart from this field, FEM is used also in other fields, such as fluid dynamics, lubrication, heat transfer, and electromagnetism and in general, can be used to approximate elastic, plastic, viscoplastic, static, dynamic, stationary, dynamic or impulsive problems.

4.2.1 Procedure

Briefly, the FEM procedure can be described as a discretization process that takes place on the studied field and it has aimed at dividing it into small domains whose behavior is known because defined a priori. Each of these domains is called "element" and the terms finite elements come from the fact that a continuous problem described in general by partial differential equations is transformed into a discrete number of domains with a precise behavior. Each element is defined by nodes which represent also the connections between elements. The final aim is to define, per each element, the stiffness relationship between the vector of applied forces F and the vector of nodal displacements f , as reported in Eq: 4.1. Once knowing the nodal displacements it will be possible to determine the displacement, strain and stress field in the entire element.

$$\{F\} = [K] \{f\} \quad (4.1)$$

The following steps will describe how to do so.

1. First of all, per each node of an element, the displacements that are relevant for a certain problem must be determined. Then, two vectors are associated with each node: a vector containing the nodal displacements of that node f_i and another vector containing the forces acting on that node, F_i . Following a predefined order, these vectors are collected in other vectors that describe

the nodal displacements and the nodal forces for an element. They are called f and F respectively.

$$\{f\} = \begin{Bmatrix} f_1 \\ f_2 \\ \dots \\ f_n \end{Bmatrix} \quad \{F\} = \begin{Bmatrix} F_1 \\ F_2 \\ \dots \\ F_n \end{Bmatrix} \quad (4.2)$$

2. The second step consists of approximating the displacement field δ , which describes the displacement of each point of an element, with a function, that is usually either a polynomial or a trigonometric function. These functions must respect the completeness and compatibility requirements, to ensure the convergence of the result when the number of degrees of freedom increases. These approximating functions are grouped into a matrix called Φ . These functions are multiplied by some coefficients, unknown at this point, called α . Eq. 4.3 describes the approximated displacement fields, where X_k indicates the coordinate of the considered point.

$$\{\delta(X_k)\} = [\Phi(X_k)] \{\alpha\} \quad (4.3)$$

3. These functions approximating the displacement field must be equal to the nodal displacement when computed at the nodes. This allows determining the unknown coefficients α_i .

$$\{\alpha\} = [A]^{-1} \{f\} \quad (4.4)$$

Where matrix A groups the values of the function Φ_{ij} computed at the nodes. It is then possible to write:

$$\{\delta(X_k)\} = [\Phi(X_k)] [A]^{-1} \{f\} = [N(X_k)] \{f\} \quad (4.5)$$

Matrix N contains the so-called shape functions which represent an interpolation of the nodal displacements and not an approximation of the displacement field as the matrix Φ ;

4. The next step consists of defining the strain field which is strictly connected to the nodal displacements one. In general, the strain field is linked to the displacement one through differentiation relationships.

$$\{\delta(X_k)\} \xrightarrow{\text{Differentiate}} \{\epsilon(X_k)\} \quad (4.6)$$

Thus:

$$\{\epsilon(X_k)\} = \text{Diff} [N(X_k)] \{f\} = [B(X_k)] \{f\} \quad (4.7)$$

Differentiating the shape functions, strains can be computed in whatever point in the element starting from the nodal displacements;

5. As well as for the strain field, it is possible to define the stress field, that relates to the first one through the material stiffness matrix. This matrix contains information about the material and eventually the geometrical characteristic of the section of the element.

$$\{\sigma(X_k)\} = [D] \{\epsilon(X_k)\} \quad (4.8)$$

6. It was stated at the beginning that the main objective was to determine the stiffness relationship of an element. What is missing at this point is the definition of the stiffness matrix of an element. To do so, the principle of virtual work will be used. This principle states that when a structure or an element is subjected to a whatever displacement field, called virtual because it is assumed, to be in equilibrium, the total work performed by the external forces that would cause the assumed displacement field is equal to the total virtual work performed by the internal stresses induced by the virtual displacement field. The vector of virtual displacements will be defined as:

$$\{f^*\} \quad (4.9)$$

The virtual work done by the external forces is:

$$L_{est}^* = \{f^*\} \{F\} \quad (4.10)$$

The virtual strain field is:

$$\{\epsilon^*\} = [B] \{f^*\} \quad (4.11)$$

The field of the stresses actually acting on an element is:

$$\{\sigma\} = [D] [B] \{f\} \quad (4.12)$$

The internal virtual work is thus:

$$dL_{int}^* = \{\epsilon^*\} \{\sigma\} dVol \quad (4.13)$$

$$L_{int}^* = \int_{Vol} \{f^*\}^T [B]^T [D] [B] dVol \quad (4.14)$$

From the equality of the works:

$$\{F\} = \int_{Vol} [B]^T [D] [B] dVol \{f\} \quad (4.15)$$

Comparing Eq: 4.1 with 4.15 allows to specify the expression of the stiffness matrix of an element. This terms are approximated because involve in their definition the shape functions.

$$\{K\} = \int_{Vol} [B]^T [D] [B] dVol \quad (4.16)$$

7. The final step consists in writing the equations linking the stresses to the nodal displacements. Recalling Eqs: 4.7 and 4.8,

$$\{\epsilon(X_k)\} = \text{Diff} [N(X_k)] \{f\} = [B(X_k)] \{f\}$$

$$\{\sigma(X_k)\} = [D] \{\epsilon(X_k)\}$$

It is possible to write:

$$\{\sigma(X_k)\} = [D] [B(X_k)] \{f\} = [H] \{f\} \quad (4.17)$$

4.3 Introduction to the Classical Laminated Plate theory

The Classical Laminated Plate (CLT) theory ³is aimed at predicting the behavior of anisotropic multi-directional laminates, which overall behavior depends on the properties and stacking sequence of the individual layers. When one dimension of a structure is much smaller than the others, for both metals and composites hold plain stress and plane strain. A significant difference relies on the fact that metals are characterized by a generalized three-dimensional isotropic elasticity, while composites are characterized by a generalized three-dimensional anisotropic elasticity, which complicates things quite a lot.

Metals and composites are different both about elastic response and failure modes. These differences will be briefly described in the following:

- Elastic response: isotropic materials can be described by two elastic constants only, any two of E , G , ν , since it holds:

$$G = \frac{E}{2(1 + \nu)} \quad (4.18)$$

Anisotropic materials could need up to twenty-one independent constants. This because in general there are six stresses and six strains and the elastic relationship is:

$$\begin{Bmatrix} \sigma_x \\ \sigma_y \\ \sigma_z \\ \tau_{yz} \\ \tau_{xz} \\ \tau_{xy} \end{Bmatrix} = \begin{bmatrix} E_{11} & E_{12} & E_{13} & E_{14} & E_{15} & E_{16} \\ & E_{22} & E_{23} & E_{24} & E_{25} & E_{26} \\ & & E_{33} & E_{34} & E_{35} & E_{36} \\ & & & E_{44} & E_{45} & E_{46} \\ & \text{Sym.} & & & E_{55} & E_{56} \\ & & & & & E_{66} \end{bmatrix} \begin{Bmatrix} \epsilon_x \\ \epsilon_y \\ \epsilon_z \\ \gamma_{yz} \\ \gamma_{xz} \\ \gamma_{xy} \end{Bmatrix} \quad (4.19)$$

Pure anisotropic materials are extremely challenging to characterize.

There exist a special class of anisotropic materials called orthotropic material in which there are two perpendicular planes of symmetry. Layer-based composites belong to this group and here four elastic constants are enough: E_x , E_y , G_{xy} and ν_{xy} . X and y are directions perpendicular to each other. Actually perfect symmetry does not exist and also this depend on the scale taken into account. Layer-based composites belong to this class of materials;

- Failure: metals are characterized by yielding and the behavior to the final rupture is quite well-known and predictable because it is related to one phenomenon only, namely, plastic deformation.

³The content of this section derives from the lecture notes of Dr. C. Kassapoglou [8]

Regarding composites, because of their heterogeneous nature, they exhibit multiple failure mechanisms that interact with each other. The most common are:

- Matrix yielding;
- Matrix cracking;
- Delamination (separation of layers in a laminate);
- Fiber cracking;
- Failure of fiber/matrix interface

It is not straightforward to understand which one happens first and how they interact. Another crucial aspect of composites' failure is the fact that it is possible to identify different failure modes depending on the analyzed scale. For example, in microscale, it is possible to recognize both defects at fibers and matrix level. At the level of some plies, it is possible to see cracks in the matrix, or if cracks do not have enough energy to break fibers, they will move along these last and delamination cracks will grow. Cracks follow the paths with the lowest energy.

When dealing with a sandwich panel, failure can interest both plies and core.

Let's now talk about the modeling of composites. They can be modeled in several different ways, depending on the chosen scale of interest. Two common approaches are:

1. Micro-mechanics;
2. Meso-mechanics;

The micro-mechanics approach is to characterize independently fibers and matrix and then predict the behavior in terms of stiffness and strength of a ply. Through this strategy, it is possible to estimate quite successfully the stiffness but not the strength. This due to the complex phenomena arising at the fiber-matrix interface. The meso-mechanics approach, instead, start with the idea of characterizing a ply to then derive the behavior of a laminate by summing up the plies contribution.

As mentioned before, layer-based composites are orthotropic. The three-dimension generalized elastic equation for an orthotropic composite is:

$$\begin{Bmatrix} \sigma_x \\ \sigma_y \\ \sigma_z \\ \tau_{yz} \\ \tau_{xz} \\ \tau_{xy} \end{Bmatrix} = \begin{bmatrix} E_{11} & E_{12} & E_{13} & 0 & 0 & 0 \\ E_{12} & E_{22} & E_{23} & 0 & 0 & 0 \\ E_{13} & E_{23} & E_{33} & 0 & 0 & 0 \\ 0 & 0 & 0 & E_{44} & 0 & 0 \\ 0 & 0 & 0 & 0 & E_{55} & 0 \\ 0 & 0 & 0 & 0 & 0 & E_{66} \end{bmatrix} \begin{Bmatrix} \epsilon_x \\ \epsilon_y \\ \epsilon_z \\ \gamma_{yz} \\ \gamma_{xz} \\ \gamma_{xy} \end{Bmatrix} \quad (4.20)$$

If the laminate is thin enough, it is possible to introduce one of the most important assumptions behind this theory, namely, the stresses in the thickness are null $\sigma_z \simeq \tau_{yz} \simeq \tau_{xz} \simeq 0$, as well as their variation through the thickness itself. Thus,

$$\begin{cases} \sigma_x = E_{11}\epsilon_x + E_{12}\epsilon_y + E_{13}\epsilon_z \\ \sigma_y = E_{12}\epsilon_x + E_{22}\epsilon_y + E_{23}\epsilon_z \\ \sigma_z = 0 = E_{13}\epsilon_x + E_{22}\epsilon_y + E_{33}\epsilon_z \\ 0 = E_{44}\gamma_{yz} \\ 0 = E_{55}\gamma_{xz} \\ \tau_{xy} = E_{66}\gamma_{xy} \end{cases} \quad (4.21)$$

From the third equation it is possible to express ϵ_z as function of ϵ_x and ϵ_y . Precisely:

$$\epsilon_z = -\frac{E_{13}}{E_{33}}\epsilon_x - \frac{E_{23}}{E_{33}}\epsilon_y \quad (4.22)$$

Substituting Eq. 4.22 in the first two equations of 4.21 it is possible to express the in-plane linear stresses as function of the linear strains only. The resulting equations are:

$$\sigma_x = \underbrace{\left(E_{11} - \frac{E_{13}^2}{E_{33}}\right)}_{Q_{xx}}\epsilon_x + \underbrace{\left(E_{12} - \frac{E_{13}E_{23}}{E_{33}}\right)}_{Q_{xy}}\epsilon_y \quad (4.23)$$

$$\sigma_y = \underbrace{\left(E_{12} - \frac{E_{13}E_{23}}{E_{33}}\right)}_{Q_{xy}}\epsilon_x + \underbrace{\left(E_{22} - \frac{E_{23}^2}{E_{33}}\right)}_{Q_{yy}}\epsilon_y \quad (4.24)$$

The equation about in-plane shear is:

$$\tau_{xy} = \underbrace{E_{66}Q_{ss}}_{Q_{ss}}\gamma_{xy} \quad (4.25)$$

Using matrix notation, the relationships between in-plane stresses and strains for an orthotropic 2D ply expressed with respect to a reference system in which one of the axes is parallel to the fibers are:

$$\begin{Bmatrix} \sigma_x \\ \sigma_y \\ \tau_{xy} \end{Bmatrix} = \begin{bmatrix} Q_{xx} & Q_{xy} & 0 \\ Q_{xy} & Q_{yy} & 0 \\ 0 & 0 & Q_{ss} \end{bmatrix} \begin{Bmatrix} \epsilon_x \\ \epsilon_y \\ \gamma_{xy} \end{Bmatrix} \quad (4.26)$$

Q_{ij} terms in Eq. 4.26, can be expressed as a function of the parameters calculated from physical testing, such as longitudinal and transverse elastic moduli. Equations 4.27, 4.28, 4.29, 4.30 report these parameters.

$$Q_{xx} = \frac{E_L}{1 - \nu_{LT}\nu_{TL}} \quad (4.27)$$

$$Q_{yy} = \frac{E_T}{1 - \nu_{LT}\nu_{TL}} \quad (4.28)$$

$$Q_{xy} = \frac{\nu_{LT}E_T}{1 - \nu_{LT}\nu_{TL}} = \frac{\nu_{TL}E_L}{1 - \nu_{LT}\nu_{TL}} \quad (4.29)$$

$$Q_{ss} = G_{LT} \quad (4.30)$$

Equation 4.26 is true when the coordinate system has one axis parallel to the fibers and the other one, perpendicular to them. When this does not hold, stresses transforms according to the coordinate transformation rule:

$$\begin{Bmatrix} \sigma_1 \\ \sigma_2 \\ \tau_{12} \end{Bmatrix} = \begin{bmatrix} \cos^2 \theta & \sin^2 \theta & 2 \sin \theta \cos \theta \\ \sin^2 \theta & \cos^2 \theta & -2 \sin \theta \cos \theta \\ -\sin \theta \cos \theta & \sin \theta \cos \theta & (\cos^2 \theta - \sin^2 \theta) \end{bmatrix} \begin{Bmatrix} \sigma_x \\ \sigma_y \\ \tau_{xy} \end{Bmatrix} \quad (4.31)$$

Being the material anisotropic, if the coordinate system changes then the definition of the stiffness terms must be updated accordingly. The constitutive equation for a ply when the coordinate system has one ax parallel to the fibers has some null terms, as reported in Eq: 4.26. When the fibers are not aligned with the reference system all the terms are non-null (Eq: 4.32)

$$\begin{cases} Q_{11}^{(\theta)} = m^4 Q_{xx} + n^4 Q_{yy} + 2m^2 n^2 Q_{xy} + 4m^2 n^2 Q_{ss} \\ Q_{22}^{(\theta)} = n^4 Q_{xx} + m^4 Q_{yy} + 2m^2 n^2 Q_{xy} + 4m^2 n^2 Q_{ss} \\ Q_{12}^{(\theta)} = m^2 n^2 Q_{xx} + m^2 n^2 Q_{yy} + (m^4 + n^4) Q_{xy} - 4m^2 n^2 Q_{ss} \\ Q_{66}^{(\theta)} = m^2 n^2 Q_{xx} + m^2 n^2 Q_{yy} - m^2 n^2 Q_{xy} + (m^2 - n^2)^2 Q_{ss} \\ Q_{16}^{(\theta)} = m^3 n Q_{xx} - mn^3 Q_{yy} + (mn^3 - m^3 n) Q_{xy} + 2(mn^3 - m^3 n) Q_{ss} \\ Q_{26}^{(\theta)} = mn^3 Q_{xx} - m^3 n Q_{yy} + (m^3 n - mn^3) Q_{xy} + 2(m^3 n - mn^3) Q_{ss} \end{cases} \quad (4.32)$$

Where $m=\cos \theta$ and $n=\sin \theta$. At this point, Eq: 4.26 transforms into:

$$\begin{Bmatrix} \sigma_1 \\ \sigma_2 \\ \tau_{12} \end{Bmatrix} = \begin{bmatrix} Q_{11} & Q_{12} & Q_{16} \\ Q_{12} & Q_{22} & Q_{26} \\ Q_{16} & Q_{26} & Q_{66} \end{bmatrix} \begin{Bmatrix} \epsilon_1 \\ \epsilon_2 \\ \gamma_{12} \end{Bmatrix} \quad (4.33)$$

What stated above is true for a single ply, but when dealing with laminates it is interesting to determine the stiffness and the strength of the whole structure as the summation and in the function of the plies constituting the laminate. This introduces the concept of strain compatibility which means that all the layers will move the same amount. Taking into account their original length, this defines plies' strain which unique for all of them $\epsilon_i = \epsilon$.

Being the behavior linear, it holds that:

$$\epsilon_i = \frac{F_i}{E_i A_i} = \frac{F_{tot}}{E_{lam} A_{lam}} \quad (4.34)$$

But, due to force equivalence

$$F_{tot} = \sum_{i=1}^n F_i \quad (4.35)$$

It also holds that:

$$(EA)_{lam} = \sum_{i=1}^n (EA)_{i\text{-th ply}} \quad (4.36)$$

Most laminates are thin compared to their in-plane dimensions. Thus, it is a good approximation to average the stresses in the thickness. So, instead of using stresses, that vary from ply to ply, it is convenient to use stress resultants, that represent forces and moments per unit width. They are defined explicitly as:

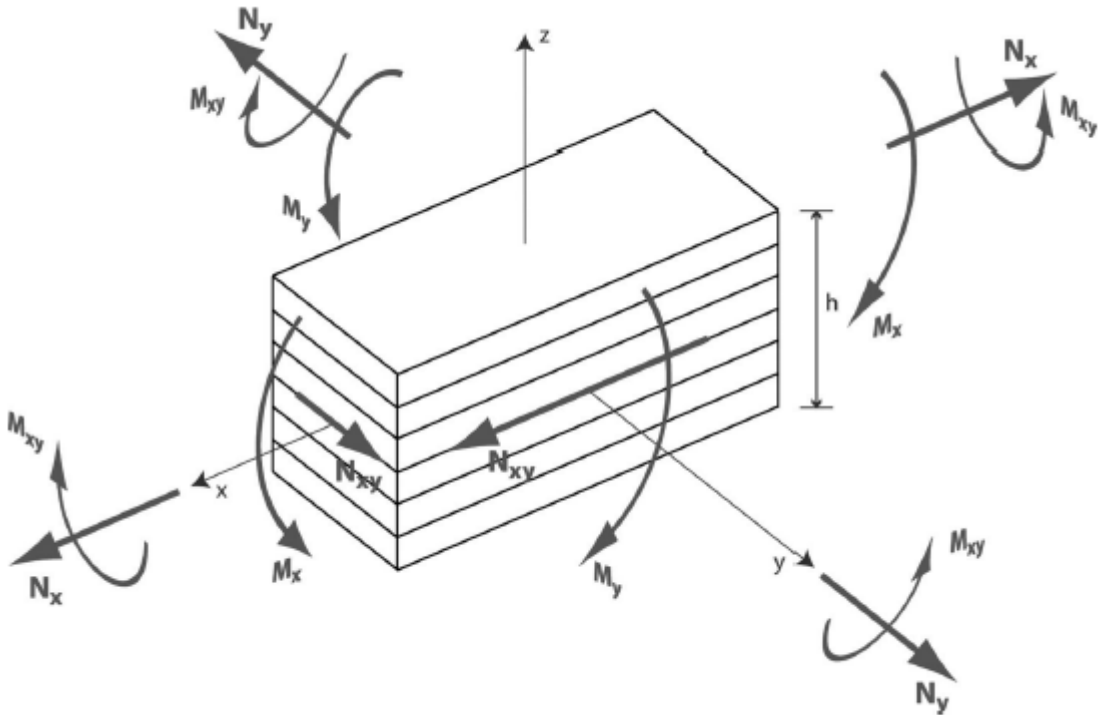


Figure 4.7: Stress resultant

$$N_1 = \int_{-h/2}^{h/2} \sigma_1 dz \quad (4.37)$$

$$N_2 = \int_{-h/2}^{h/2} \sigma_2 dz \quad (4.38)$$

$$N_{12} = \int_{-h/2}^{h/2} \tau_{12} dz \quad (4.39)$$

$$M_1 = \int_{-h/2}^{h/2} \sigma_1 z dz \quad (4.40)$$

$$M_2 = \int_{-h/2}^{h/2} \sigma_2 z dz \quad (4.41)$$

$$M_{12} = \int_{-h/2}^{h/2} \tau_{12} z dz \quad (4.42)$$

It is possible, now, to introduce the topic of the membrane (in-plane) behavior. This is based on some assumptions. They are:

- The structure is loaded by in-plane loads only. No bending;
- The lay-up is symmetric.

These hypotheses lead to the fact that the strains ϵ_1 , ϵ_2 and γ_{12} are constant through the thickness and equal to the mid-plane strains $\epsilon_{1,0}$, $\epsilon_{2,0}$ and $\gamma_{12,0}$.

Let's consider now Eq. 4.33, and let's integrate the equation along z . The first equation will be:

$$\int_{-h/2}^{h/2} \sigma_{11} dz = \int_{-h/2}^{h/2} Q_{11} \epsilon_{1,0} dz + \int_{-h/2}^{h/2} Q_{12} \epsilon_{2,0} dz + \int_{-h/2}^{h/2} Q_{16} \gamma_{12,0} dz \quad (4.43)$$

Though the definition of the stress resultant and because the strains are constant, Eq: 4.43 can be rewritten as:

$$N_1 = \underbrace{\int_{-h/2}^{h/2} Q_{11} dz}_{A_{11}} \epsilon_{1,0} + \underbrace{\int_{-h/2}^{h/2} Q_{12} dz}_{A_{12}} \epsilon_{2,0} + \underbrace{\int_{-h/2}^{h/2} Q_{16} dz}_{A_{16}} \gamma_{12,0} \quad (4.44)$$

The term A_{11} indicates the relationship between the longitudinal force per unit width and the in-plane shear strain.

Repeating the integration for the other equations and defining the terms accordingly, lead to the matrix equation which defines the relationships between unit-width loads, in-plane stiffness terms and in-plane strains.

$$\begin{Bmatrix} N_1 \\ N_2 \\ N_{12} \end{Bmatrix} = \begin{bmatrix} A_{11} & A_{12} & A_{16} \\ A_{12} & A_{22} & A_{26} \\ A_{16} & A_{26} & A_{66} \end{bmatrix} \begin{Bmatrix} \epsilon_1 \\ \epsilon_2 \\ \gamma_{12} \end{Bmatrix} \quad (4.45)$$

In general, the terms A_{ij} can be defined as:

$$A_{ij} = \int_{-h/2}^{h/2} Q_{ij} dz \quad (4.46)$$

But because of the terms Q_{ij} are constant within each ply, the integral can be substituted by a summation. Here k denotes the k -th ply, and N is the total number of plies in the laminate.

$$A_{ij} = \sum_{k=1}^N \underbrace{(z_k - z_{k-1})}_{\text{Ply thickness}} \quad (4.47)$$

Let's now consider the out-of-plane behavior, namely, when subjected to bending. Based on the standard plate theory, the starting point is the assumption that the strains in the thickness vary linearly. They appear as:

$$\epsilon_1 = \epsilon_{10} - \frac{\partial^2 w}{\partial x^2} z = \epsilon_{10} + zK_1 \quad (4.48)$$

$$\epsilon_2 = \epsilon_{20} - \frac{\partial^2 w}{\partial y^2} z = \epsilon_{20} + zK_2 \quad (4.49)$$

$$\gamma_{12} = \gamma_{120} - 2 \frac{\partial^2 w}{\partial x \partial y} z = \gamma_{120} + zK_{12} \quad (4.50)$$

K_1 , K_2 , K_{12} are the curvatures. It should be noticed that the origin of the coordinate system is in the laminate mid-plane. Furthermore, for pure bending, there are no in-plane strains, and so $\epsilon_{10} = \epsilon_{20} = \gamma_{120} = 0$.

To determine the relationship between the moments per unit-width with respect the curvatures, let's take Eq: 4.33, multiply both sides by z and integrate through the thickness of the laminate. The first equation becomes:

$$\int_{-h/2}^{h/2} z \sigma_{11} dz = \int_{-h/2}^{h/2} z Q_{11} \left(-z \frac{\partial^2 w}{\partial x^2}\right) dz \quad (4.51)$$

Using the definition of for M_1 :

$$M_1 = - \int_{-h/2}^{h/2} z^2 Q_{11} \left(\frac{\partial^2 w}{\partial x^2}\right) dz - \int_{-h/2}^{h/2} z^2 Q_{12} \left(\frac{\partial^2 w}{\partial y^2}\right) dz - \int_{-h/2}^{h/2} 2z^2 Q_{16} \left(\frac{\partial^2 w}{\partial x \partial y}\right) dz \quad (4.52)$$

For pure bending the curvatures are constant, thus:

$$M_1 = K_1 \int_{-h/2}^{h/2} z^2 Q_{11} dz + K_2 \int_{-h/2}^{h/2} z^2 Q_{12} dz + K_{12} \int_{-h/2}^{h/2} 2z^2 Q_{16} dz \quad (4.53)$$

Since Q_{ij} are constant for each ply, after integration, the equation appears as:

$$M_1 = K_1 \underbrace{\sum_{k=1}^N Q_{11}^{(k)} \frac{z_k^3 - z_{k-1}^3}{3}}_{D_{11}} + K_2 \underbrace{\sum_{k=1}^N Q_{12}^{(k)} \frac{z_k^3 - z_{k-1}^3}{3}}_{D_{12}} + K_{12} \underbrace{\sum_{k=1}^N Q_{16}^{(k)} \frac{z_k^3 - z_{k-1}^3}{3}}_{D_{16}} \quad (4.54)$$

Repeating the process for the remaining equations and using matrix notation, the relationship that expresses the moments per unit-width as function of the curvatures is:

$$\begin{Bmatrix} M_1 \\ M_2 \\ M_{12} \end{Bmatrix} = \begin{bmatrix} D_{11} & D_{12} & D_{16} \\ D_{12} & D_{22} & D_{26} \\ D_{16} & D_{26} & D_{66} \end{bmatrix} \begin{Bmatrix} K_x \\ K_y \\ K_{xy} \end{Bmatrix} \quad (4.55)$$

Equations 4.45 and 4.55 show the relationships between forces per unit-width as a function of the in-plane strains and the moments per unit-width as a function of the curvatures respectively. Composites exhibit also coupling phenomena between the in-plane and the out-of-plane behaviors. This means that in-plane loads could generate out-of-plane bending or pure bending could introduce in-plane strains. In other words, some composites may experience bending or twisting when subjected to pure in-plane loads and vice-versa, some other laminates could stretch when loaded by pure bending or torsional moments. So, let's take into account the constitutive equation 4.33. Considering Eqs: 4.48, 4.49, 4.50, each equation can be rewritten as:

$$\sigma_1 = Q_{11}(\epsilon_{10} + zK_1) + Q_{12}(\epsilon_{20} + zK_2) + Q_{16}(\gamma_{120} + zK_{12}) \quad (4.56)$$

Integrating with respect to z and using the definition of the resultant stresses:

$$N_1 = A_{11}\epsilon_{10} + K_1 \int_{-h/2}^{h/2} Q_{11} z dz + A_{11}\epsilon_{20} + K_2 \int_{-h/2}^{h/2} Q_{12} z dz + A_{16}\gamma_{120} + K_{12} \int_{-h/2}^{h/2} Q_{16} z dz \quad (4.57)$$

The integrals can be turned into summations:

$$N_1 = A_{11}\epsilon_{10} + A_{12}\epsilon_{20} + A_{16}\gamma_{120} + K_1 \underbrace{\sum_{k=1}^N Q_{11}^{(k)} \frac{z_k^2 - z_{k-1}^2}{2}}_{B_{11}} + K_2 \underbrace{\sum_{k=1}^N Q_{12}^{(k)} \frac{z_k^2 - z_{k-1}^2}{2}}_{B_{12}} + K_{12} \underbrace{\sum_{k=1}^N Q_{16}^{(k)} \frac{z_k^2 - z_{k-1}^2}{2}}_{B_{16}} \quad (4.58)$$

The overall stress-strain relationship for a laminate is:

$$\begin{Bmatrix} N_1 \\ N_2 \\ N_{12} \\ M_1 \\ M_2 \\ M_{12} \end{Bmatrix} = \begin{bmatrix} A_{11} & A_{12} & A_{16} & B_{11} & B_{12} & B_{16} \\ A_{12} & A_{22} & A_{26} & B_{12} & B_{22} & B_{26} \\ A_{16} & A_{26} & A_{66} & B_{16} & B_{26} & B_{66} \\ B_{11} & B_{12} & B_{16} & D_{11} & D_{12} & D_{16} \\ B_{12} & B_{22} & B_{26} & D_{12} & D_{22} & D_{26} \\ B_{16} & B_{26} & B_{66} & D_{16} & D_{26} & D_{66} \end{bmatrix} \begin{Bmatrix} \epsilon_1 \\ \epsilon_2 \\ \gamma_{12} \\ K_x \\ K_y \\ K_{xy} \end{Bmatrix} \quad (4.59)$$

To summarize,

- A_{ij} terms relate in-plane strains with in-plane loads.

$$\begin{Bmatrix} N_1 \\ N_2 \\ N_{12} \\ M_1 \\ M_2 \\ M_{12} \end{Bmatrix} = \begin{bmatrix} A_{11} & A_{12} & A_{16} & B_{11} & B_{12} & B_{16} \\ A_{12} & A_{22} & A_{26} & B_{12} & B_{22} & B_{26} \\ A_{16} & A_{26} & A_{66} & B_{16} & B_{26} & B_{66} \\ B_{11} & B_{12} & B_{16} & D_{11} & D_{12} & D_{16} \\ B_{12} & B_{22} & B_{26} & D_{12} & D_{22} & D_{26} \\ B_{16} & B_{26} & B_{66} & D_{16} & D_{26} & D_{66} \end{bmatrix} \begin{Bmatrix} \epsilon_1 \\ \epsilon_2 \\ \gamma_{12} \\ K_x \\ K_y \\ K_{xy} \end{Bmatrix} \quad (4.60)$$

- B_{ij} terms represent the coupling terms between in-plane behavior and out-of-plane one.

$$\begin{Bmatrix} N_1 \\ N_2 \\ N_{12} \\ M_1 \\ M_2 \\ M_{12} \end{Bmatrix} = \begin{bmatrix} A_{11} & A_{12} & A_{16} & B_{11} & B_{12} & B_{16} \\ A_{12} & A_{22} & A_{26} & B_{12} & B_{22} & B_{26} \\ A_{16} & A_{26} & A_{66} & B_{16} & B_{26} & B_{66} \\ B_{11} & B_{12} & B_{16} & D_{11} & D_{12} & D_{16} \\ B_{12} & B_{22} & B_{26} & D_{12} & D_{22} & D_{26} \\ B_{16} & B_{26} & B_{66} & D_{16} & D_{26} & D_{66} \end{bmatrix} \begin{Bmatrix} \epsilon_1 \\ \epsilon_2 \\ \gamma_{12} \\ K_x \\ K_y \\ K_{xy} \end{Bmatrix} \quad (4.61)$$

- D_{ij} entries specify the bending behavior, relating out-of-plane resultant loads to out-of-plane curvatures.

$$\begin{Bmatrix} N_1 \\ N_2 \\ N_{12} \\ M_1 \\ M_2 \\ M_{12} \end{Bmatrix} = \begin{bmatrix} A_{11} & A_{12} & A_{16} & B_{11} & B_{12} & B_{16} \\ A_{12} & A_{22} & A_{26} & B_{12} & B_{22} & B_{26} \\ A_{16} & A_{26} & A_{66} & B_{16} & B_{26} & B_{66} \\ B_{11} & B_{12} & B_{16} & D_{11} & D_{12} & D_{16} \\ B_{12} & B_{22} & B_{26} & D_{12} & D_{22} & D_{26} \\ B_{16} & B_{26} & B_{66} & D_{16} & D_{26} & D_{66} \end{bmatrix} \begin{Bmatrix} \epsilon_1 \\ \epsilon_2 \\ \gamma_{12} \\ K_x \\ K_y \\ K_{xy} \end{Bmatrix} \quad (4.62)$$

There are some particular cases:

- Symmetric laminates: in the laminate, per each ply with a certain orientation, there is a symmetric one with respect to the mid-plane. In this case, B_{ij} terms vanish;
- Balanced laminates: per each ply oriented with an angle θ , there is another ply in the laminate oriented at $-\theta$. In this case, $A_{16} = A_{26} = 0$ which means that in-plane stretching and compression are decoupled to in-plane shear;
- Anti-symmetric laminate: when $D_{16} = D_{26} = 0$ bending and torsion are uncoupled.

Eq. 4.59, allows to determined the stress resultant on the laminate once knowing strains and rotations. Usually the situation is the opposite and so Eq. 4.63 defines the so-called inverted stress-strain relationship.

$$\begin{pmatrix} \epsilon_1 \\ \epsilon_2 \\ \gamma_{12} \\ K_x \\ K_y \\ K_{xy} \end{pmatrix} = \begin{bmatrix} \alpha_{11} & \alpha_{12} & \alpha_{16} & \beta_{11} & \beta_{12} & \beta_{16} \\ \alpha_{12} & \alpha_{22} & \alpha_{26} & \beta_{12} & \beta_{22} & \beta_{26} \\ \alpha_{16} & \alpha_{26} & \alpha_{66} & \beta_{16} & \beta_{26} & \beta_{66} \\ \beta_{11} & \beta_{12} & \beta_{16} & \delta_{11} & \delta_{12} & \delta_{16} \\ \beta_{12} & \beta_{22} & \beta_{26} & \delta_{12} & \delta_{22} & \delta_{26} \\ \beta_{16} & \beta_{26} & \beta_{66} & \delta_{16} & \delta_{26} & \delta_{66} \end{bmatrix} \begin{pmatrix} N_1 \\ N_2 \\ N_{12} \\ M_1 \\ M_2 \\ M_{12} \end{pmatrix} \quad (4.63)$$

Experimental tests must be performed to link A_{ij} , B_{ij} and D_{ij} to actual physical quantities.

Chapter 5

The SC17 project

The SC17 prototype has been developed after a deep reorganization of the team. The team was affected by internal discontents and aversion between departments. Because of this the team has been completely dismissed and recreated again from zero. The number of members of the new team was significantly smaller than the old one: about eight people instead of more than seventy. This, in addition to the fact that the new team has been established in late October, influenced some of the decisions behind the design of the new prototype. By looking at the geometries, and in particular, to the monocoque, it is possible to appreciate simple shapes and rational design. This was an attempt to minimize both design and manufacturing lead-time. But this idea has been applied to every component of the car. The entire SC17 project was reliability driven, and thus simple and predictable shapes have been used where possible. This also to limit costs. The diagram reported in figure 5.1 summarizes the steps performed during the design of the chassis of the SC17.

The first step in the design of the new prototype consisted of a deep analysis of the previous one.

The previous vehicle, the SCXV, was properly designed and mechanically reliable, but suffered severe electrical reliability issues.

Its main advantages were:

- Mechanical reliability;
- Manufacturing quality;
- Maintainability and accessibility;
- Visibility.

Its main disadvantages were instead:

- Electrical reliability;
- Waterproofing;

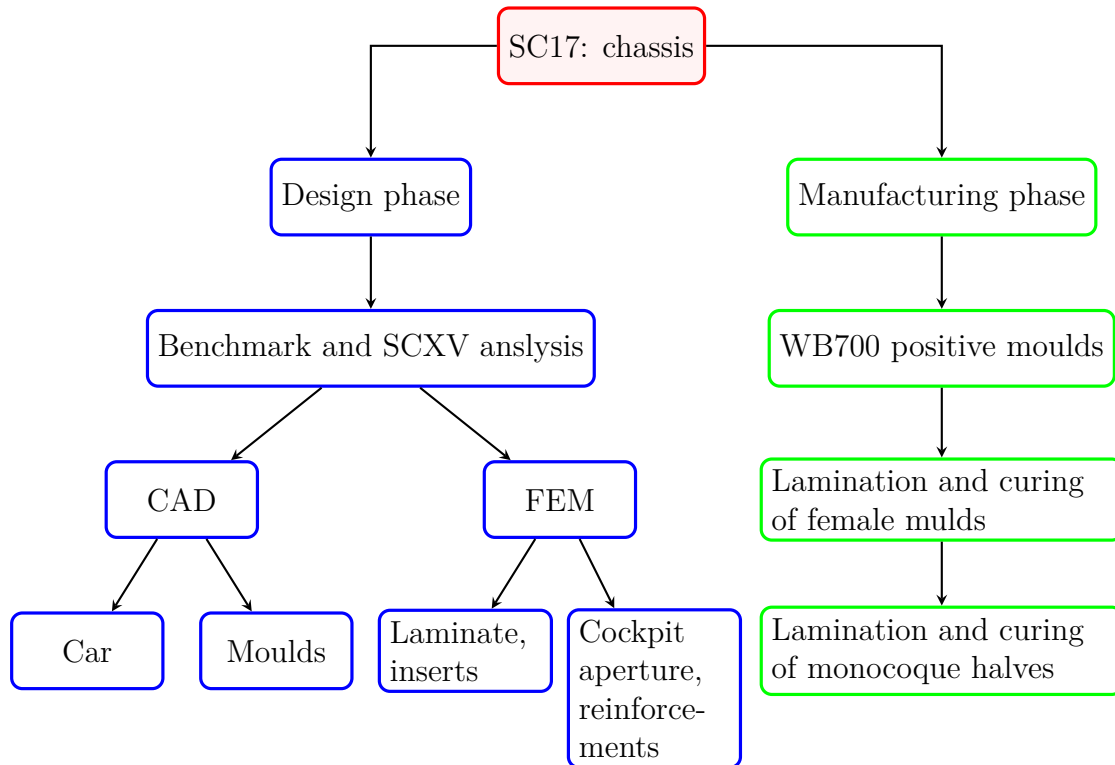


Figure 5.1: SC17 chassis design process

- Dimensions (Bulky rear-end);
- Weight;
- Height of the centre of gravity;

Picture 5.2 illustrates a section of the SCXV, from which it is possible to appreciate the packaging.

About waterproofing, FSAE rules state that all the electric prototypes participating in a certain competition must be subjected to the so-called "rain test". It consists of leaving the vehicle with its electrical systems turned-on under a set of water sprays for a certain time. The test aims to access the electrical system insulation to guarantee drivers' safety.

When the insulation properties are lacking, as it was for the SCXV prototype, the usual practice was to use an enormous amount of silicone and other sealants, such as tapes and so forth, to try to overcome this test. This induced a non-negligible increase of the mass which was repeated event after event, which in turn traduced into a loss of performances.

The design targets for the SC17 project were mainly driven by specific stiffness. The high torsional stiffness target provided by the vehicle dynamic department and

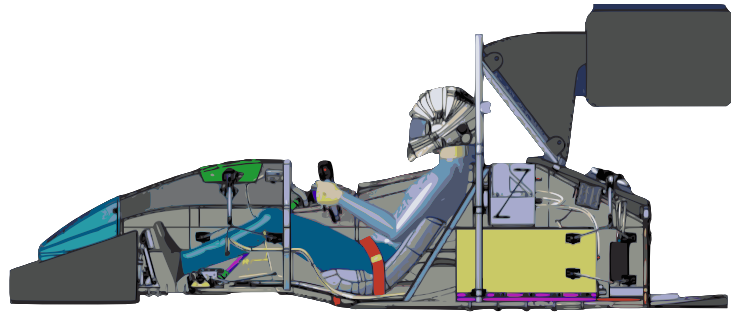


Figure 5.2: Packaging of the prototype SCXV

the loading conditions demanded by the FSAE required, for the first time, the need to study the influence on the torsional stiffness over the mass ratio of the cockpit opening. A detailed torsional stiffness test campaign has been conducted on the SCXV (described in detail in 3.4.1, page: 30). Briefly, this test underlined how the cockpit opening represents the region of the chassis which induces the greatest loss in terms of torsional stiffness.

Thus, the main objectives for the SC17 project were:

- Improving overall reliability and, in particular, electrical one;
- Reducing the height of the center of gravity (Estimated reduction at the beginning of the project of about 10%: from 230 mm to 209 mm);
- Reducing the overall mass of the vehicle. This was achieved by revisiting and optimizing the design of all vehicle components. One of the greatest achievement in this regards has been obtained thanks to a new battery pack design which involved new Li-ion cells, new cooling, and new packaging;
- Improve the torsional stiffness behavior in the cockpit opening region.
- Improve the dynamic performances of the vehicle and solve some critical issues related to the SCXV suspension geometry (jacking force which tent to rise the inside rear wheel during a turn).

These overall targets traduced to some specific objectives for the monocoque itself. They were:

1. Mass \leq 22 kg (SCXV reference);
2. Torsional stiffness \geq 180 kNm/rad (SCXV reference).

As mentioned above, the series of events that brought to the born of the new team limited, even more, the time available to design the new prototype. This constrained some aspects of the design. Among all of them, the most relevant for the

monocoque was the impossibility to test new materials and lay-up configurations to try to improve the sandwich panels used in the regulated areas of the chassis which dictate the chassis' mass. This is the reason behind the fact that the regulated laminates of the SC17 monocoque are the same as the SCXV. Several interesting ideas have been discarded because of a lack of time to manufacture the specimens and to perform the tests. Some examples are represented by the concept of using different core sizes for different regions (Smaller cells where critical mechanical properties were required, more coarse honeycomb in less stressed regions) or the usage of asymmetric laminated sandwich panels to improve bending behavior (One of the tests required by the SAE is three points bending test). To be approved and legal, a sandwich panel must be able to withstand a prescribed load when undergoing this test.

5.1 Load-cases

The first step when designing a new component is understanding to which loads will be subjected to during running conditions.

This section contains the details of all the load-cases used during the simulations. In addition to the standard running load-cases, which consider both forces and moments acting at the tyre-ground contact patch, and the ones defined by the FSAE rules-book, it has been decided to introduce specific load cases for the cockpit opening analysis, namely, the action of the pilot on the cockpit opening sides when exiting the car. This because FSAE rules states that, because of safety reasons, the driver must be able to exit from the chassis with fastened seat belts in less than five seconds (Egress test). This traduces in a dynamic action in which the driver pushes with his/her hands on the cockpit sides to exit as fast as possible, which in turns means an non negligible load on the cockpit sides. Since the rules imposes to design the chassis to host up to a 95-th percentile male, which weights on average about 98 kg, this figure has been used to define the relative load-case. To be precise in this particular load-case the width of a 95-th percentile male specimen hand has been considered (Reference: <https://msis.jsc.nasa.gov/sections/section03.htm>). This in order to define properly the areas in which the loads will be acting. A RBE3 has been used to distribute the loads on the sides.

In addition to the load-cases mentioned above, some other ones have been taken into consideration for the final structural assessment of the firewall and the surrounding structures, namely:

- The loads due to the inertia of the pilot during the maximum acceleration phase;
- The reaction forces due to the application of the brake force during the most severe braking phases.

For both conditions, both the weight and the bio-metric data in terms of hip region width and inner shoulders of the 95-th percentile male specimen has been used (same NASA source previously mentioned). In particular, the hip region for a 40 years old American 95-th percentile male is about 423 mm, while the inner width of back in the shoulder area is about 454 mm. These measures have been used to model a RBE3 element to distribute the load on the firewall. This choice allowed the design to both comply with FSAE rules and to have some more structural margin, since the mass of all pilots was lower than this one.

Numerically, considering a maximum longitudinal acceleration of 1.6g, with an assumed driver weight of 98.5 kg, the resulting load on the firewall would be a compression force acting along the x-direction of about 1546N. On the other hand, considering a force exerted by the driver on the brake pedal, during maximum braking conditions, of about 200 kg, the reaction force compressing the firewall

is about 1962 N. Being the load direction the same, only the second case has been modelled, being more severe. Considering the load in this way is actually conservative because the longitudinal deceleration probably tends to reduce the pressure on the firewall.

Table 5.1: Running load-cases: forces and moments at the tyre-ground contact patch

	Front Axle			Rear Axle			Mz Front [Nmm]	Mz Rear [Nmm]
	x	y	z	x	y	z	z	z
<i>Coordinates of TCP [mm]</i>	0	650	-260	-1525	600	-260	-	-
<i>Pure acceleration (1.6g long.) [N]</i>	-	-	-	-1865	0	1166	-	8114
<i>Pure Braking (-2.5g long.) [N]</i>	3249	0	1300	-	-	-	12348	-
<i>Pure Turn (2.0g lat.) [N]</i>	<i>Outer</i>	0	-2594	1297	0	-3880	1552	-
	<i>Inner</i>	0	-420	210	0	-201	80	-
<i>Pure Turn (2.5g lat.) [N]</i>	<i>Outer</i>	0	-3582	1433	0	-3880	1552	-
	<i>Inner</i>	0	-185	74	0	-201	80	-
<i>Brake-In-Turn (1.5g lat. + -1.5g long) [N]</i>	<i>Outer</i>	2233	-2233	1489	2233	-2233	1489	-
	<i>Inner</i>	1010	-1010	674	1010	-1010	674	-
<i>Acceleration-In-Turn (1.5g lat. + 1.5g long) [N]</i>	<i>Outer</i>	-2378	-2378	1586	-2378	-2378	1586	-
	<i>Inner</i>	-1054	-1054	702	-1054	-1054	702	-

Table 5.2: FSAE alternative frame rules load-cases

Load-case name	Application point	Boundary conditions	x-comp.	y-comp.	z-comp.	Max allowable deflection [mm]
AF4.1	Top of Main Roll Hoop	Fixed displacement (x, y, z) but not rotation of the bottom nodes of both sides of the front and main roll hoops.	6.0	5.0	-9.0	25
AF4.2	Top of Font Roll Hoop	Fixed displacement (x, y, z) but not rotation of the bottom nodes of both sides of the front and main roll hoops.	6.0	5.0	-9.0	25
AF4.3	Between Front and Main Hoop. Impactor radius: 127 mm	Fixed displacement (x, y, z) but not rotation of the bottom nodes of both sides of the front and main roll hoops.	0	7.0	0	25
AF4.4	Attachment points between the impact attenuator and the front bulkhead	Fixed displacement (x, y, z) but not rotation of the bottom nodes of both sides of the main roll hoop and both locations where the main hoop and shoulder harness tube connect.	120	0	0	25
AF4.7	Attachment points between the impact attenuator and the front bulkhead	Fixed displacement (x, y, z) but not rotation of the bottom nodes of both sides of the main roll hoop and both locations where the main hoop and shoulder harness tube connect.	120	10.5	0	25

5.2 SC17 FEM model

This section analyzes the FEM models used to simulate the behavior of the chassis when subjected to different loading conditions.

This corresponds to the right-hand side of the FEM branch reported in figure 5.1.

To obtain the most accurate results with the lowest amount of computational resources, several best practices have been followed during the model set-up. Some of these include: the most simple element type capable of describing properly the behavior of a specific component has been chosen, the mesh size for the monocoque has been determined via a convergence analysis, more efficient Hexa elements have been used to replace Tetra ones in mappable solids. Mappable, in this regard, means that it can be meshed by extruding Quadrilateral and Triangular (Tria) bi-dimensional elements to create Hexa and Penta tri-dimensional ones.

The number of Tria elements and their locations have been attentively analyzed, minimizing their presence in the region of interest, compatibly with the local geometry. Further local mesh refinements have been successively studied in the cockpit opening area.

The following section describes in detail the steps carried-out to determine the most appropriate mesh size.

5.2.1 Monocoque CAD model: the surfaces resulting from the first design phase

This section describe which were the design considerations that brought to the first geometries that have been used as input for the calculations about the cockpit. In particular, this section focuses on the reasons that guided the design of the cockpit opening.

The main guidelines which drove the shapes of the aperture and its reinforcement were:

1. FSAE rules. As mentioned in section 3.5, the rules state the minimum dimensions of the opening via a template which is used to assess rules compatibility during technical inspections;
2. The need to host properly the driver. At the beginning of the project the driving position was set to be 30° with respect to the horizontal. This allowed the shoulders of the driver to be almost completely inside the opening. The first attempt of the opening was then as close as possible to the FSAE template. It could be though as an offset of the template perimeter.

Unfortunately, because of visibility problems, the angle of the back restraint was raised to 35° . This traduced into the impossibility of using the former designed shape due to the shoulders position, and thus a bigger cut-out has been

necessary. Picture 5.4 illustrates a render of the monocoque with the original cut-out shape. On the other hand, picture 5.5 shows the actual position of the pilots during driving position. As it is possible to see, its shoulder comes out of the opening. The resulting aperture is shown in pictures 5.6;

3. The need to reinforce the cockpit opening. A solution capable of both improving the inertia and the bending stiffness of the edges, as well as increasing the lamination quality was employed. As introduced in figure 3.21, a solution constituted by a reinforcement in the edges, if properly designed is capable of increasing the panel stiffness and allow to overlap properly the laminate plies. For this purpose Rohacell foam has been used. Its superior capability of being shaped through milling processes, together with its mechanical properties, allowed to design a reinforcement which shape smoothly connected the surrounding sandwich panels with the edges of the opening.

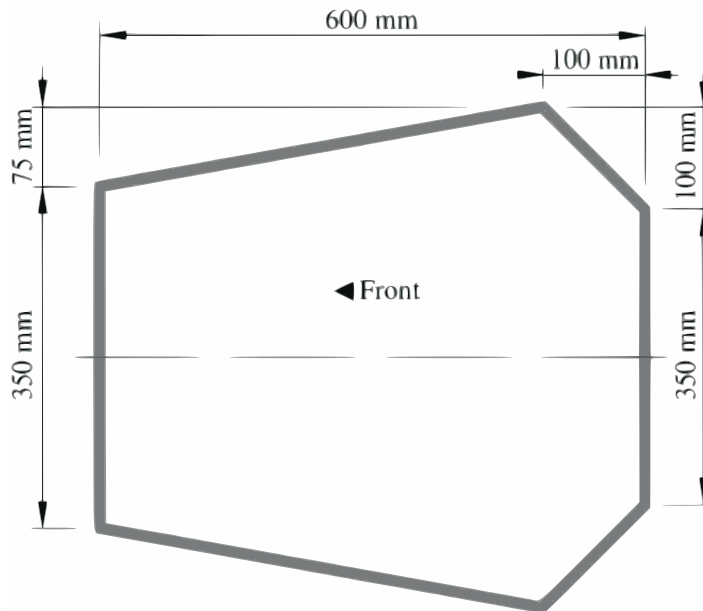


Figure 5.3: Cockpit opening FSAE template

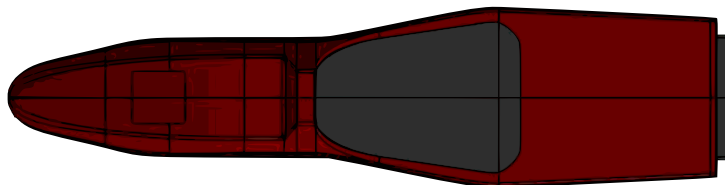


Figure 5.4: First cockpit opening geometry



Figure 5.5: Actual position of driver shoulder during driving conditions



Figure 5.6: SC17 actual cockpit opening geometry

5.2.2 Monocoque convergence analysis

This section describes the process followed to determine the global mesh-size of the monocoque in the model subsequently used to perform the calculations necessary for both the laminate optimization, the detailed study of the cockpit opening and, finally, the structural assessment.

Solely torsion load-case has been considered for the convergence study of the chassis. The mesh size of the other components has been determined through both the experience of the author and the element's dimensions used in the FEM models of the previous prototype.

A first coarse mesh, 20mm average element size, was used to perform the first simulation. This process has been repeated several times, refining the mesh-size at each iteration. The refinements steps were:

- 20 mm;
- 15 mm;
- 10 mm;
- 5 mm.

Convergence has been reached with 10 mm mesh size.

Pictures 5.7, 5.8, 5.9, 5.10 represents the models mentioned before. In particular, image 5.11, shows the detail of a 5 mm mesh size monocoque.

The z-coordinate displacement of the force application point of the left-hand side upright has been measured and used to compute the torsional stiffness of each model. This process has been repeated for all the steps mentioned before. Picture 5.12 represents the way through which the torsional stiffness has been calculated.

After measuring the positive z-coordinate displacements of the force application point on the upright and defining the error between two successive models through formula 5.1, results proved that the convergence has been reached with a mesh-size of 10 mm. the outcomes of this convergence analysis are summarized in table 5.3.

$$\Delta e_{j-1} = \frac{d_z(j) - d_z(j-1)}{d_z(j-1)} \quad (5.1)$$

Where:

- $d_z(j)$ is the z-coordinate displacement of model j;
- $d_z(j-1)$ is the z-coordinate displacement of model j-1;

The model resulting from the convergence analysis is an effective and efficient FE model, capable for both stiffness and structural assessment of the monocoque. Its main features are:

Table 5.3: Convergence analysis summary

<i>Model j-th</i>	<i>Average mesh size</i>	<i>Number of nodes</i>	<i>% of tria</i>	<i>Run time [s]</i>	<i>z-displ. [mm]</i>	<i>Delta ej-1</i>	<i>Error</i>
1	20	51764	1.0%	40	2.77	-	11.0
2	15	60825	0.9%	98	3.00	8.3	2.7
3	20	86111	0.7%	171	3.08	2.7	Ref
4	5	212126	0.03%	589	3.13	1.6	-

- Monocoque average mesh size of 10 mm, with a number of tria of about 0.7 %;
- Efficient brick tri-dimensional elements where possible;
- One-dimensional elements for the main roll-hoop, A-arms, push-rod and suspension dummy damper;
- First order tetra elements for the upright, modelled with a pretty rough mesh. Here the intent is to have a good estimation of their stiffness, so it is not required to have a fine mesh, as it would be for the structural assessment;
- Two-dimensional shell elements for the monocoque, its rear cover and the front roll-hoop

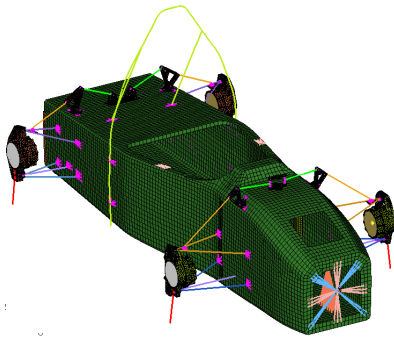


Figure 5.7: FEM model: mesh-size 20 mm

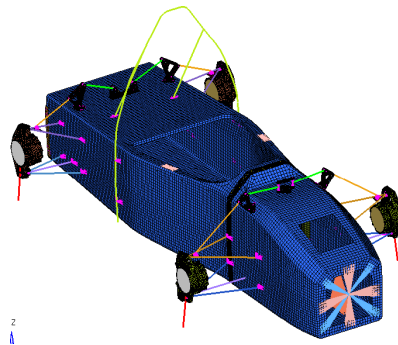


Figure 5.8: FEM model: mesh-size 15 mm

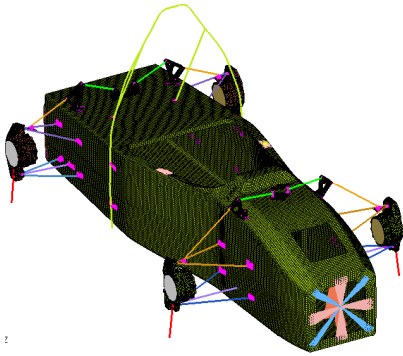


Figure 5.9: FEM model: mesh-size 10 mm

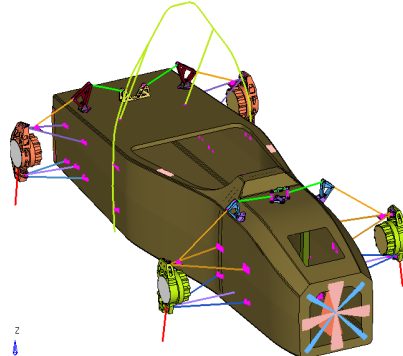


Figure 5.10: FEM model: mesh-size 5 mm

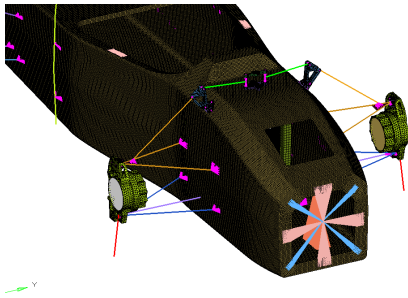


Figure 5.11: FEM model detail: mesh-size 5 mm

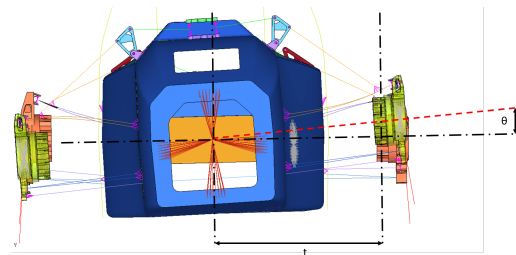


Figure 5.12: Torsional stiffness calculation

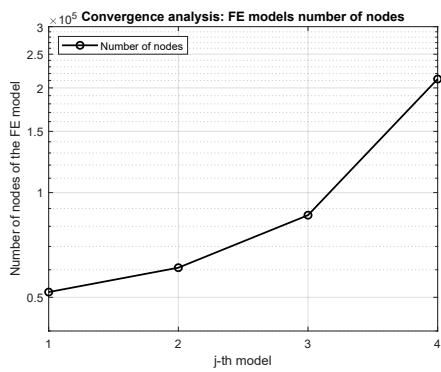


Figure 5.13: Convergence analysis: number of nodes per iteration

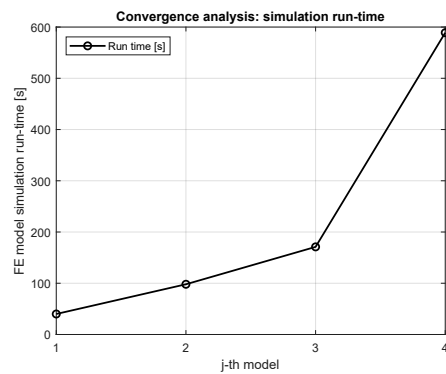


Figure 5.14: Convergence analysis: run-time per iteration

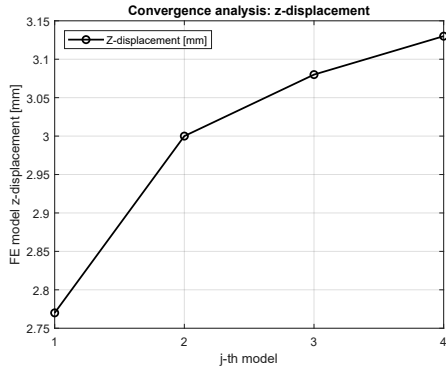


Figure 5.15: Convergence analysis: z-displacement per iteration

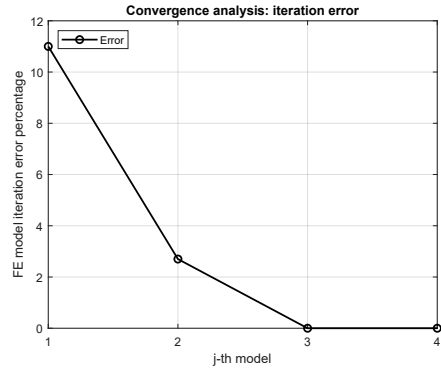


Figure 5.16: Convergence analysis: error percentage per iteration

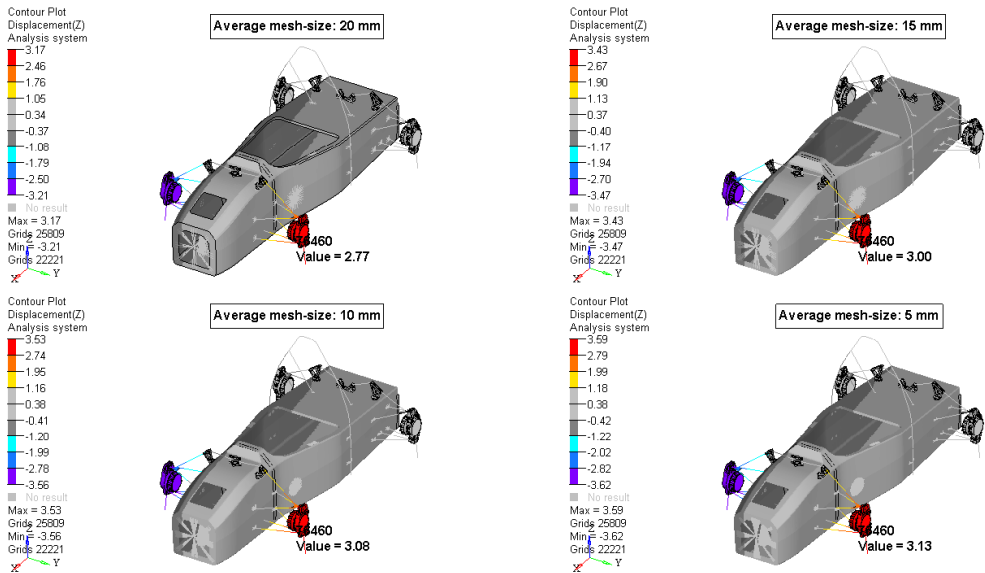


Figure 5.17: Convergence analysis: displacements comparison

5.3 Cockpit-opening detailed analysis

Once the global mesh-size of the monocoque has been determined, the attention moved to the analysis of the cockpit opening. As suggested by the studies carried-out in section 3.4.2, to increase the mechanical properties of the panels surrounding the aperture and to allow a more appropriate arrangement of plies overlap, a reinforcement increasing the cross-sectional area of the edges could be employed. Rohacell has been used for this purpose because of its versatility in terms of shape. Its mechanical properties allow to mill it even in small thicknesses, improving the design freedom. Moreover, it allows for achieving a continuous geometrical transition much easier than the honeycomb. The shape of the reinforcement has been designed taking into consideration four main aspects:

1. The transition between the side sandwich panel and the edge of the opening has been done so to be smooth, avoiding stress concentrations and abrupt stiffness change;
2. The width of the top of the reinforcement has been defined so to be big enough to improve the stiffness but not too bulky to force the monocoque being too wide;
3. The cross-section of the ring is not uniform and varies according to the local needs: it is bigger in the corners, where the flexural moments are the biggest, while it is thinner in the middle to exploit at the maximum the material;
4. Its cross-sectional shape has been designed so to facilitate the shifting of overlapping of the plies.

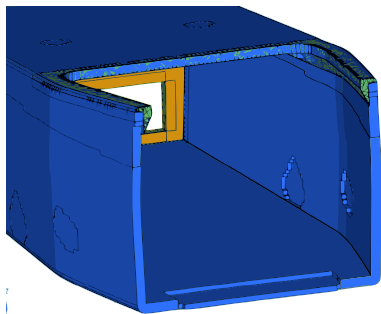


Figure 5.18: FEM model with ring

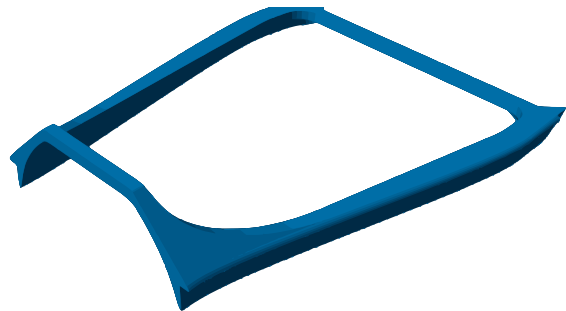


Figure 5.19: Detail of the Rohacell ring

Concerning the simulation aspects, the Rohacell reinforcement has been integrated into the laminate model. In particular, second-order solid tetrahedral elements have been used for this component. This to not overestimate its stiffness, providing more accurate results, closer to the reality.

Evonik Industries provide Rohacell with different densities and consequently mechanical properties. Thus, during the analyses, all the solutions available have been taken into account. Figure 5.20 summarizes the contribution of the different Rohacell on the torsional stiffness.

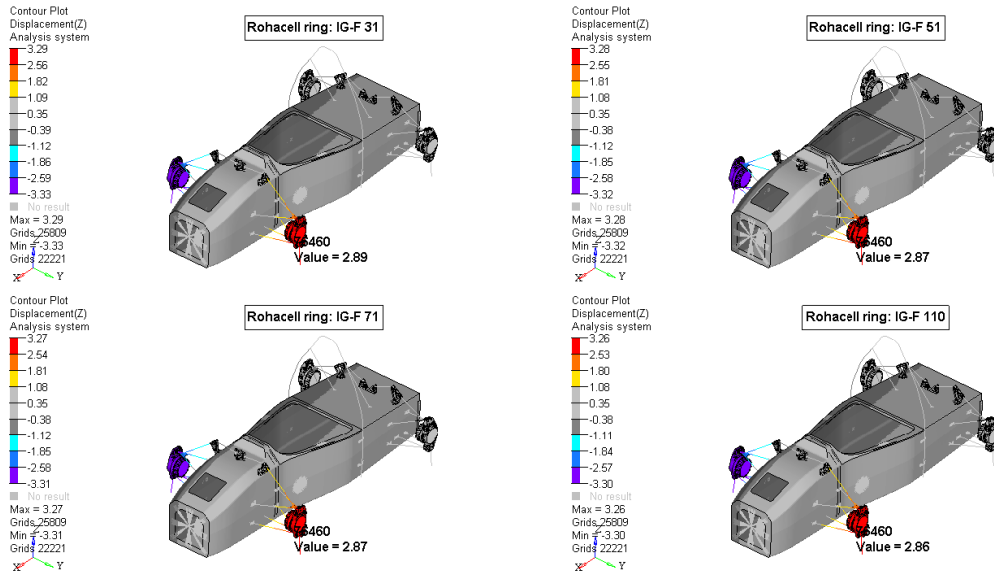


Figure 5.20: Study of the influence of Rohacell density on torsional stiffness

Picture 5.21 shows the strain energy density of the reinforcement modeled with the four different materials. The picture shows that when the vehicle is subjected to torsion, the regions of the rings more involved are the corners and the front part. This supports the choice that has been done concerning the shape. The ring is thicker in these regions.

The mechanical properties of the Rohacell improve increasing the density. Being the specific torsional stiffness the most important parameter to evaluate the static achievements of a chassis, to select the most performing solution, their contribution in terms of percentage increase of specific torsional stiffness with respect the baseline without the reinforcement ring has been evaluated. Figure 5.22 illustrates a bar chart, in which each bar describe the contribution to the specific stiffness. The highest contribution has been given by Rohacell IG-F 51 and thus this material has been chosen for the ring.

Together with the Rohacell support, to further reinforce this region, some plied of Uni-Directional (UD) plies have been employed. They have been arranged to form a ring all around the aperture. Their usage has been limited to two plies. In fact, with all the improvements the overall stiffness target has been reached without the need to add other plies. Figure 5.23 illustrates the contribution of the UD to the torsional stiffness when added to the different Rohacell rings. Figure 5.24 compare the baseline to two improvements.

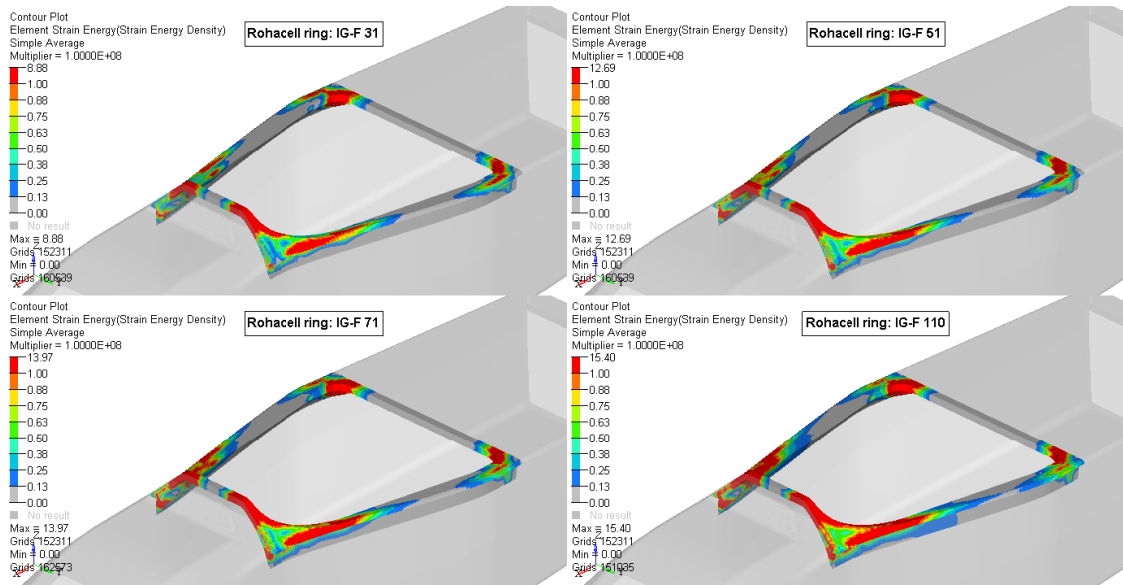


Figure 5.21: Strain energy density of the different Rohacell solutions

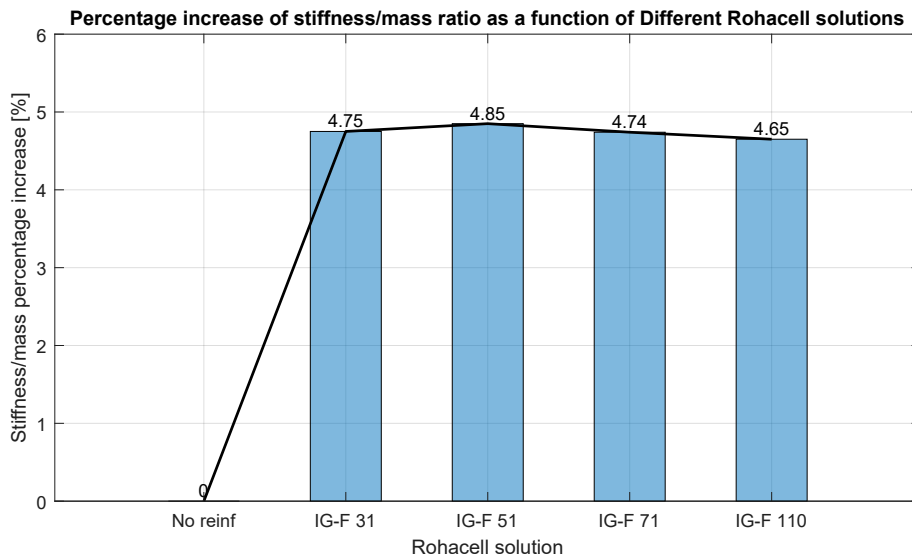


Figure 5.22: Percentage increase of stiffness/mass ratio as a function of different Rohacell solutions

The next step in the design process was to analyze the fixed firewall frame. FSAE rules specify in detail the properties of this component. It must be strong enough to protect the driver and made with materials that allow the electrical insulation of the driver from the tractive system compartment that contains the battery pack. It must be capable of supporting an indentation test performed with a screwdriver.

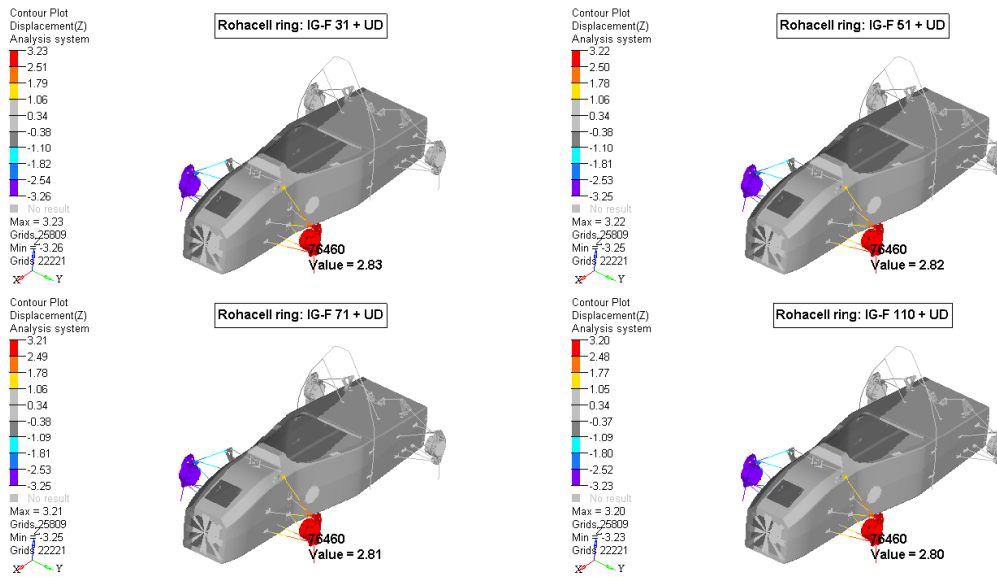


Figure 5.23: Study of the influence of Rohacell density and UD on torsional stiffness

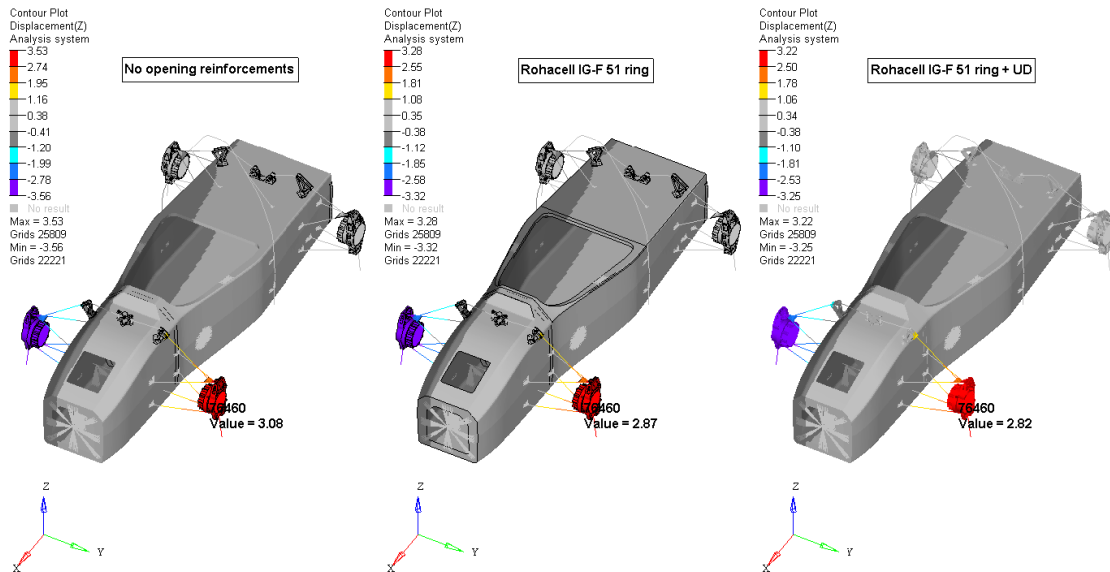


Figure 5.24: Z-coordinate displacement comparison between baseline model (left), Rohacell reinforcement (centre) and Rohacell and UD (right)

Rules specify also that the side facing the battery pack must be made of aluminum and must be grounded. For these reasons, the laminate has been defined using Kevlar and Nomex honeycomb. Nomex is an aramidic honeycomb. To provide stiffness and strength plies of CFRP have been inserted inside the laminate, between the Kevlar and the aluminum. Three types of carbon fiber have been analyzed:

plain T200, twill M46J and UD-K63712. The second is a High Module (HM) while the third one is an Ultra High Module (UHM) carbon fiber. The first two materials have been analyzed with different orientations, namely, at 0° and 45° . The third one has been simulated arranged in two balanced plies at $\pm 45^\circ$. Results show that the orientation was not particularly relevant. Figure 5.25 illustrates the analyses with T200 oriented in two different ways. In the fashion, image 5.26 shows the same kind of results but using M46J. Figure 5.27 illustrates the comparison between the three materials.

M46J has been chosen because of its good performance and because of its better drapability which helped during manufacturing.

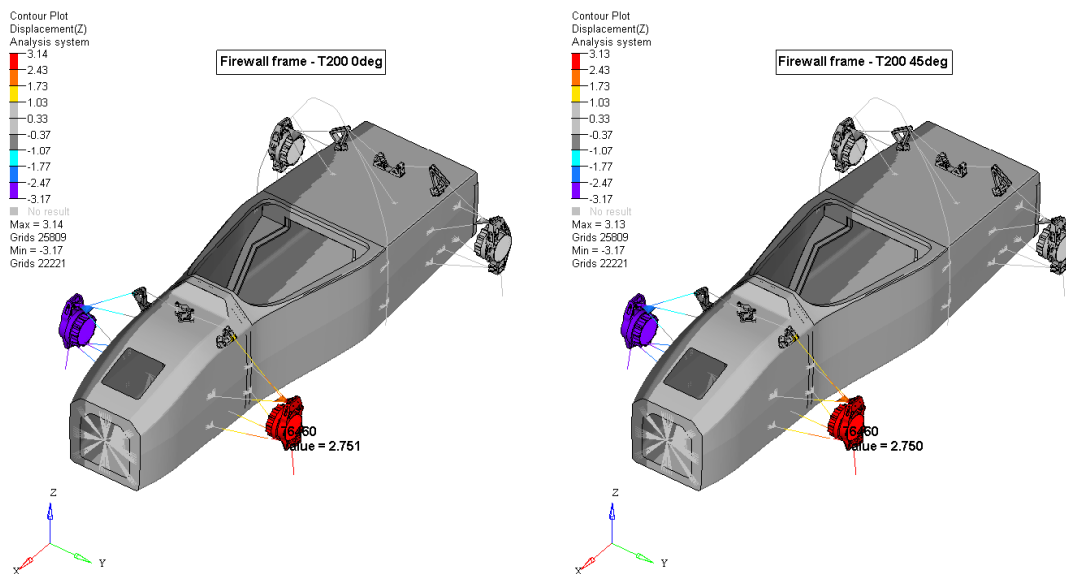


Figure 5.25: Z-coordinate displacement comparison between firewall fixed frame with: T200 at 0° (left) and T200 at 45° (right)

The experience achieved simulating the firewall fixed frame has been directly transferred into the firewall itself. The FSAE rules about strength and insulation are valid also for this component. In this case, only two solutions have been tested between Kevlar and aluminum. A first with M46J only and a second with UD, in the same fashion as for the frame. Again UD did not bring a considerable contribution, thus it was discarded. Figure 5.28 reports the results of this comparison. What should be underlined is that the frame alone did not contribute substantially to the specific torsional stiffness. This changed when the firewall has been added.

Figure 5.29 illustrates the strain energy density of the entire chassis when the vehicle is subjected to symmetric torsion. Picture 5.30 shows the strain energy density of the maximum envelopes of the running and FSAE alternative frame rule load-cases. The resulting model featured a series of improvements which brought the torsional stiffness from 172 kNm/rad to 202 kNm/rad (Figure 5.31).

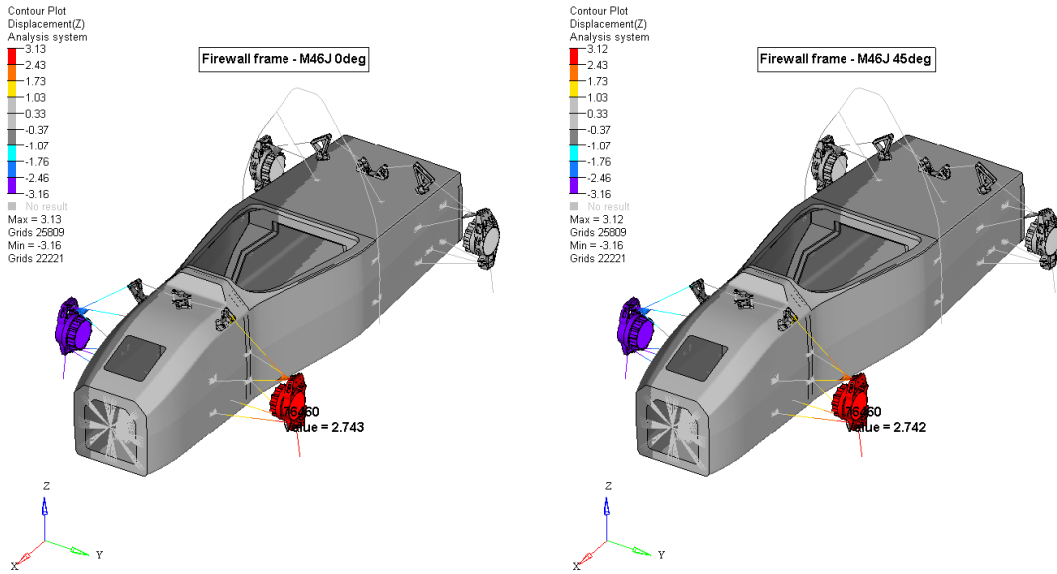


Figure 5.26: Z-coordinate displacement comparison between firewall fixed frame with: M46J at 0° (left) and M46J at 45° (right)

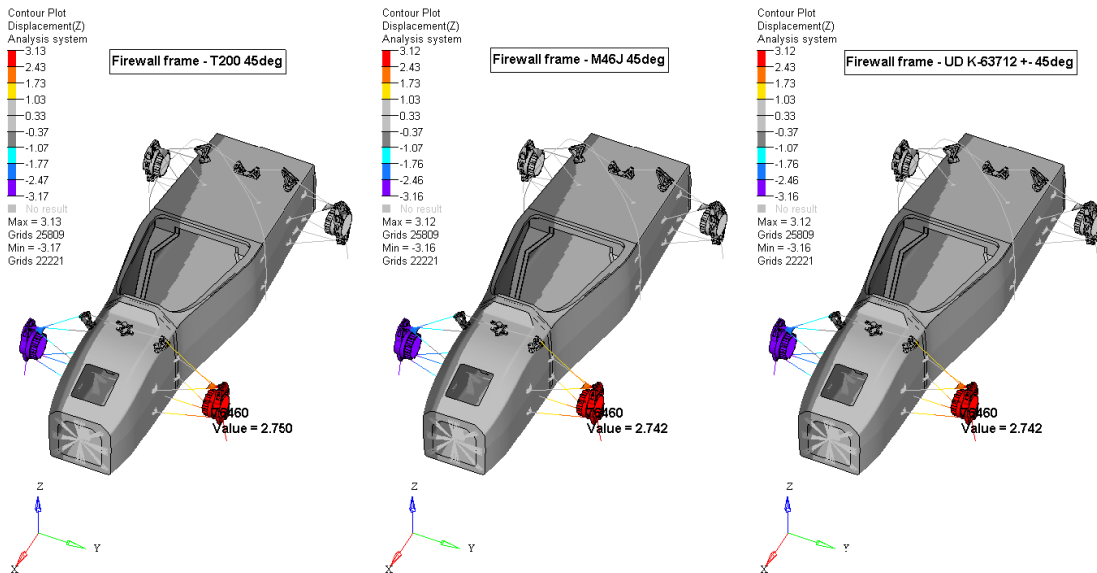


Figure 5.27: Firewall fixed frame z-coordinate displacement comparison between: T200 (left), M46J (centre), UD (right)

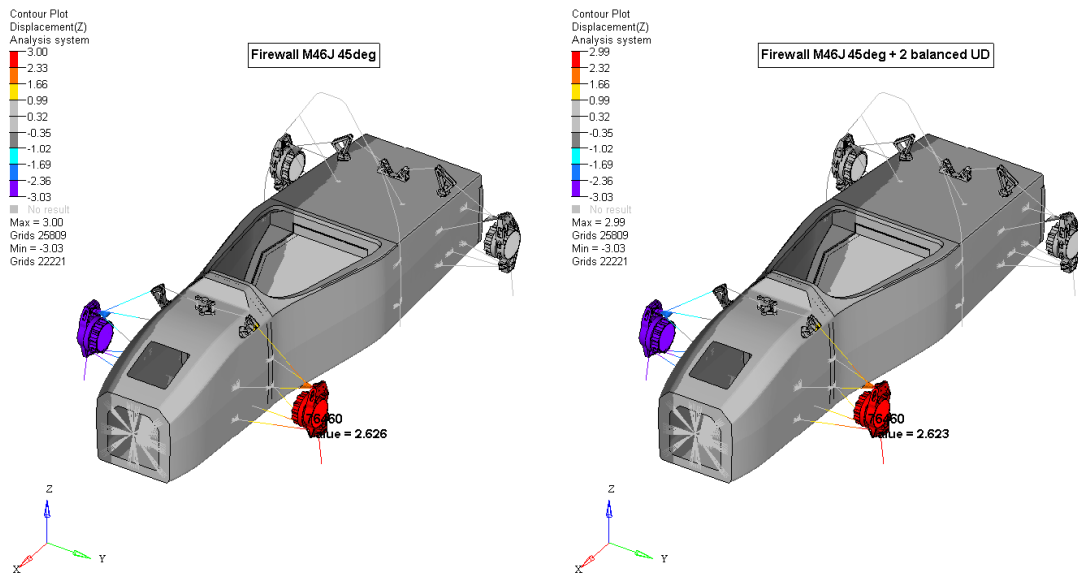


Figure 5.28: Z-coordinate displacement comparison between two firewall laminate solutions: fixed frame M46J laminate (left), same laminate but with additional two UD balanced plies (right)

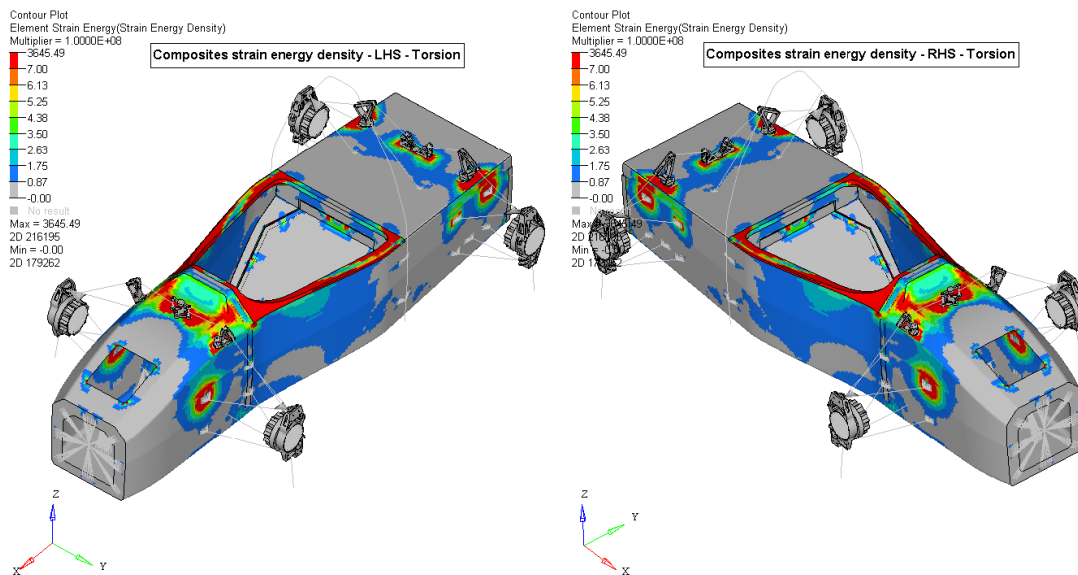


Figure 5.29: Strain energy density of the resulting model when subjected to torsion

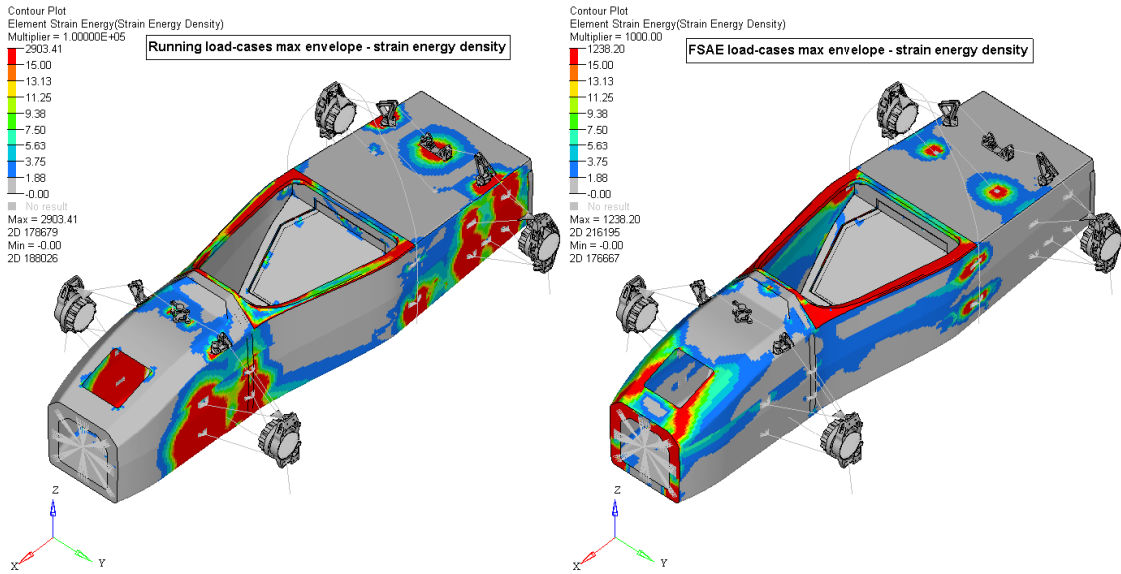


Figure 5.30: Strain energy density of the resulting model when considering maximum envelope of: running load-cases (left), FSAE alternative frame rules (right)

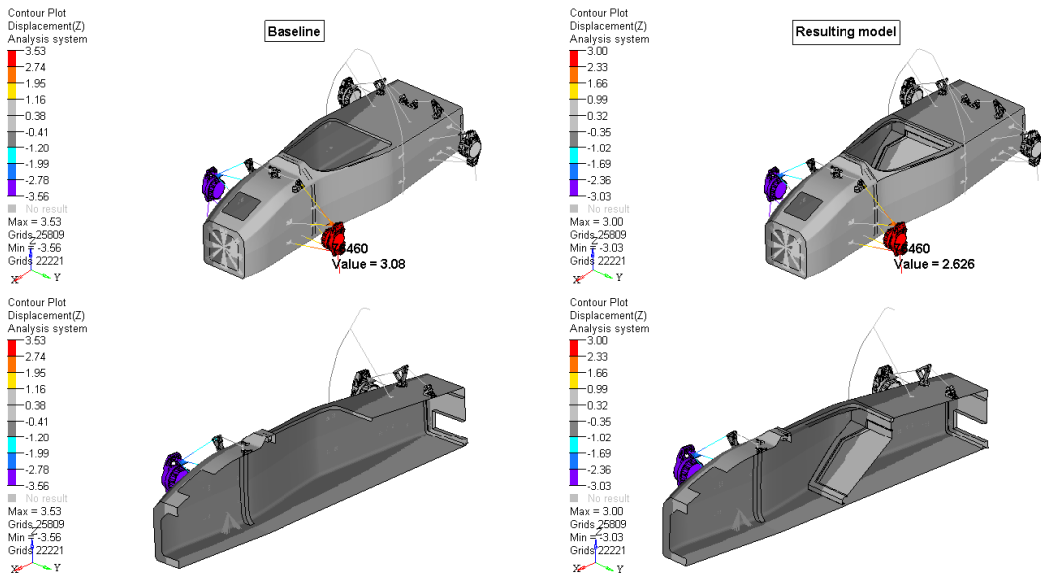


Figure 5.31: Comparison between the baseline model (left) and the resulting model (right)

5.4 Practical implementation of the designed solutions

This section contains some pictures which illustrate how the solution studied in the previous section have been physically implemented on the car.

Figure 5.32 illustrates the lamination process of the upper half of the monocoque. In particular, on the left side, it is possible to appreciate the mating of a honeycomb panel and the Rohacell reinforcement. About this last, it is possible to notice the thicker triangular parts at its extremities. This demonstrates in practice the cross-section management mentioned above.



Figure 5.32: Lamination of the top half of the monocoque

Figure 5.33 illustrates in detail the front-end of the reinforcement. This region has been quite difficult to design because of the presence of the reinforcement, the front roll-hoop, the steering wheel support and the internal edges of the opening. The shape of the ring has been defined, as already mentioned, to create a smooth transition between the sections of the laminate.

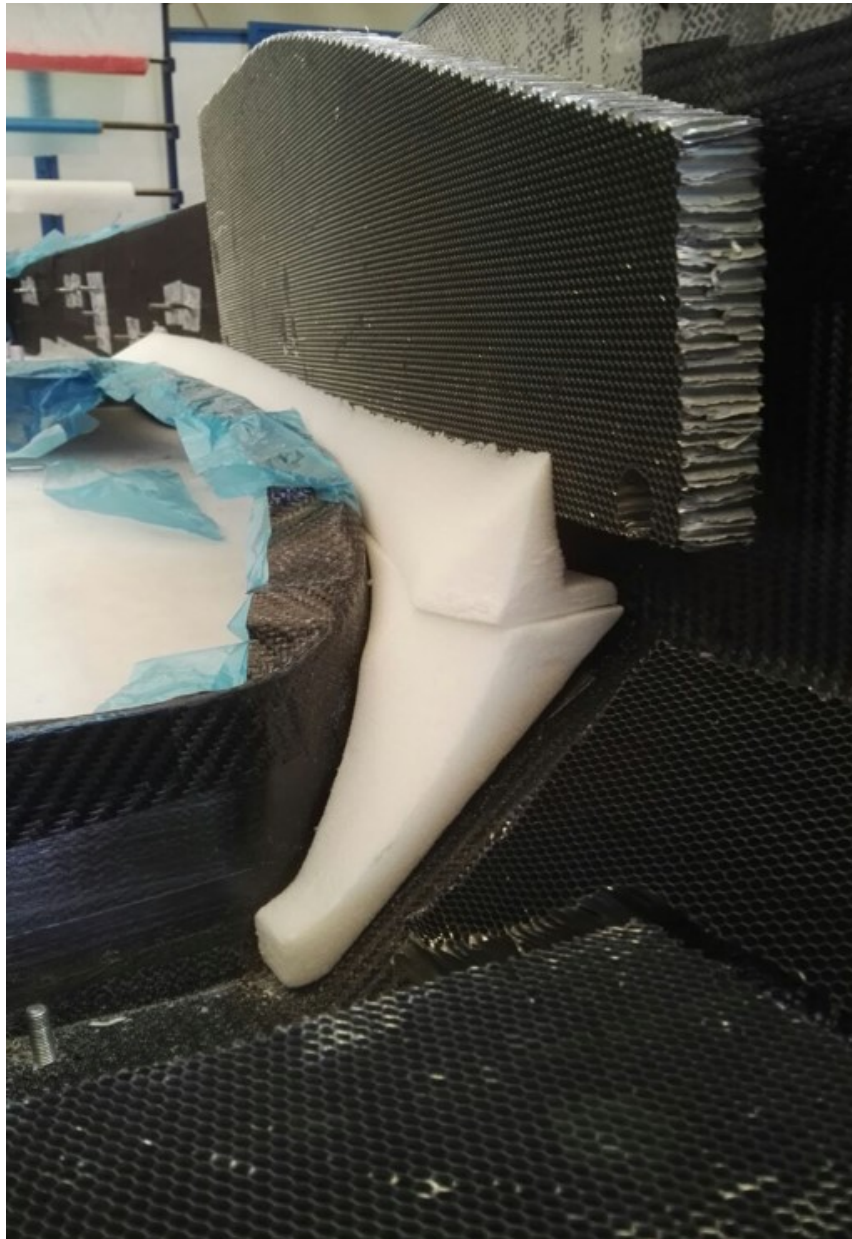


Figure 5.33: Lamination of the top half: detail of the cockpit opening Rohacell reinforcement

Figure 5.34 reports detail of the integrated firewall frame with the opening for the firewall. It is difficult to appreciate because of the conductive dark paint but around the internal edge, there is a seal that was compressed by the screwed firewall to further enhance the water-proofing capabilities.



Figure 5.34: Integrated firewall frame

5.5 The SC17: a brief overview of the project results

The results presented in the previous sections describe the steps followed during the design phase of the SC17, in the winter of 2016. The design phase has been abandoned once the manufacturing started, in early 2017. This section takes inspiration by an analogous section in [4], and it is aimed at providing an overview of the SC17 prototype, at the end of its manufacturing and assembly phase, with its main features and characteristics.

The main characteristics of the SC17 are:

- Composite monolithic monocoque;
- Four-Wheel-Drive (4WD) with hub-motors (the electric motor are mounted outboard, directly on the uprights);
- AMK electric motors with a peak-power of 35 kW;
- Two-stage epicycloidal transmissions mounted in series of the motors in the hubs;
- Push-rod suspensions both at front and rear with glass-fiber anti-roll bar;
- Pirelli tyres 13";
- Complete aero-package constituted by front wing, rear wing and side-pods;
- Ion-polymers cells battery pack with total capacity of 7.46 kWh;
- Double direction telemetry;
- Total mass of 215 Kg;
- Maximum power (limited by rules) of 80 kW;
- Acceleration from 0 to 100 km/h in less than 3 seconds.

As already mentioned at the beginning of Chapter 5, the main goal for this project was to pursue reliability, peculiarity which was missing in the previous projects, causing poor results. Dramatic improvements have been achieved during the SC17 projects and a complete testing season before the races enhanced the competitiveness of the vehicle. Concerning electronics, the weakest points of the previous projects, most of the problems have been solved by using predictable and reliable standard components. Also under the mechanical point of view, it has been decided to choose simple and reliable solutions.

This resulted in a winning approach: the team has been able to manufacture and assembly the car respecting the schedule set-up at the beginning of the project and the car participated to three Europeans races, achieving the best results of the pure-electric era.

The improved performances are the consequence of a deep re-arrangements of the packaging, allowed by changing the pilot driving position. Picture 5.35 illustrates a section view of SC17, through which it is possible to discover the arrangements of the components contained inside the monocoque. A deep analysis carries out with the pilots about the driving position, especially concerning the inclination of the back restraint with respect the horizontal, determined that the minimum inclination which did not compromised visibility was 35° . Once defined this, the other components have been positioned so to minimize the distance from the yaw axis and from the ground. In figure 5.35, the inverter is behind the integrated back restraint, followed by the battery pack. On top of this there was the ECU. Comparing picture 5.2 and picture 5.35 is it possible to see how bulky the rear end of the SCXV was compared to the SC17.

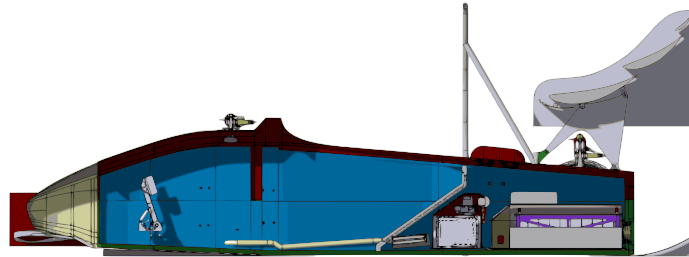


Figure 5.35: Packaging of the prototype SC17

Other innovative aspects of the SC17 dwell in the usage of innovative technologies, such as additive manufacturing (AM). This last has been used to optimize the cooling of the inverter, substituting a massive steel cooling plate with optimized aluminum ones, with a considerable mass reduction. AM has been also used to produce the cooling jackets of the electric motor. Additive technologies allowed the design of a helix which improved the thermal exchange.

Concerning aerodynamics, it has been studied utilizing Computational Fluid Dynamics (CFD) software and then validated in the wind tunnel. Image 5.37 illustrates the SC17 in the wind tunnel of Centro Ricerche FIAT. The aero-package generates 350 N of downforce at 60 km/h. It has a drag coefficient (c_x) of 1.13 and a downforce coefficient (c_z) of 1.96. Picture 5.36 illustrates a CFD simulation, while image 5.37 is the SC17 in the wind tunnel.

The unsprung masses architecture remained the same as SCXV. They have been

re-designed to improve reliability and saving weight.

As mentioned above, uprights hosted the electric motors. This allowed improving traction and implementing torque vectoring, which means managing the torque on each wheel individually, depending on the driving conditions. AMK motors were characterized by low torque (21 Nm) and high rotational speed (20000 rpm). This required a reduction system capable of increasing the output torque. To do so, a two-stage reduction system, with a transmission ratio of 1:16 has been used.

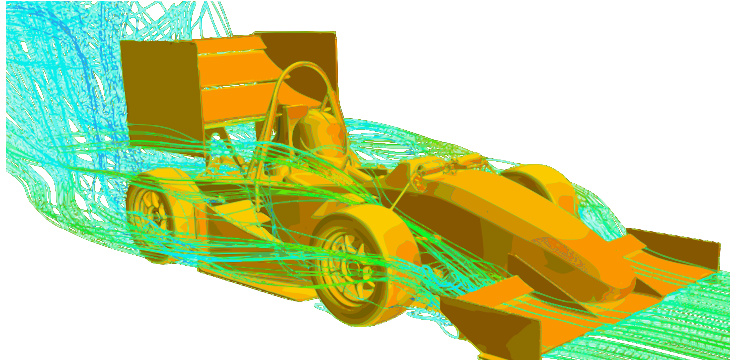


Figure 5.36: CFD simulation of the SC17



Figure 5.37: SC17 in the wind tunnel of Centro Ricerche FIAT during the validation of the aero-pack

5.6 Possible future developments

This section contains some ideas that could be investigated for future developments. They consider both design and manufacturing aspects, and are both based on the experience of the author.

- Rib-reinforced composite sandwich designed for Three-Point Bending (3PB) test. Picture 5.38 ([9]) shows how a sandwich panel could be reinforced either acting on its geometry or adding a rib of foam. Another interesting solution could be to use an asymmetric lamination of the plies which are used to construct the panel. Further studies about 3PB tests and composite specimens can be found in [18];
- Sandwich cores can also be exploited wisely to improve the specific stiffness and strength of a composite structure. Aluminum honeycomb probably represents the best choice in terms of performances and core with smaller cells, and so heavier, could be used for the most stressed regions, while lighter honeycomb could be used in the remain parts. Honeycombs, in general, are not easy to deal with during the manufacturing phase. Some team, as illustrated in picture 5.39, used foam layers glued one on top of each other, allowing a much simpler management of the thicknesses and the transitions;
- Concerning manufacturing, the SC17 monocoque is a monolithic structure, cured in one cycle only. The obtained results suggested that probably this choice was not the best. Aesthetically the uppermost layer shown lack of resin and structurally there where some dry fibers all over the chassis. Another important aspect is the debulk pressure. When dealing with composite lay-up, in order to maximise the adhesion of the plies to the mould, it is usual to perform a pure pressure cycle with the first ply and then the first set of plies. The debulk of the SC17 has been carried out at 4.5 bar. This because the debulk of the SCXV was performed at the same pressure. The suggestion here is to experiment higher pressure to improve even more the adhesion between the plies and the mould and between the plies themselves, with structural benefits;
- Curing represent another milestone in the manufacturing process of a composite component. As mentioned earlier, the SC17 was produced with a unique curing cycle. It is advisable, after a high-pressure debulk, to cure the external plies. Once the panels are finished a final curing can then be performed. Looking at what other teams did, it is also wise to think about a non-monolithic monocoque (extremely demanding in terms of lamination at the interface between upper and lower halves) but two halved glued afterwards;

- The integrated firewall frame improved dramatically the waterproofing capabilities of the prototype. About the SC17, it has been glued by means of structural glue afterward. Another solution which would increase the final quality and the waterproofing capabilities is dedicated curing process, eventually with a local bag;
- During the manufacturing process of the SC17, a non negligible amount of time has been spent producing the Rohacell fillets to interpose between the sandwich panels, in order to have a uniform pressure distribution during curing. A much simpler solution is expanding filler, which increase their volume during curing;

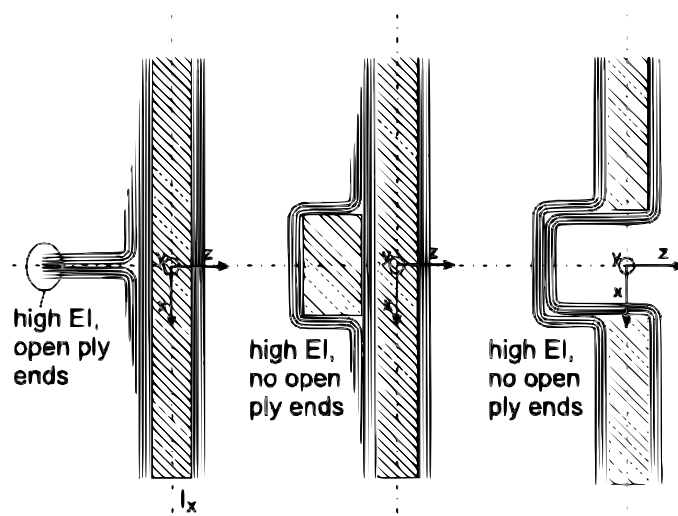


Figure 5.38: Stiffened composite panel



Figure 5.39: Monocoque sandwich foam core

Chapter 6

Further studies on the cockpit opening

This section contains some further studies performed a posteriori with respect to the investigations completed in the previous section. Some peculiar aspects have been investigated and, in particular, their effects on the specific torsional stiffness. They were:

- Cockpit opening fillet radii in top-view;
- Cockpit opening fillet radii in side-view;
- Aperture width;
- Aperture length;
- Aperture shape;
- Reinforcements

In an attempt to increase the precision of the models, and being the opening region the restricted area in which stresses have been measured, a local mesh refinement has been performed. A local mesh-size of about 2.5 mm has been used. The convergence parameter chosen this time was the maximum stress in the opening region. Picture 6.1 illustrates these results and table 6.1 summarizes the steps performed.

Convergence, in this case, has not been reached clearly as for the case of the monocoque global mesh size. The percentage difference between the chosen mesh size and the previous step is quite remarkable. Thus, being the run time acceptable even with the finer mesh, it has been decided to use a local mesh-size of 2.5mm.

In the following analyses, the front part of the aperture has not been analyzed deeply as the rear one. This because of the presence of the steering wheel and

Table 6.1: Local convergence analysis summary

<i>Model j-th</i>	<i>Average local mesh-size</i>	<i>Number of nodes</i>	<i>% of tria</i>	<i>Run time [s]</i>	<i>Stress cockpit opening [MPa]</i>	<i>Delta ej-1</i>	<i>Error</i>
1	10	86111	0.7%	171	49.0	-	23.4%
2	5	97876	1.4%	246	50.0	2.0%	21.4%
3	2.5	132256	1.8%	347	67.7	21.4%	Ref

the necessity to move it comfortably. When this portion of the aperture has been designed, the minimum amount of space required has already been considered. This defined the shape of the aperture in top-view. A clearance of about 20 mm from the hands has been left. Neither issue nor criticalities have been reported by the driver in this regard.

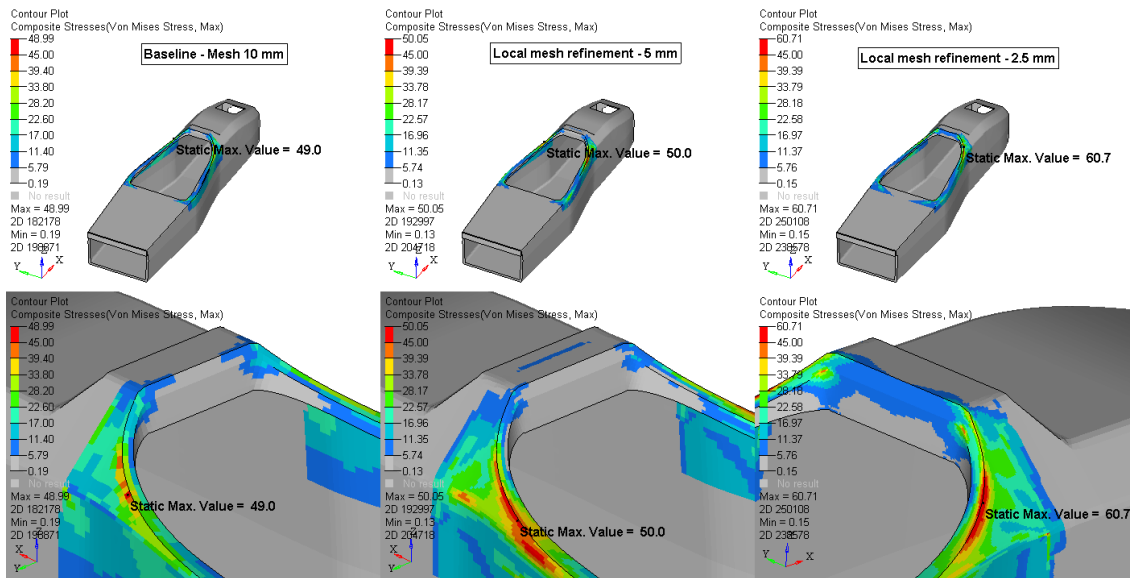


Figure 6.1: Local convergence analysis. Stress in the cockpit opening

6.1 Influence of fillet radii

This section presents the main results related to the sensitivity analysis performed on the opening region when dealing with different fillets. The complex geometry of the monocoque in this region allows defining fillets in different areas and fashions. In this analysis, they have been considered, for the sake of simplicity, divided into two macro-categories depending on their orientation: fillets in side-view (xz plane) and fillets in top view (xy plane).

The monocoque model utilized in these studies did not consider any kind of cockpit opening reinforcement.

Pictures 6.2, 6.3 and 6.4 illustrate the results of the analyses performed considering the rear-end aperture fillets, in top-view only. The baseline geometry has been compared to an extreme case, in which rear-end fillets were completely missing. A fillet with a radius of 100 mm has been modeled and finally, in another model, its radius was increased to 134 mm. This last particular figure was the result of considerations about the position of the FSAE opening template with respect to the opening itself. As mentioned before this set of analyses focused only on the rear part of the opening. Therefore, the space at disposal to move the FSAE template was quite limited. A radius of 134 mm was the biggest feasible radius that allowed to have a safety margin from the template itself.

On the other hand, figures 6.5, 6.6 report the results of the analyses performed on the fillets in side-view.

Table 6.2 summarizes analyses results.

In view of the above, it is possible to draw some conclusions:

- Top-view rear fillets influence mainly the values of the stresses. There were no dramatic variations when changing the values of the radii, no even with the complete absence of the fillet;
- Front fillets in side-view influence much more the stiffness. This probably because of the shape of the stricture in this region. A closer look at the monocoque in this area highlights how the side fillets link the side panels to the top of front-hoop housing, extending on a remarkable amount of length. In fact, in the extreme case in which these fillets have been removed, the torsional stiffness loss was more than 10%;
- The rear end side-view fillets analysis gave an interesting result. Contrary to the expectations, the torsional stiffness degraded. Post-processing of the results revealed that the higher height of the opening wall, with no reinforcement, allowed a wider motion, with a consequence reduction of the stiffness of the opening region;
- The major influence of the fillets is about the peaks of stress. Even if the local

maxima are quite different from case to case, the effect is local and does not represent a dramatic condition for the laminate, which remain usually safe.

Table 6.2: Influence of fillet radii on torsional stiffness over mass ratio

	Model	Max stress [MPa]	Delta stress %	Z-displ [mm]	Delta displ %	Mass m [kg]	Torsional stiffness Kt [kNm/rad]	Torsional stiffness/mass Kt/m [kNm/(rad*kg)]	Delta Kt/m %
Fillets in the x-y plane	Baseline 2.5 mm (rear)	54.5	Ref	3.2	Ref	20.73	167	8.1	Ref
	No rear fillets	96.6	77%	3.2	1%	20.73	166	8.0	-1%
	R = 100 mm	18.1	-81%	3.2	-2%	20.73	169	8.1	2%
	R = 134 mm	1.0	-95%	3.1	0%	20.74	169	8.2	0%
Fillets in the x-z plane	Baseline 2.5 mm (front)	60.7	Ref	3.2	Ref	20.73	167	8.1	Ref
	No front fillet	102.2	68%	3.6	13%	20.74	148	7.1	-12%
	Additional structure at rear	77.2	27%	3.3	5%	20.75	160	7.7	-5%

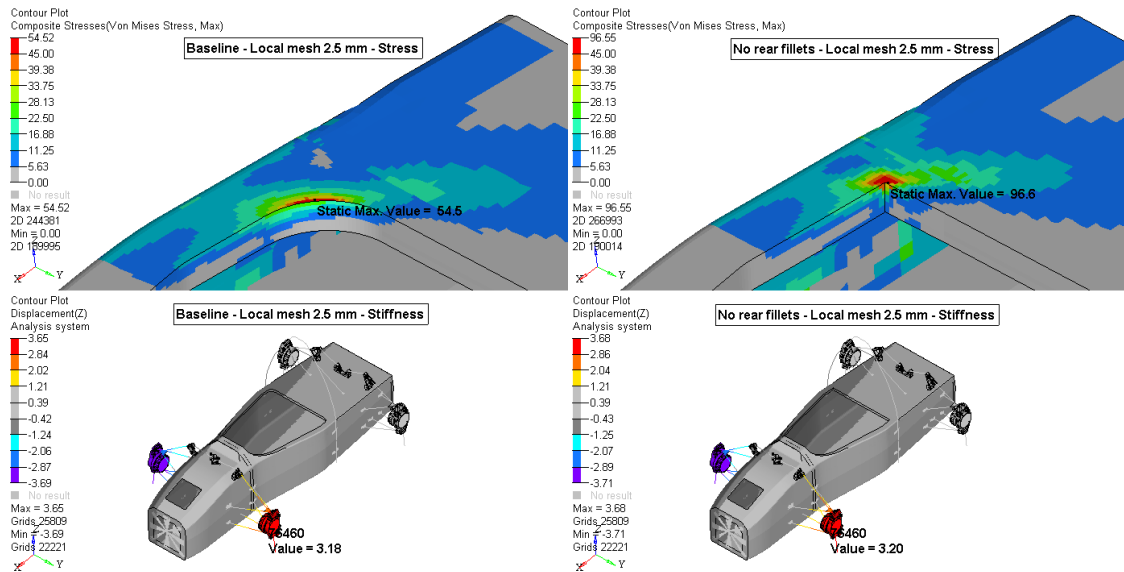


Figure 6.2: Baseline geometry (left) and absence of rear-end fillets (right)

It is interesting to look at what other teams do. Pictures 6.8 and 6.7 illustrates the solutions of AMZ (ETH Zurich) and TuFast (TU Munich) respectively. As it is possible to appreciate, top-view shapes are similar and both teams opted for big fillet radius, solutions which is aligned to the results of the simulations presented in this section. TuFast’s aperture narrower in the front, while AMZ one seems to be wider. Anyway, this is just a subjective perception.

6.1 – Influence of fillet radii

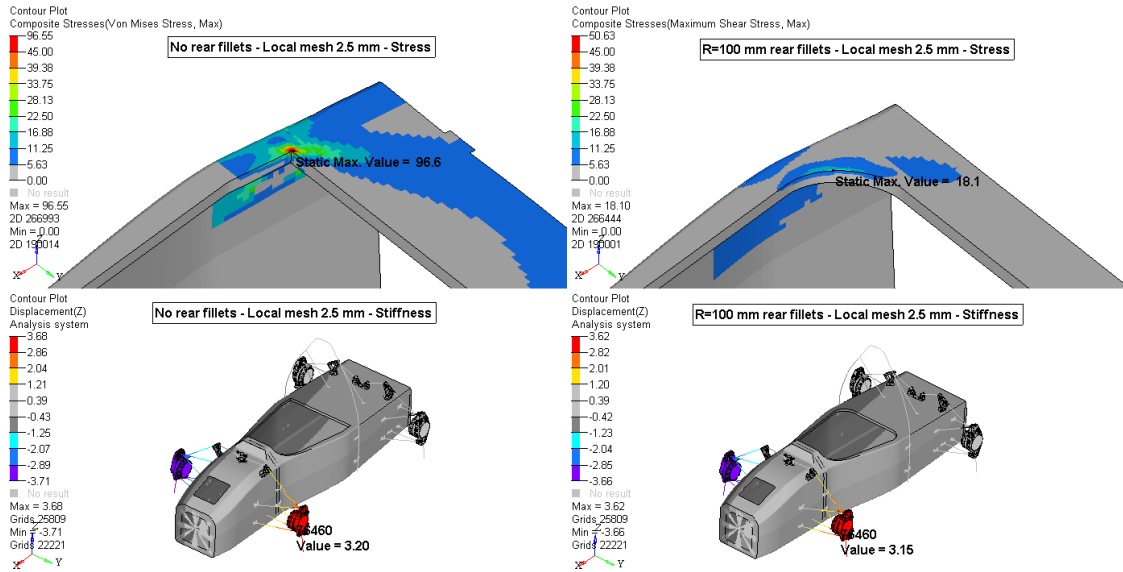


Figure 6.3: Absence of rear-end fillets (left) and a fillet $R=100$ mm (right)

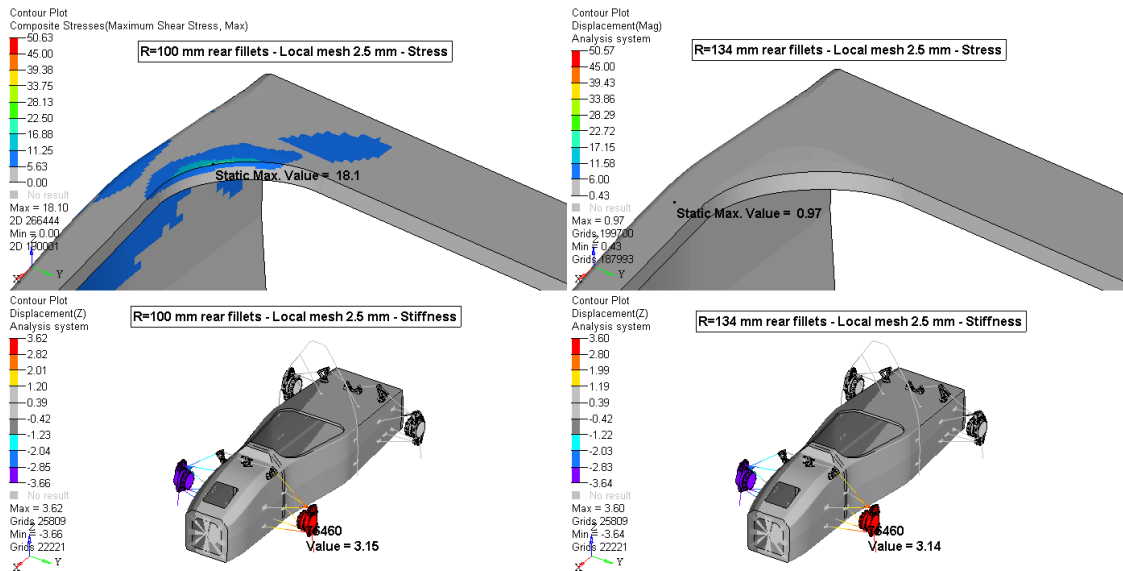


Figure 6.4: Fillet $R=100$ mm (left) and fillet $R=134$ mm (right)

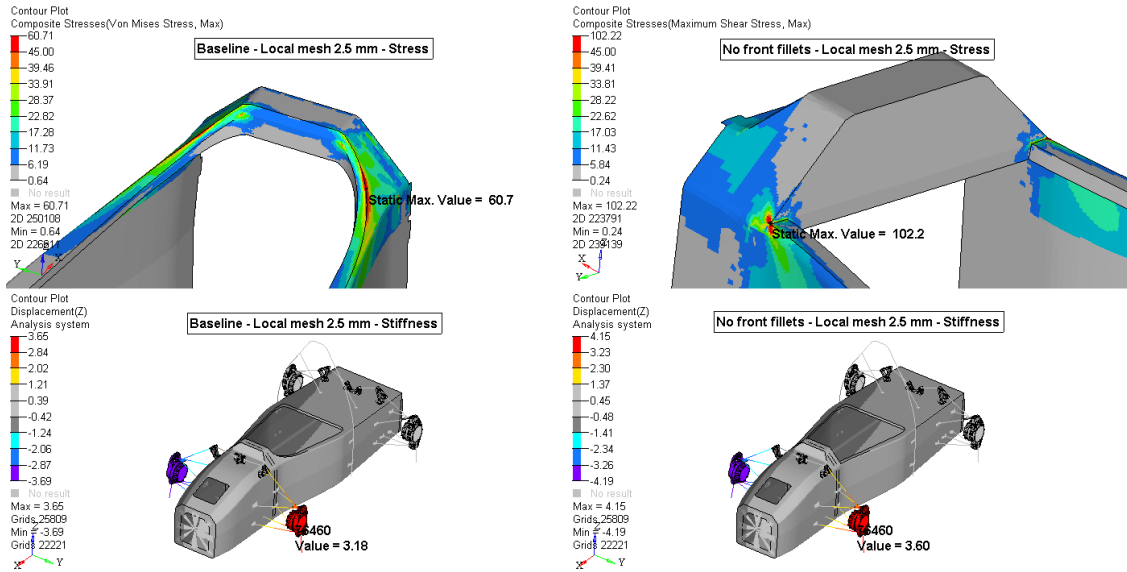


Figure 6.5: Baseline geometry (left) and absence of front-end fillets (right)

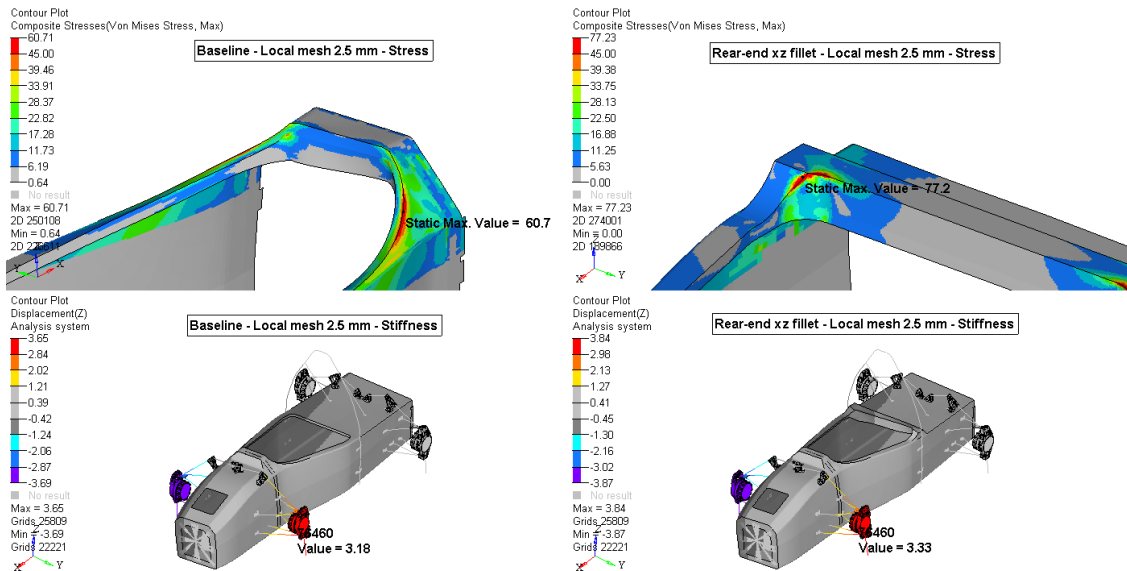


Figure 6.6: Baseline geometry (left) and rear-end with additional structure (right)

6.2 Influence of aperture dimensions

This section reports briefly the results of the analyses performed to determine the effect of the opening width on the torsional stiffness. No studies have been carried out on the effect of the length. The reason behind this choice is that the aperture considered was defined around an extreme driving position, with a back-rest inclination of 35° with respect to the horizontal. Being usually the driving position more vertical, the opening will be smaller with improvements in terms of stiffness.

Figure 6.9 illustrates the comparison between the produced shape and an aperture exactly equal to the FSAE template. This last, despite being an extreme case, induce a quite interesting increase in stiffness. Image 6.10 shows how increasing the width 5 mm per each side did not induce major losses.

In addition to these analyses, shape optimization has been performed on the opening. The idea was to leave to the solver the task of defining an aperture capable of minimizing the stresses, starting from the minimum allowed one, namely, the opening with the same dimension of the FSAE template. Unfortunately, the optimization did not bring the expected results. With more time available, a dedicated analysis could be successful.

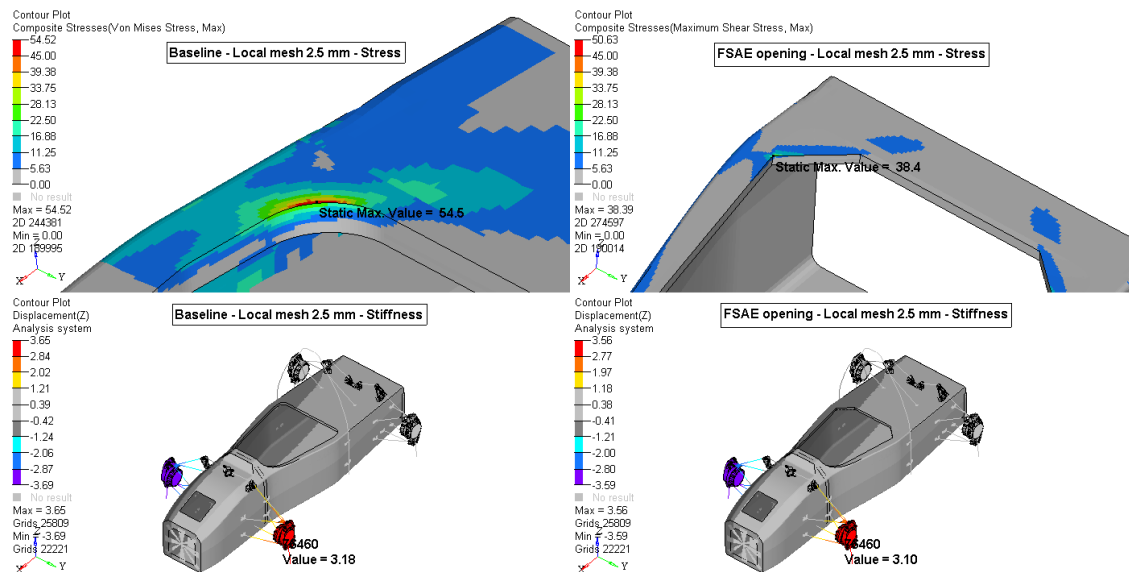


Figure 6.9: Baseline geometry (left) and aperture at the limit with the FSAE dimensions (right)

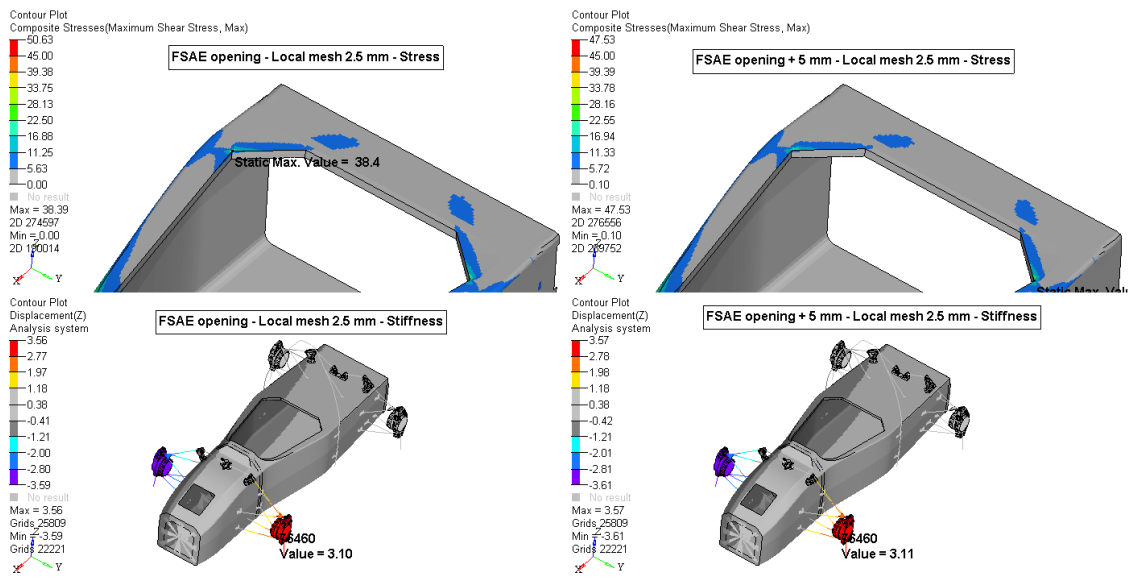


Figure 6.10: Aperture at the limit with the FSAAE dimensions (left) and the same geometry but 5 mm wider

Chapter 7

Conclusion

This paper presented in detail one specific aspect of the design process followed during the conceptual phase of the chassis of the SC17. In addition to this, some further analyses have been performed in order to increase the understanding of the geometry of the cockpit opening aperture on the stiffness over mass ratio.

The solutions designed and analyzed presented in this thesis did not remain a virtual study but have been manufactured and then assembled in what became the SC17. During the 2017 Formula Student season, in fact, the SC17 took part in races in Italy, Czech Republic, and Spain with remarkable results for the team.

The resulting monocoque (manufactured) containing all the improvements developed in this paper shown a total mass of 21.7kg. The actual torsional stiffness was not tested because of the lack of time before the races. Priority was given to testing the car to verify the absence of major issues and to develop vehicle dynamic controls. Thus, the estimation of the torsional stiffness is a theoretical value of about 202 kNm/rad.

The outcomes of this work demonstrated that:

- The design target in terms of torsional stiffness has been reached;
- The maximum mass target of 22 kg has been respected;
- The stiffness of the monocoque was high enough to allow the proper functioning of the suspensions and the other vehicle dynamic components.

The major problems suffered by this project were related to manufacturing. Because of the inexperience of the author, some choices about the production process lead to an increase in the production time and poor aesthetic quality of the final laminate.

To conclude, this monocoque represented a further step ahead in terms of design and waterproofing, thanks to opening reinforcement and to integrated firewall frame.



Figure 7.1: Squadra Corse team together with the teams's faculty advisor during design event in Varano 2017



Figure 7.2: SC17 team during the prizegiving in Varano 2017 - Third place overall

Bibliography

- [1] Ever J. Barbero. *Introduction to Composite Materials Design, Third Edition*. 2017. ISBN: 9781138196803. DOI: 10.1201/9781315296494.
- [2] Jonathan Brivio. “Design, manufacturing and testing a sandwich monocoque for a formula student race car”. PhD thesis. 2014.
- [3] Alessio Canuto. “Design of a composite monocoque for Formula Student single-seater racing car”. PhD thesis. 2017.
- [4] Elisabetta Carboneri. “Progettazione e produzione di Sospensioni e Masse non Sospese per una vettura di formula SAE”. Master. Politecnico di Torino, 2018.
- [5] Andrew Deakin et al. “The effect of chassis stiffness on race car handling balance”. In: *SAE Technical Papers 724* (2000). ISSN: 26883627. DOI: 10.4271/2000-01-3554.
- [6] Leonard Hamilton et al. “Production of a composite monocoque frame for a formula SAE racecar”. In: *SAE Technical Papers 2*. June (2013). ISSN: 26883627. DOI: 10.4271/2013-01-1173.
- [7] Alexander L Kalamkarov and Alexander G Kolpakov. *Analysis, design and optimization of composite structures*. Vol. 1. Wiley New York, 1997.
- [8] Christos Kassapoglou. *Design and analysis of composite structures: with applications to aerospace structures*. John Wiley & Sons, 2013.
- [9] Jannis D.G. van Kerkhoven. “Design of a Formula Student Race Car chassis”. In: (2008), p. 66.
- [10] Laszlo P Kollar and George S Springer. *Mechanics of composite structures*. Cambridge university press, 2003.
- [11] Stefano Manzi. “Progettazione e produzione di un telaio monoscocca per una vettura Formula SAE”. PhD thesis. 2015.
- [12] Frank L Matthews et al. *Finite element modelling of composite materials and structures*. Elsevier, 2000.

BIBLIOGRAPHY

- [13] Alessandro Moroni. “Racing Car Chassis Torsional Stiffness and its Influence on the Car ’ s Transient Handling Performance”. In: November (2008), pp. 1–22.
- [14] Ozden O Ochoa and Junuthula Narasimha Reddy. “Finite element analysis of composite laminates”. In: *Finite Element Analysis of Composite Laminates*. Springer, 1992, pp. 37–109.
- [15] SAE. “SAE International”. 2016. URL: <https://www.sae.org/students/>.
- [16] Enrico Sampo’, Aldo Sorniotti, and Andrew Crocombe. “Chassis torsional stiffness: Analysis of the influence on vehicle dynamics”. In: *SAE Technical Papers* (2010). ISSN: 26883627. DOI: 10.4271/2010-01-0094.
- [17] SquadraCorse. *Squadra Corse PoliTo | Politecnico di Torino | Italia*. URL: <https://www.squadracorsepolito.com/>.
- [18] Robert Story. “Design of Composite Sandwich Panels for a Formula SAE Monocoque Chassis”. In: (2014). URL: <https://ir.library.oregonstate.edu/xmlui/handle/1957/46918>.
- [19] RL Taylor and Olgierd Cecil Zienkiewicz. *The finite element method*. Butterworth-Heinemann, 2013.
- [20] Olgierd Cecil Zienkiewicz et al. *The finite element method: solid mechanics*. Vol. 2. Butterworth-heinemann, 2000.